

AD-A 085 945

TECHNICAL
LIBRARY

TECHNICAL REPORT — RL-80-6

QUANTITATIVE NONDESTRUCTIVE
EVALUATION

Dallas G. Smith
John A. Schaeffel, Jr.
Ground Equipment and Missile Structures Directorate
US Army Missile Laboratory

October 1979



U.S. ARMY MISSILE COMMAND

Redstone Arsenal, Alabama 35809

Distribution approved for public release; distribution unlimited.

AAA

DEFIC QUALITY INSPECTED 1

DISPOSITION INSTRUCTIONS

DESTROY THIS REPORT WHEN IT IS NO LONGER NEEDED. DO NOT RETURN IT TO THE ORIGINATOR.

DISCLAIMER

THE FINDINGS IN THIS REPORT ARE NOT TO BE CONSTRUED AS AN OFFICIAL DEPARTMENT OF THE ARMY POSITION UNLESS SO DESIGNATED BY OTHER AUTHORIZED DOCUMENTS.

TRADE NAMES

USE OF TRADE NAMES OR MANUFACTURERS IN THIS REPORT DOES NOT CONSTITUTE AN OFFICIAL ENDORSEMENT OR APPROVAL OF THE USE OF SUCH COMMERCIAL HARDWARE OR SOFTWARE.

UNCLASSIFIED

SECURITY CLASSIFICATION OF THIS PAGE (When Data Entered)

REPORT DOCUMENTATION PAGE		READ INSTRUCTIONS BEFORE COMPLETING FORM
1. REPORT NUMBER TR-RL-80-6	2. GOVT ACCESSION NO.	3. RECIPIENT'S CATALOG NUMBER
4. TITLE (and Subtitle) QUANTITATIVE NONDESTRUCTIVE EVALUATION		5. TYPE OF REPORT & PERIOD COVERED Technical Report
		6. PERFORMING ORG. REPORT NUMBER
7. AUTHOR(s) Dallas G. Smith John A. Schaeffel, Jr.		8. CONTRACT OR GRANT NUMBER(s)
9. PERFORMING ORGANIZATION NAME AND ADDRESS Commander US Army Missile Command ATTN: DRSMI-RL Redstone Arsenal, Alabama 35809		10. PROGRAM ELEMENT, PROJECT, TASK AREA & WORK UNIT NUMBERS
11. CONTROLLING OFFICE NAME AND ADDRESS Commander US Army Missile Command ATTN: DRSMI-RPT Redstone Arsenal, Alabama 35809		12. REPORT DATE October 1979
		13. NUMBER OF PAGES 176
14. MONITORING AGENCY NAME & ADDRESS (if different from Controlling Office)		15. SECURITY CLASS. (of this report) Unclassified
		15a. DECLASSIFICATION/DOWNGRADING SCHEDULE
16. DISTRIBUTION STATEMENT (of this Report) Distribution approved for public release; distribution unlimited.		
17. DISTRIBUTION STATEMENT (of the abstract entered in Block 20, if different from Report)		
18. SUPPLEMENTARY NOTES		
19. KEY WORDS (Continue on reverse side if necessary and identify by block number) Nondestructive Evaluation Nondestructive Inspection Nondestructive Testing		
20. ABSTRACT (Continue on reverse side if necessary and identify by block number) This work represents the completion of an effort begun in 1976 with the preparation of the Army report <u>Fracture Mechanics Design Handbook</u> and continued with preparation of <u>Fracture Mechanics Design Handbook for Composite Materials</u> . The purposes of those reports was to provide an introduction to fracture mechanics fundamentals and to provide a convenient source of fracture mechanics information for structural designers, stress analysts, and engineers. That idea is continued here. Fracture mechanics and quantitative nondestructive evaluation (NDE) are		

20. ABSTRACT (Concluded)

closely related; both combined are required to design for structural reliability. Fracture mechanics assumes flaws of given locations, shapes, and dimensions; NDE provides the means of finding those flaws. A program of fracture control must include both fracture mechanics calculations and nondestructive inspection considerations. The stress analyst and the fracture specialist must be familiar not only with flaw tolerance calculations but also with the methods used to find those flaws: how sensitive and how reliable those methods are, how they are carried out and the provisions which must be made for them during design. A knowledge of fracture mechanics without some knowledge of NDE is incomplete, and visa versa. The definition of each should perhaps be broadened to include a portion of the other. Fracture mechanics calculations have diminished worth without an inspection method to verify the absence or presence of flaws of calculated critical size; and NDE likewise has limited value without fracture mechanics to provide a rational accept/reject criteria.

This manual has been prepared primarily for the non-NDE specialist. Its aim is to increase understanding of NDE capabilities among those involved in structural design and fracture mechanics calculations, and to provide physical details pertaining to most of the important NDE techniques. Since NDE has been so actively applied in the aerospace industry most of the application examples discussed here are related to aerospace structures; however the basic ideas apply to any structure containing fracture critical components. A brief introduction together with comments on the relationship of fracture mechanics and quantitative NDE is included in Chapter 1. The present practice of NDE, including military specifications, airplane inspection manuals, and inspector training are discussed in Section 2. The "big five" methods of NDE — liquid penetrant, magnetic particle, ultrasonic inspection, eddy current, and radiography — are introduced in Section 3. Certain advanced inspection methods — methods still undergoing development — are included in Section 4. The state-of-the-art, the sensitivity and reliability, of various methods along with the statistical analysis for determining flaw detection probability and confidence levels is presented in Section 5. Excerpts from two actual airplane inspection manuals are included in the appendix to illustrate the degree to which instructions to inspectors are detailed and specified.

This report is only an introduction to quantitative nondestructive testing; it is not a training manual or handbook on how to apply the various techniques. Other sources provide that. No pretense of originality is made. Information included was gathered from many sources; appreciation is extended to all those authors whose work is cited and apologies to any who may have been overlooked or inadvertently omitted.

CONTENTS

Section	Page
I. Introduction	09
A. Role of Nondestructive Evaluation	09
B. Literature of NDE	11
C. Relationship of NDE to Fracture Mechanics	13
II. The Practice of Nondestructive Evaluation	14
A. Damage Tolerance Requirements	15
B. Inspection Practice	17
C. NDE Personnel	18
III. The Basic NDE Methods	21
A. Liquid Penetrants	21
B. Magnetic Particle	24
C. Eddy Current Testing	29
D. Ultrasonics	35
E. Radiography	57
IV. Advanced NDE Methods	69
A. Neutron Radiography	69
B. Acoustic Emission	72
C. Liquid Crystals	82
D. Holographic Interferometry	83
E. Acoustical Holography	87
F. Speckle Interferometry	89
G. Acoustical Speckle Interferometry	93

CONTENTS (Concluded)

Section	Page
V. The Sensitivity and Reliability of Inspection Methods	96
A. State-of-the-Art Detection Capabilities	96
B. Reliability of Flaw Detection	107
C. The Human Factor in NDE	112
References	121
Appendix A	131
Appendix B	149

ILLUSTRATIONS

Figure	Page
1. Initial Flaw Assumptions [24].....	16
2. NDT Method Symbols Used in the Inspection Manual for the DC-10 [35].....	19
3. Penetrant Seeps into the Crack	23
4. Rinsing the Penetrant from the Surface	25
5. The Developer Draws the Penetrant Out of the Crack Like a Blotter	25
6. Leakage Field Around a Surface Flaw, Subsurface Flaw, and a Parallel Flaw ..	26
7. Circular Magnetism Produced by Current Flowing Through Wire or Rod	27
8. Longitudinal Magnetism Produced by a Circular Coil.....	27
9. Magnetic Field Between Electrical Contacts	28
10. Eddy Current Generated in a Flat Plate by a Magnetic Field	30
11. Eddy Currents Produced in a Cylindrical Body by an Encircling Coil	30
12. Depth of Penetration in Plane Conductors [17]	31
13. Coil Impedance for Variations in Test Frequency or Conductivity and Specimen Radius for a Nonferromagnetic Cylinder Encircled by a Test Coil [17]	32
14. Coil Impedance for Variations in Test Frequency or Conductivity and Per- meability or Radius for a Ferromagnetic Cylinder Encircled by a Test Coil [17]	33
15. Two Identical Secondary Coils in Series Used to Detect Difference in Test Material from A to B	34
16. Types of Coils	36
17. Example of Absolute (a) and Differential (b) Bobbin Coil	37
18. The Pulse-Echo and Through-Transmission Methods	39
19. An Example of the A-Scan Method	40
20. The B-Scan Method	41
21. The C-Scan Method	42
22. Longitudinal and Shear Waves.....	43
23. Incidence of Longitudinal Wave on Interface Between Two Materials Showing the Partial Mode Conversions	46
24. Mode Conversion and Reflection at a Steel Air Interface	48

Figure	Page
25. Mode Conversion at Plexiglas-Steel Interface for Angle of Incidence in Range 29 to 61 Degrees	49
26. The Angle Probe	50
27. Beam Spread as Influenced by Frequency and Transducer Crystal Size	51
28. Example Contact Test Indications	52
29. Immersion Testing for Disbond of Bearing Bush and Box [15]	53
30. An Angle Probe [15]	54
31. Angle Probe, Pulse-Echo Inspection of Weld Seam Showing (a) Principle of Detection, and (b) Probe Movement [15]	55
32. Surface Wave Applications Showing (a) Inspection of a Hollow Extrusion, and (b) Surface Crack Search in a Fitting [14]	56
33. The Boeing Ultrasonic Fastener Hole Scanner	58
34. The Basic Radiographic Setup	59
35. Basic X-Ray Tube	60
36. Arrangement and Operation of Typical Isotope Camera	63
37. Penumbra Caused by Finite Source Size and Finite Specimen-Film Distance	64
38. Three Kinds of Radiation Scattering	66
39. Image Distortion Due to Source-Specimen-Film Misalignment	67
40. Influence of Ray Divergence on Recorded Flaw Location	67
41. Influence of Relative Crack and Ray Orientation on Detection Sensitivity	68
42. Standard Penetrameter for a 1-inch Thick Specimen	68
43. Typical Arrangement for Thermal Neutron Radiography — Direct Method of Imaging Shown	71
44. Acoustical Emission Monitoring System Showing Some Typical Filter and Amplifier Values	74
45. Acoustical Emission Activity as a Function of Specimen Stress in Terms of: (a) Pulse Rate, and (b) Accumulated Counts [56]	76
46. Fatigue Corrosion Test Showing How the Acoustical Emission Count can Serve as a Precursor of Unstable Crack Propagation [53]	77
47. Total Stress Waves Emitted Correlated With K_{MAX} from a Fatigue Cracking Test [53]	78
48. Relationship Between Fatigue Crack Growth Rate and Stress Wave Emission for Two Conditions of D6aC Steel [53]	79

ILLUSTRATIONS (Continued)

Figure	Page
49. Relationship Between Acoustical Emission Rate and the Stress Intensity Factor for a High Strength Steel Undergoing Hydrogen Embrittlement Cracking [54]	80
50. The Relationship Between Acoustical Emission and Stress Intensity Factor [54]	81
51. Steps in the Liquid Crystal Solution Application	84
52. Liquid Crystal Film Test	85
53. Typical Optical Geometry for Making Holographic Interferograms	86
54. Holographic Interferogram of Composite Tube With Circular Embedded Teflon Tape Flaw at Center of Tube	88
55. Typical Acoustical Holography NDT Configuration	90
56. Typical Optical Configuration for Making Laser Speckle Interferograms	91
57. Typical Reconstructed Diffraction Halo Modulated by Light and Dark Bars of Light	92
58. Typical Configurations for Acoustical Speckle Interferometry	94
59. Echo-Return Correlation in Acoustical Speckle Interferometry	95
60. Sensitivity of Five NDT Methods to Surface Flaws [21,23,36,65]	97
61. Inspection Sensitivity for Surface Cracks in Thin Aluminum Plates [66]	98
62. Inspection Sensitivity for Surface Cracks in Thick Aluminum Plates [66]	98
63. Detectable Surface Flaw Size Data [21,23,36,67]	100
64. Estimated NDE Capabilities for Flaw Detection for the B-1 Program [30]	101
65. Crack Detection Probability for Surface Cracks in 2219-T87 Aluminum at 95 Percent Confidence Level [68,69]	102
66. Sensitivity of Four Methods for Finding Surface Fatigue Cracks in 4330V Steel [28]	103
67. Production Inspection Capability of Two Methods for Finding Surface Flaws in Titanium Plates [70]	105
68. The Accuracy of Three NDT Methods for Cracks in Aluminum and Steel Cylinders [28]	106
69. Round Robin Test Results of Eleven Laboratories	108
70. Comparison of Lower-Bound Fatigue Crack Detection Probability by Three Different Plotting Methods (95 Percent Confidence Limits [76,77])	113
71. Bolted-Joint Fatigue-Cracked Specimen Used in an Inspection Program [78] ...	115
72. Comparison of Inspectors for Finding Cracks in Bolted Joints [78]	116

ILLUSTRATIONS (Concluded)

Figure	Page
73. Number of Inspectors Detecting Cracks of Various Sizes in a Bolted Joint [78].	117
74. Crack Detection Ability of Several Inspectors Using the Magnetic Particle Method [73]	118
75. Crack Detection Ability of Several Inspectors Using Delta Scan for Semi-Circular Surface Flaws [73]	119

TABLES

Table	Page
1. Degrees of Inspectability [24]	17
2. Code Letter for Equipment Callout Used in the Manual for the DC-10 [35]....	19
3. The Five Basic NDI Methods [43]	22
4. Example Wave Velocities in Typical Materials [14]	45
5. Typical Applications Versus Tube Voltage [17]	61
6. Characteristics of Four Isotopes Used for Radiography	62
7. Lower Bound Probability of Detection as Function of Successful Inspection Detections in a Lot of 30 with Confidence Limit of 95 Percent [77]	111

I. INTRODUCTION

Fracture control of modern structures is accomplished by a combination of applied fracture mechanics and quantitative nondestructive evaluation (traditionally called nondestructive testing). The role of fracture mechanics in fracture control was previously described in the Army reports *Fracture Mechanics Design Handbook* [1], and *Fracture Mechanics Design Handbook for Composite Materials* [2]. This present work is an extension of those two reports; it discusses the role and principles of quantitative nondestructive evaluation (NDE) in fracture control.

Most structural designers are familiar with the term nondestructive testing (NDT) — a method of testing a structure or component without damaging that test subject. Properly applied, NDT (or NDE) increases safety, conservation, and productivity. It can help prevent technological disasters. For its full potential to be realized, however, NDE must be included in the design phase of a product and so it is becoming important for designers and managers to have more than an elementary understanding, to gain familiarity with basic NDE methods, and to gain some notion of the capabilities and limits of NDT.

Because it conveys a more accurate description of the overall process, in general usage the terms nondestructive evaluation (NDE) is replacing nondestructive testing (NDT). Prompted by the emergence and widespread use of fracture mechanics and its flaw tolerance philosophy, the term *quantitative* nondestructive evaluation has in the last ten years arisen. The word “quantitative” is significant; it refers to two things: (1) an ability to quantify a detected flaw by determining its location, orientation, shape and size, and (2) the ability to statistically determine flaw detection reliability — i.e., the probability of detecting flaws of a given size range.

In the following the terms nondestructive testing (NDT) and nondestructive evaluation (NDE) are both used when speaking of the technology in general. In addition the term nondestructive test (NDT) will refer to a particular test method such as eddy current, etc. The term nondestructive inspection (NDI) refers to an application of NDT methods for inspecting materials or components.

A. Role of Nondestructive Evaluation

Three broad forces, as indicated by Berger [3], tend to increase the use of improved nondestructive testing — safety, conservation, and productivity. Safety is an

obvious concern in the case of modern structures, the failure of which can lead to loss of a great number of lives. Energy and material conservation can be affected through NDT by minimizing the waste of producing defective components, and by reducing over design. Increased production is promoted by NDT when a defective component or material is discovered before being assembled into the finished product. This permits saving the additional material and energy of further fabrication with the defective component. Many potential economic benefits possible through improved NDT were studied by the National Materials Advisory Board [4] and by Forney [5]. Savings can be effected through NDT if in-service defective components are detected and repairs made before extensive damage occurs. The operational and support costs of an airplane for example constitute the major portion of the life cycle costs [5]. If a higher reliability of the airplanes fracture critical components can be assured through more reliable NDT then substantial reductions in maintenance costs — and hence total life cycle costs — can result. If NDT technology is not sufficient to assure the integrity of advance composite airplane structures then proof testing of each component may be necessary to satisfy the requirements of US Military standard 1530, “Aircraft Structural Integrity Program” [6,5]. The cost of proof testing empennage components is known to be from 2.75 to 3.75 times more expensive than conventional NDT of those structures [5]. If NDT can provide the required assurance then a substantial cost savings is apparent. Under present conservative practice, certain critical airplane engine turbine disks are replaced when a calculated one percent probability exists that a small crack has developed [5]. These disks are then discarded whether or not a crack can be found. Most of them have substantial useful life remaining — possibly as much as 90 percent [5]. Since some disks cost as much as \$20,000, such a practice is wasteful. If NDE can determine a more rational disk replacement scheme based on inspection rather than calculated fatigue crack existence then a considerable savings would result. Early failure of structures due to flawed components can result in personal injuries and loss of life — a major risk associated with product liability. Product liability lawsuits are increasing in cost and frequency [4]. Reference [4] reported that in a single incident involving a faulty artillery shell, Army contractors were held liable in a judgment totaling several million dollars.

The importance of preventing technological disasters was discussed by McMaster [7]. His example is enlightening. Suppose an engineering system costing \$200 million is totally lost, then in a country such as the United States having a population of about 200 million the eventual cost to every man, woman and child is \$1 apiece — an amount, McMasters argues, which would be more than detectable if forcibly extracted from the pocket book of each person on the day of the disaster.

Examples of such disasters are too easy to find. The recent crash of a DC10 commercial jet following an engine pylon failure claimed 275 lives [8,9]. The plane which was totally destroyed was valued in the tens of millions of dollars. The plane's manufacturers are already the target of millions of dollars in lawsuits [10]. Following the crash, the entire US registered fleet of 138 DC10's, as well as most foreign registered DC-10's, was grounded. The revenue loss associated with the grounding of the domestic fleet alone was estimated at \$92 million [11].

B. Literature of NDE

Due to the prevalent use of high strength materials to meet missile and aerospace requirements and the flaw tolerant ideas of fracture mechanics, NDE is emerging as an integral part of design. This has been slow in coming about. Traditionally, NDT was sought "after the fact" to locate flaws in suspect parts [4]. Thus hampered, the value of NDT was diminished because the installed part was uninspectable or because the applied test was inadequate. Awareness and recognition of the potential impact of NDT on product quality and reliability are lacking [4]. Too, designers and analysts have low regard for NDE because of a lack of understanding of its limitations and capabilities.

The topic of NDT is an old one extending back to the ancients when the ringing sound of a sword was an indication of the blade's quality. But even modern methods date back further than one might expect. For example an industrial radiography unit was installed at the Army Ordnance Arsenal, Watertown, Massachusetts as early as 1922 [12].

Partly because NDE involves so many disciplines, the literature on the subject has been rather diffused — appearing in several different journals, conference proceedings contractor reports, and so on. Some excellent books are available on NDT techniques. Edited by McMaster [13], *The Nondestructive Testing Handbook*, is comprehensive and rich in practical details of the methods in use at the time of its publication. The book by McGonnagle [14] and the book by Schall [15] each give simple discussions of the major NDT methods. The Army pamphlet, *Quality Assurance, Guidance to Nondestructive Testing Techniques* [16] contains excellent elementary explanations and descriptions of the more widely-used NDT methods.

A couple of summary reports on NDT were prepared by NASA through contractors. The Southwest Research Institute undertook a comprehensive review of NDE resulting in the 1973 report *Nondestructive Testing — A Survey* [17]. A technology survey was conducted by Martin Marietta Corporation, resulting in the 1975 report, *NDE — An Effective Approach to Improved Reliability and Safety — A Technology Survey* [18]. This report contains the interpreted abstracts of about 100 key documents related to NDE.

A series of training handbooks or manuals were prepared by NASA through a contractor on each of the five most widely used NDT methods: liquid penetrants, magnetic particles, ultrasonics, eddy currents, and radiography. This series constitutes 18 volumes which are available from the American Society for Nondestructive Testing (ASNT). The series contains a handbook for each method together with one or more programmed manuals. These books, listed in Reference [18] provide training on principles, apparatus, and procedure for each of the five methods.

Nondestructive evaluation was the topic of a study of the National Materials Advisory Board (NMAB) in 1969 [19]. Among the conclusions of that study was “. . . it is necessary that nondestructive evaluation be deliberately considered for incorporation into every phase of the design-production-service cycle.” It was indicated that the term nondestructive evaluation was more appropriate than nondestructive testing or inspection for the reasons that the discipline requires evaluation of tests and inspection and “testing” and “inspection” did not properly connote the theoretical aspects of the field. In 1977 NDE was again the topic of a study by NMAB [4]. That study emphasized the economic and management aspects of NDE in aerospace manufacturing.

An international concern for adequate NDE of aerospace structures is reflected by meetings of the NATO Advisory Group for Aerospace Research and Development (AGARD) in 1975 and 1978. Proceedings of these meetings, known as AGARDograph 201 [20] and AGARD 234 [21], respectively, provide a rich source of NDE problems related to aerospace equipment.

ASTM committee E-7 on Nondestructive Testing was formed in 1938. As of 1975 Forty-seven nondestructive testing standards had been prepared and appeared in the Annual Book of ASTM standards. In addition a number of military specifications and standards have been

prepared on NDT. ASNT and ASME are involved in the preparation of standards and personnel certification procedures for nondestructive testing. The 1976 ASTM special technical publication STP 624 *Nondestructive Testing Standards — A Review* [22] contains the latest information on present standards.

The quantitative capabilities and limitations of NDE were the emphasis of a materials/design forum held by the American Society of Metals 1974. The proceedings of this meeting entitled *Prevention of Structural Failure, The Role of Quantitative Nondestructive Evaluation* [23] contains many papers discussing flaw detection capabilities and limitations.

As an up-to-date source of information, ASNT publishes a monthly journal *Materials Evaluation*, which publishes timely articles on development of new NDE techniques and novel applications of NDE.

C. Relationship of NDE to Fracture Mechanics

NDE is used during fabrication to control material quality and to locate defects caused by fabrication processes. NDE is used during in-service to find in-service induced flaws such as fatigue cracks, corrosion, etc. During design, fracture mechanics is used to calculate critical flaw sizes for all fracture critical locations in the structure. Initial flaw sizes are assumed in accordance with, for example, military specifications 83444 [24] which specify initial flaw dimensions; crack growth notes are used to determine the time-to-failure of flaws. This places a burden then on NDE to locate all such flaws before they grow to critical length. It is important that the critical flaw be of sufficient size to be readily detected by the planned NDT method. This means that the NDE specialist and fracture mechanics specialist must work together so as to plan an inspection procedure suitable for locating a given flaw at a given location. The planning for the in-service NDE must be an integral part of the design. Considerations must be given to the confidence for which a given flaw can be detected at a given location. Access to the component must be provided by removable access plates, etc.

The use of fracture mechanics together with the increased use of high strength flaw sensitive materials to meet aerospace requirements has placed an increased burden on NDE to detect ever smaller and smaller flaws — and not only to detect flaws but to quantify the ability of the NDT process to find a given flaw. This topic of quantification — quantitative NDE — is a fairly recent one, brought about by the demands of fracture mechanics requirements.

A lack of appreciation or understanding of the limits of NDE in quantifying flaws has been a hindrance in structural reliability. The crash of an F-111A in 1969 due to a crack in the D6ac wing pivot fitting [25,26] is a good example. Forney [26] indicates "... that the fracture condition existed basically because of the existence of smaller critical crack sizes and more rapid subcritical crack growth properties of the component steel than realized, as well as a *general overconfidence in NDI capabilities and practices under the circumstances*" [emphasis added]. Another example of unrealistic expectations of NDI performance was related by Kent [27]. It was necessary to inspect some 4000 fastener holes in a transport airplane every 9 months to detect a crack in the material approaching a length of 1 mm under a fastener head. The inspector was required to work in the open air. When inspecting 2000 of the fastener holes on the lower wing surface the NDI inspector had to hold the probe above his head while attempting to read an instrument setting at his feet. According to Kent, the inspector had about a 15 percent chance of finding a significant crack during the two day operation.

Such examples indicate a strong need for quantification of NDT methods — a need to know the smallest flaw which can be detected with a high probability at a given confidence level under actual inspection conditions. This need has become widely recognized. For example Military Specification MIL-A-83444, "Airplane Damage Tolerance Requirements" [24] now set forth the damage tolerance requirements of military aircraft. These include the assumption that a structure will contain small flaws, whose assumed dimensions are specified. These must be taken into account in the structural design and in the selection of NDI techniques and inspection intervals. Thus the NDI becomes an integral part of the design. A technical applications manual is prepared for the given airplane during the design of both military and civil commercial airplanes. This manual specifies in detail all the NDI procedures required by the maintenance schedule.

II. THE PRACTICE OF NONDESTRUCTIVE EVALUATION

Fracture mechanics and modern NDE have been primarily developed within the aerospace industry, although their present use extends far beyond that into the nuclear power industry and so on. The two disciplines, fracture mechanics and NDE, are so closely related that the two together may appropriately be considered as one. Fracture mechanics assumes the existence and sizes of flaw and uses these assumptions to make structural strength and life calculations. NDI provides the means of finding and measuring assumed flaws — both flaws developed during manufacturing and flaws such as fatigue cracks and corrosion developed in-service. The combined use of fracture mechanics methodology and NDI for increased

structural reliability has been discussed by a number of researchers, including Pachman, et. al. [25,28], Hastings [29], Ehret [30], Kaplan and Reiman [31], and Davidson [32].

The best example of the application of NDI and fracture mechanics methodology is to be found in the aerospace industry. Whereas a few years ago there was only a sort of ad hoc application of NDI, certain procedures have now become standard practice, governed by precise written requirements. The present fracture control practice of the aerospace industry can serve as a good example — if not model — to follow for other industries concerned with brittle fracture problems. Because of this it is instructive to consider the aerospace application of NDE in some depth.

A. Damage Tolerance Requirements

The damage tolerance requirements of military airplanes are controlled by the military specification MIL-A-83444 “Airplane Damage Tolerance Requirements” [24], and military standard MIL-STD-1530, “Aircraft Structural Integrity Program Airplane Requirements” [6]. These were recently discussed by Forney [26]. The primary feature of these documents is the requirement that the designer assumes that an airplane inherently contains crack-like defects at delivery. These cracks must be taken into account in the initial design and in setting the NDI program, including method of inspection, interval of inspection, parts to be inspected, etc. Military standard MIL-I-6870C, “Inspection Program Requirements, Nondestructive Testing: For Aircraft and Missile Materials and Parts” [33] requires that a review of the NDT plan be an integral part of the design review.

MIL-A-83444 allows a choice between a fail safe structure where crack stoppers or a multiply load path is provided and slow crack growth structures where crack growth is depressed so that critical crack length is not reached during the inspection interval. The initial flaw assumptions of 83444 are summarized in *Figure 1*. Flaw shapes and sizes are given for hole locations and other locations. At a hole location for slow crack growth it is seen that a corner flaw with a 0.05 inch radius is assumed if the material is thicker than 0.05 inch. If the material thickness is less than 0.05 inch then a through-crack of length 0.05 inch is assumed. For fail safe the crack is a 0.02 inch corner flaw for thickness greater than 0.02 inch and a 0.02 inch through flaw if thickness is less than 0.02 inch. As the table shows, a similar situation exists for flaws at locations other than at holes. The specified initial flaw sizes presume the inspection of 100 percent of all fracture critical regions of all structural components. Smaller initial flaws than those listed in *Figure 1* may be assumed but if so an NDT demonstration program must be performed to verify that all flaws equal to or greater than the design flaw size have at least a 90 percent probability of detection with a 95 percent confidence level.

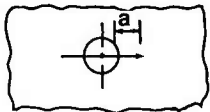
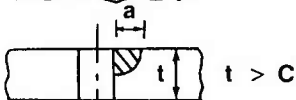
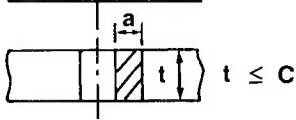
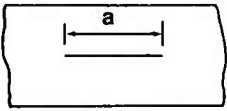
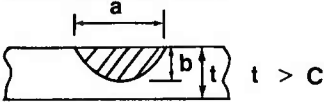
		SLOW CRACK GROWTH	FAIL SAFE	
AT HOLE LOCATION		a	0.05	0.02
	 	c	0.05	0.02
AT LOCATIONS OTHER THAN HOLES		a	0.250	0.10
		b	0.125	0.050
		c	0.125	0.050

Figure 1. Initial flaw assumptions [24].

The ease or difficulty of finding a given flaw depends upon the flaw's access and is referred to as the flaw's degree of inspectability. Some flaws may become immediately evident in-flight in which case the flaw is referred to as in-flight evident inspectable. Other flaws may be obvious to ground personnel in which case the flaw is ground-evident inspectable. The less inspectable a component (i.e., the more inaccessible) the more conservative the design must be in order to insure the necessary safe period of service within the inspection interval. The degrees of inspectability and the associated required minimum periods of service specified in 83444 are shown in *Table 1*.

B. Inspection Practice

In Air Force practice, official NDI technical applications manuals are written for each system (aircraft, missile system, etc.). These manuals entitled "Nondestructive Inspection Procedures" detail all the NDI procedures required by the maintenance schedule [26]. These manuals are referred to as technical orders (TO's). The TO's are published with designations such as TO-IF-111A-36 for the F-111A aircraft, TO-IJ-57-9 for the J-57 turbojet engine [26]. The inspection for each aircraft is referred to as its "dash 36 manual," for each engine its "dash 9 manual" and so on. A "dash 6" manual entitled "Periodic Inspection Requirements" is also issued for each system. This manual details the specific timing of each inspection action [26]. A general manual, TO33B, establishes uniform procedures for conducting the five basis NDI procedures. Example pages of a "dash 36" for two planes are included in Appendix A.

TABLE 1. DEGREES OF INSPECTABILITY [24]

Degree of Inspectability	Typical Inspection Interval	Required Minimum Period of Unrepaired Service Usage
In-Flight Evident	One Flight	Return to Base
Ground Evident	One Flight	One Flight
Walkaround Visual	Ten Flights	5 x Inspection Interval
Special Visual	One Year	2 x Inspection Interval
Depot or Base Level	1/4 Lifetime	2 x Inspection Interval
Non-Inspectable	One Lifetime	Two Lifetimes

The best reported example of NDE practice for commercial aircraft is contained in a series of articles by Hagemmaier, et. al. [34,35,36] based on NDI of the DC-10 [34], development of the NDT testing manual for the DC-10 [35], and a discussion of the state-of-the-art inspection of aircraft structures [36]. Requirements for commercial aircraft in general comply with the Air Transport Association (ATA) [37]. The philosophy of the NDI for commercial airplanes is similar to that for military airplanes although slightly different — for military airplanes the NDI is more demanding [36].

During the initial stages of manufacturing an airplane preplanning is necessary, so that accessibility to a given structural component can be provided. The NDI methods and techniques are determined from considerations of expected defect location and orientation. The NDI program includes indoctrinating designers and maintenance personnel with the basic concepts of NDI. An NDT manual is prepared which specifies the NDI procedures for each fracture-critical component.

The preparation of the NDI manual for the DC-10 was a considerable undertaking requiring two years to complete. The manual contained 31 sections, 1337 pages and cost about \$300,000 [35]. Although practices vary somewhat from company to company this manual might be considered to be typical for large commercial aircraft.

The NDT manual for the DC-10 is too complex to explain in detail here but a few key ideas will serve to illustrate its preparation and use. The manual is divided into chapters by aircraft zones — a chapter for each zone of the plane. In addition the manual contains a general chapter on the main NDT methods. Specific areas of the aircraft are illustrated by drawings. The particular NDT method for each location is indicated by an NDT symbol. *Figure 2* [35] shows the NDT symbols used in the manual. Equipment is called out by the use of code letters for each piece of equipment, *Table 2*.

As an example of an NDT manual the Appendix includes pages taken from the Boeing Commercial Jet NDT manual (these pages also are included in AGARDograph 201 [20]). A scan of these will give an idea of the specificity of the NDI manuals presently in use.

C. NDE Personnel

As noted above, both specific NDT requirements and detailed NDT manuals exist for a given aircraft system. The various NDI procedures, however, must ultimately be carried out by human inspectors. These inspectors must be skilled and competent in the inspection methods. This is a basic and critical requirement: that the inspection job is carried

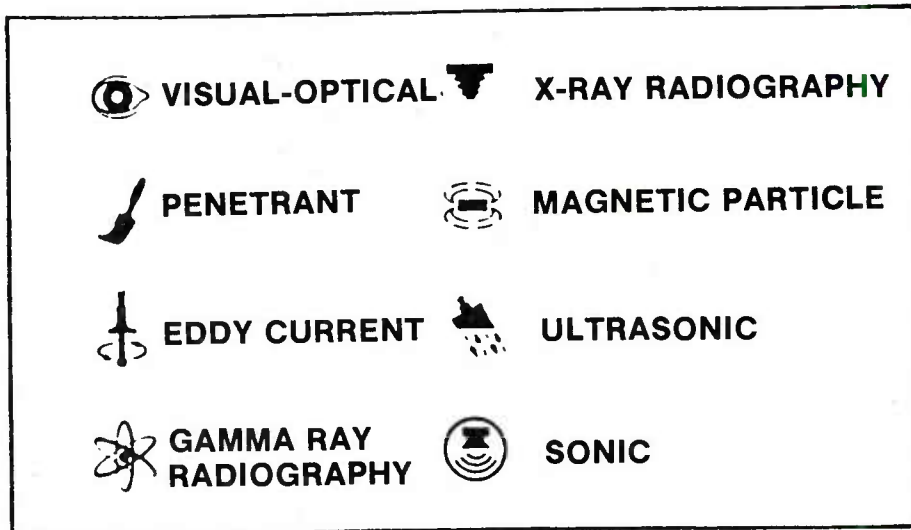


Figure 2. NDT method symbols used in the inspection manual for the DC-10 [35].

TABLE 2. CODE LETTER FOR EQUIPMENT CALLOUT USED IN THE MANUAL FOR THE DC-10 [35]

Code	Equipment or Material	Code	Equipment or Material
A	Portable X-Ray Machine	H	Eddy Current Reference Standards
B	X-Ray Film	J	Penetrant Kit
C	Portable Ultrasonic Instrument	K	Black Light
D	Ultrasonic Search Units (1) Angle Beam (2) Straight Beam (3) Surface Beam	L	Borescopes
E	Ultrasonic Reference Standards	M	Flashlight
F	Portable Eddy Current Instrument	N	Inspection Mirror
G	Eddy Current Probes	P	Magnifying Glass
		Q	Magnetic Particle
		R	Sonic

out by well-qualified personnel — qualified by virtue of their education, training and experience; and not only qualified but certified as such. Toward this goal a set of recommended practices [38] for personnel qualification and certification was published by ASNT in 1966, later revised in 1975. The revisions were recently discussed by Berry [39]. This document [38], known as ASNT Recommended Practice SNT-TC-1A, establishes three levels of qualification denoted by Levels I, II, and III. The scope of operation as well as the experience requirements for each level are specified. These were summarized succinctly by Hovland [40].

In general, an NDT Level I performs specific tests within an NDT method and under the direction of a Level II or Level III. A Level II, in addition to directing the activities of an NDT Level I, must be able to set up and calibrate equipment and be familiar with equipment capabilities and limitations. A Level II must be able to apply suitable inspection techniques, interpret indications and evaluate them in terms of applicable codes and specifications. An NDT Level III must be capable of establishing techniques, interpreting specifications and codes, designating the particular test method and techniques to be used, and interpreting test results. He must be capable of evaluating results in terms of existing codes or specifications or assist in establishing test criteria when none exists.

In addition recommended training courses were developed for each NDT method, an examination or test system whereby applicants could demonstrate their qualifications was prepared, and recommendations were made for the administration of NDT personnel certification. It was made the responsibility of the employer of the NDT inspector to establish written procedures concerning all phases of certification. The Level III individual is responsible for conducting examinations of NDT Levels I and II personnel. The philosophy of the original ASNT document was that the Level III is an administrative person representing management and was therefore designated by management. The employer, however, was to document the education, training and experience of the Level III individual. In this area some apparent misuse of Level III certification occurred by employers appointing Level III individuals without properly documenting their training, etc. In response to criticism of this particular practice, SNT-TC-1A was revised in 1975 so that ASNT could certify Level III (only Level III, not Levels I or II) personnel on a voluntary basis. Thus the Level III individual can now be certified by either ASNT or the employer.

The point to be made is that due to SNT-TC-1A a uniform procedure does exist for training and certifying NDT personnel. Non-destructive inspection is not an ad hoc procedure haphazardly carried out by technicians untrained in the applicable techniques. Moreover application of SNT-TC-1A is fairly general. It has been voluntarily adopted by many manufacturers and suppliers and has been incorporated into other standards such as the

ASME Boiler and Pressure Vessel Code. Military standard MIL-STD-410D “Nondestructive Testing Personnel Qualification and Certification” [41] similarly provides for the certification of military inspectors. Still, the human element in the NDI process is of great concern and it will be dealt with further in Section 5.

III. THE BASIC NDE METHODS

As a casual scan of Vary [42] shows, there are a great many methods of inspections. Aside from visual inspection, however, there are five commonly used methods of NDI:

- Liquid penetrants.
- Magnetic particle.
- Eddy current.
- Ultrasonics.
- Radiography.

The following includes a brief introduction to each of these methods. The explanations are elementary and brief, meant only to provide a basic introduction to a beginning student or someone such as a designer or stress analyst wishing to gain a basic understanding of how the methods work. *Table 3* from [43] shows a summary of the five methods.

A. Liquid Penetrants

In the penetrant test a low viscosity fluid is applied to the test piece. After time has been allowed for the penetrant to seep into the cracks the excess penetrant is washed from the surface and a developer is applied. The penetrant then seeps out of the cracks into the developer and provides a visible indication of the cracks. This method makes invisible cracks apparent to the eye.

Many penetrants are commercially available. Basically there are two types: dye penetrants and fluorescent penetrants. The fluorescent penetrants are viewed under a black or ultraviolet light. The dye penetrants contain a red dye designed to give a high color contrast between the penetrant and the developer. The dye penetrant requires only white light and is most useful on site where a source of ultraviolet light is not available.

TABLE 3. THE FIVE BASIC NDI METHODS [43]

	Liquid Penetrant Testing	Magnetic Particle Testing	Radiographic Testing	Eddy Current Testing	Ultrasonic Testing
Definition	Uses a penetrating liquid to seep into a surface discontinuity thus providing a visible indication.	Uses electrical current to create a magnetic field in a specimen while magnetic particles indicate where the field is broken by a discontinuity.	Uses electromagnetic rays (x-rays and gamma rays) to penetrate material, recording on film discontinuities in the material.	Uses an electrical current in a coil to induce eddy currents into a specimen. Indicators reveal discontinuities that alter the path of the induced currents.	Uses ultrasound to penetrate material, indicating discontinuities on an oscilloscope screen.
Uses	Used on metal, glass, ceramics to locate surface discontinuities. Simple to use and does not require elaborate equipment.	Used on metal which can be magnetized (ferromagnetic) to detect surface or subsurface discontinuities. Simple to use and equipment is portable for field testing.	Used on any metal stock or articles, as well as a variety of other materials to detect (and record on film) surface or subsurface discontinuities, film provides a permanent record of the discontinuities.	Used on metals to detect surface and subsurface discontinuities, hardness, and thickness, plating coating (non-metallic), and sheet thickness measurements.	Used on metal, ceramics, plastics, etc., to detect surface and subsurface discontinuities. When automated, indications are recorded on paper, providing a permanent record. Also measures material thickness.
Limitations	Does not detect discontinuities beneath the surface of a specimen.	Cannot be used on metal which cannot be magnetized. Requires electrical power.	High initial cost. Requires electrical power source. Potential safety hazard to personnel.	Inspection depth limited to less than one inch. Does not give physical shape of discontinuities.	Moderately high initial cost. Requires electrical power source. Interpretation of test results requires highly-trained personnel.

The steps in performing a penetrant inspection are [14]:

- Clean the surface.
- Apply the penetrant.
- Remove the excess penetrant from the surface.
- Apply the developer.
- Inspect and interpret the indication.

It is essential that the surface be clean and free of oil, paint, dirt, scale, etc. — anything which will clog the cracks preventing the penetrant from entering or anything which will retain the penetrant causing a false indication. The penetrant is applied to the surface by brushing, spraying or dipping. After a period of time, anywhere from 1 to 30 minutes depending upon the type of penetrant and material being inspected, the penetrant seeps into the crack, *Figure 3*. After the proper penetration time the penetrant is rinsed from the surface by a water spray

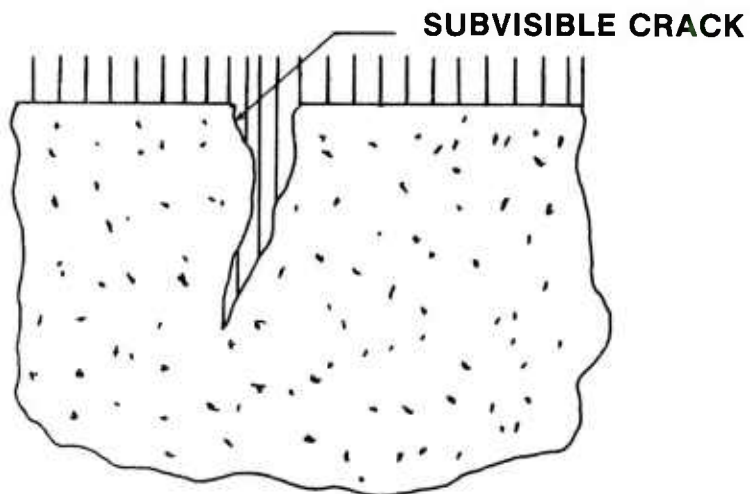


Figure 3. Penetrant seeps into the crack.

leaving the penetrant in the crack, as shown in *Figure 4*. The penetrants typically require an emulsifier to make them mix with water so that they can be readily rinsed from the surface. Many penetrants come prepared with the emulsifier already mixed in. For those that do not an additional step is required before rinsing: the emulsifier must be applied over the penetrant. The penetrant then mixes with the emulsifiers, becoming “water washable,” so that it can be rinsed away by water. This is known as post-emulsification. A penetrant without the emulsifier, the “post-emulsification” kind, seeps into the crack much more readily and is much more sensitive than the emulsified type.

After rinsing, the specimen is developed and dried. The order in which this occurs depends upon whether the developer is “dry” or “wet.” If the developer is dry the specimen must be dried first; if the developer is wet the specimen is dried after development. Drying is done with a hot air gun or by allowing to stand in the air.

The developer consists of finely ground powder such as talc. When spread over the surface, acting as a blotter, it draws the penetrant out of the crack, and this provides a visual indication of the crack as shown in *Figure 5*. The dry developer is a powder spread over the surface by any convenient means. Excess powder may need to be removed by tapping or shaking the specimen or with gentle air pressure. The wet developer consists of the fine particles suspended in water or a quick-drying carrier.

The penetrant method has a number of limitations. The method will only detect surface connected cracks; and even for surface cracks, the flaw depth cannot be determined. The method will not work on porous materials because the penetrant is absorbed into the pores, masking flaw indications. The penetrant can wash out of shallow cracks — cracks less than 0.02 to 0.04 inch causing those cracks to be missed. Other cracks, their surfaces smeared together by machining or burred together by shot peening may escape detection. In any case one must have sufficient access to the part to thoroughly clean it and to apply the penetrant; this is not always possible in the case of in-service inspection of a structure. Still penetrant inspection is very cost-effective, and it applies to one of the most serious types of flaws, the surface crack.

B. Magnetic Particle

In the use of the magnetic particle method a part to be inspected is magnetized. Magnetic particles are then distributed over the surface of the test piece. At a flaw location the magnetic field or flux is distributed. This causes the magnetic particles to be attracted to the flaw. The pattern of magnetic particles around the flaw provide a visual indication of the

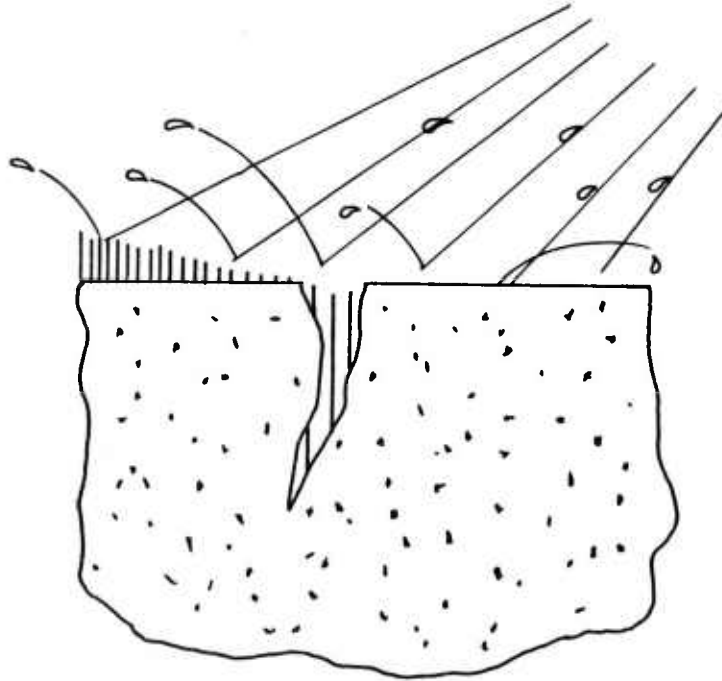


Figure 4. Rinsing the penetrant from the surface.

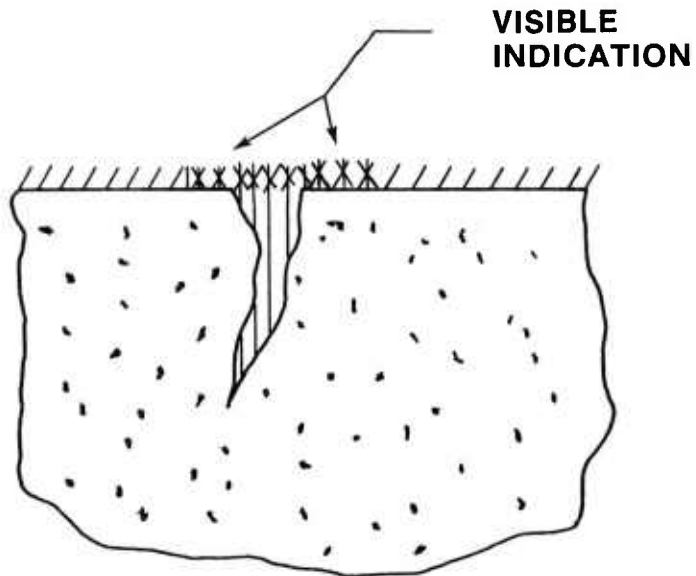


Figure 5. The developer draws the penetrant out of the crack like a blotter.

location and size of the flaw. The magnetic particles or powder can be either dry or suspended in a liquid. The particles are colored to give contrast between the specimen and powder; some particles are fluorescent for increased sensitivity, requiring viewing under ultraviolet light. The method can be used to locate either surface or subsurface flaws so long as the subsurface flaws are not too deep or too small. Surface flaws produce a sharply defined pattern consisting of a heavy powder build up tightly held. Subsurface flaws produce a less sharply defined pattern because the particles are less tightly held.

Figure 6 illustrates the magnetic flux disturbance or leakage field around two transverse flaws — one surface the other subsurface — and around a parallel flaw. It can be seen that even the subsurface flaw causes the flux lines to stray out if the plane of the flaw is substantially transverse to the magnetic field lines, whereas if the flaw plane is parallel to the field, as the third flaw in *Figure 6*, little or no disturbance of the field is produced. Hence, the method is most sensitive to flaws perpendicular to the magnetic field.

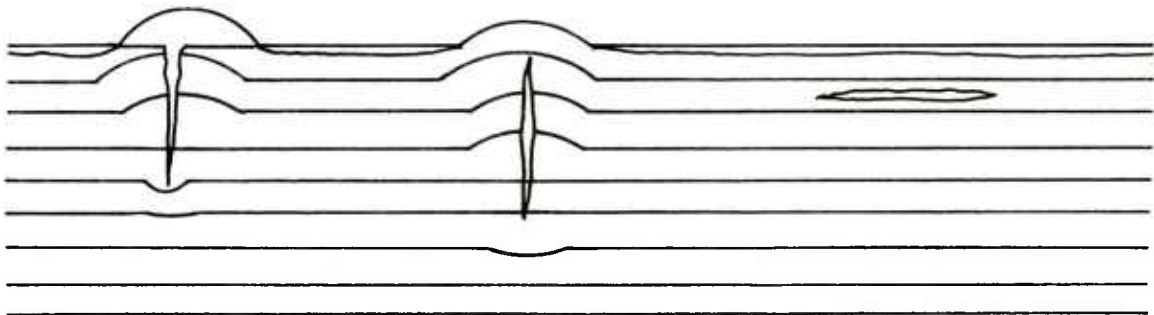


Figure 6. Leakage field around a surface flaw, subsurface flaw, and a parallel flaw.

The magnetic field may be set up by running a current through a conductor near the specimen or by running a current through the specimen itself. If a current is run through a wire or a rod, *Figure 7*, the magnetic field lines will be circular at right angles to the current direction. It can be seen that for that arrangement, longitudinal cracks and 45° cracks would be detected. Therefore this is a valid inspection scheme. *Figure 7* shows another principle. If the circular part of *Figure 7* is a wire which is wrapped in the form of a solenoid around a rod specimen, say, as shown in *Figure 8* the magnetism field lines for each loop will all combine to form longitudinal field lines in the rod. Thus the arrangement of *Figure 8* can be used to inspect for circumferential and 45° cracks as shown.

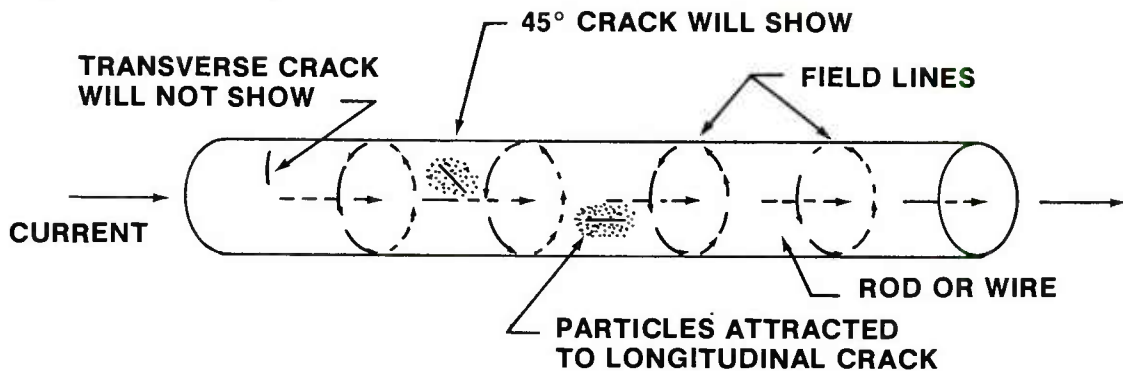


Figure 7. Circular magnetism produced by current flowing through wire rod.

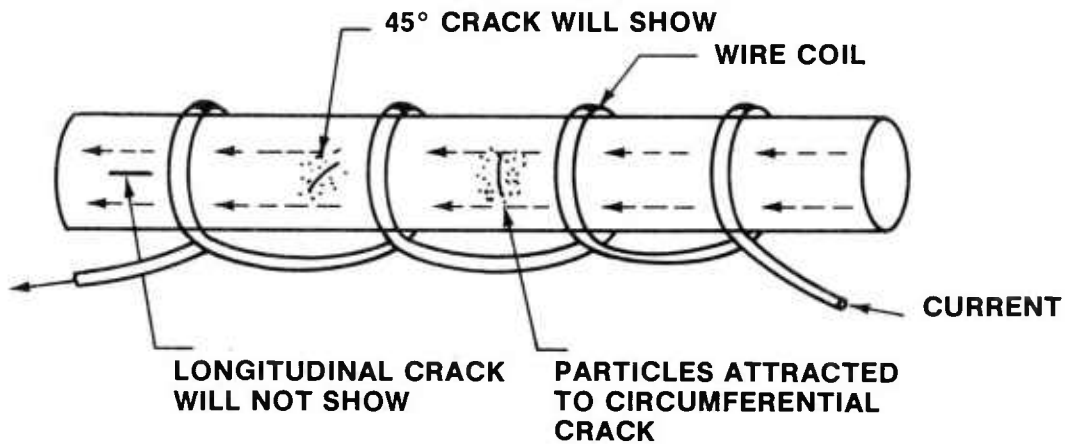


Figure 8. Longitudinal magnetism produced by a circular coil.

In many cases it is not practical to magnetize the whole specimen. *Figure 9* shows how magnetism can be introduced into a position of a test piece by the use of electrical contacts to produce a current in part of the specimen. A crack parallel to the current flow between the two prods would be detected. The prod contact area must be clean to allow current passage without arcing or burning. Additionally, low voltage is used to prevent burning the surface. The current is turned on after the prods are applied and turned off before they are removed to prevent arcing.

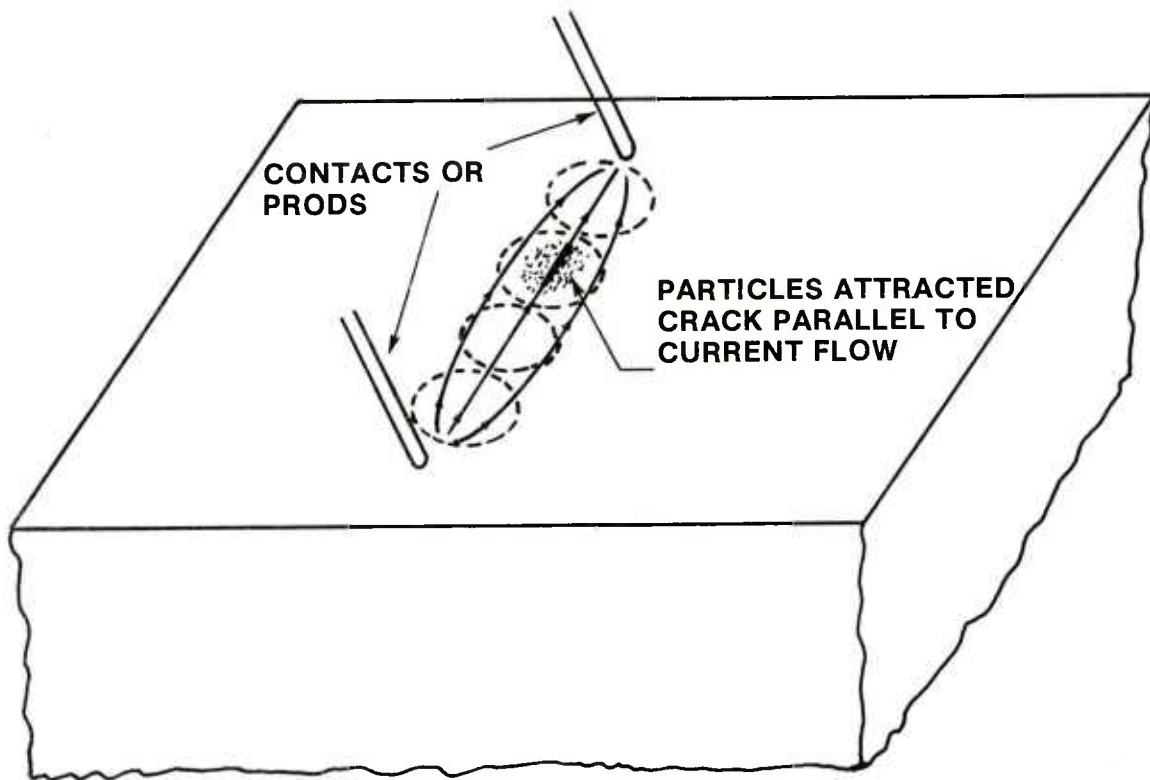


Figure 9. Magnetic field between electrical contacts.

AC or DC current may be used. The DC field penetrates deeper into the specimen than the AC field. Since the AC field is confined to the surface of the specimen AC current is best suited for finding surface flaws. The geometries shown in *Figures 7, 8, and 9* are simple shapes. However, the method can easily be applied to various shapes and sizes.

In many cases it is necessary to remove the residual magnetic field after the inspection. This may be true if the part is to be machined again to prevent the attraction of particles (swarf) or if the part is an aircraft component where residual magnetism could affect compasses and other instruments. To remove the residual magnetism the part is subjected to a reversing magnetic field which is continually decreasing.

The magnetic particle method is advantageous in many cases, however, it can only be applied to magnetic materials. The cost of the method is low and with portable equipment it can be applied almost anywhere.

C. Eddy Current Testing

Eddy current inspection is a method of detecting surface and slightly subsurface flaws in electrically conductive materials. The test article is placed near an electrical coil which carries alternating current. The electromagnetic field produced by the coil induces electrical currents in the test piece. The direction of these currents is opposed to the direction of the primary field induced by the coil. These currents travel in a closed path similar to the eddies in fluid flow; therefore they are called eddy currents. The strengths of the eddy currents depend upon many things including the frequency of the applied field, the conductivity of the test piece, and the magnitude of the applied field. The eddy current field in close proximity to the test coil influences the impedance of the test coil. A crack or inhomogeneity will distort the path of the eddy currents. Since the eddy currents influence the impedance of the test coil a crack that changes the eddy current field will also change the apparent impedance of the test coil. The change in apparent impedance of the test coil can be measured and used as an indication of a crack or inhomogeneity. This is the single coil approach. Another way is to use a second sensor that can sense the induced eddy current fields.

Figures 10 and 11 show examples of eddy current fields induced by test coils. The first shows the eddy currents induced in a flat plate by a coil held over it. The second shows the eddy currents induced in a cylindrical body by an encircling coil. The currents are concentrated near the surfaces of the body exhibiting a skin effect. The current decays exponentially with distance from the surface. The penetration distance δ to which the current is $1/e$ (about 37%) times its surface value is given by:

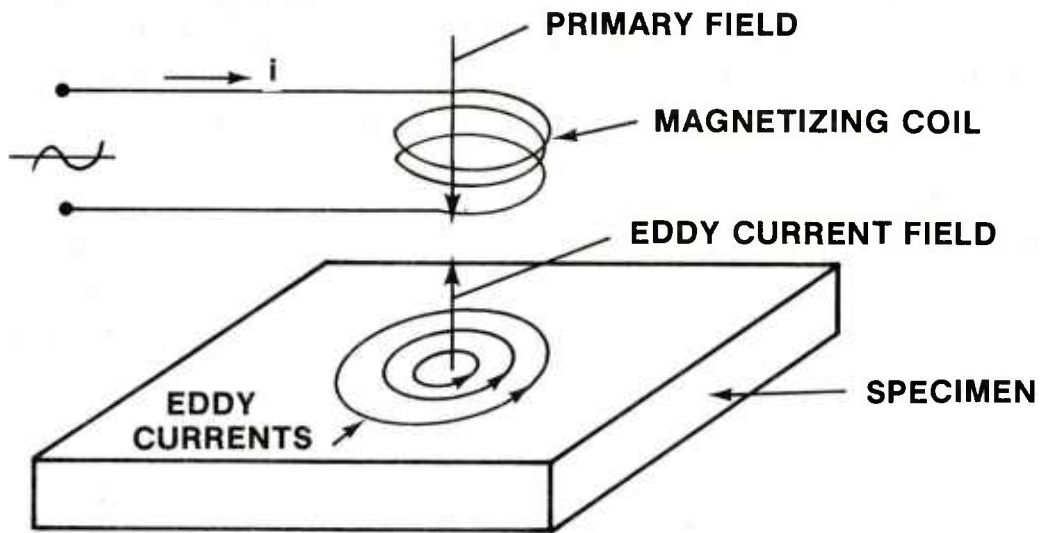


Figure 10. Eddy current generated in a flat plate by a magnetic field.

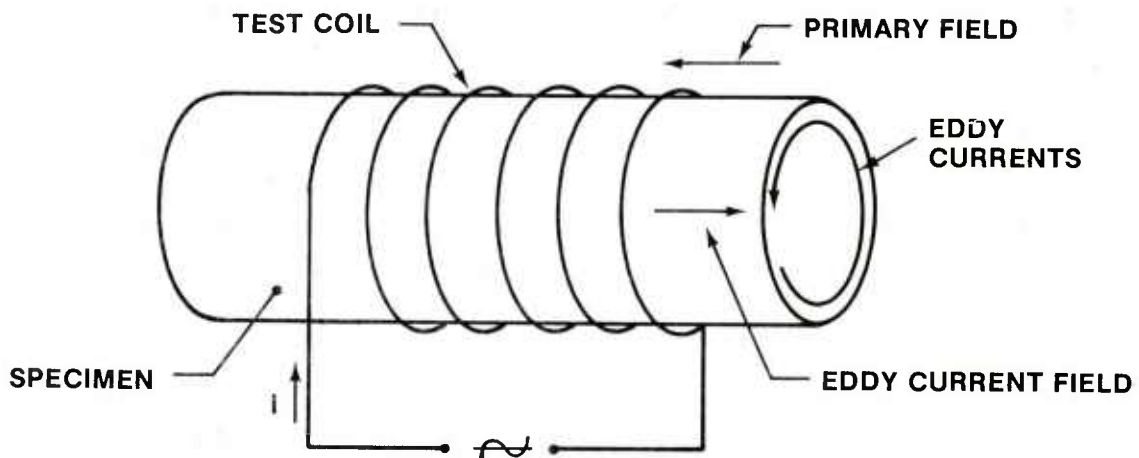


Figure 11. Eddy currents produced in a cylindrical body by an encircling coil.

$$\delta = \frac{1}{(2\pi f\mu\sigma)^{1/2}} \quad (1)$$

where

- δ = depth of penetration, meters
- f = frequency, Hertz ($\omega=2\pi f$)
- μ = magnetic permeability
- σ = volume electrical conductivity

Equation (1) only applies to flat surfaces and uniform fields. Consequently it should be used only as a guide, not accounting for test coil geometry or curved specimen surfaces. As an example the depth of penetration for a number of materials is illustrated in *Figure 12*, which shows that in order to obtain significant penetration for subsurface flaws low frequencies are needed.

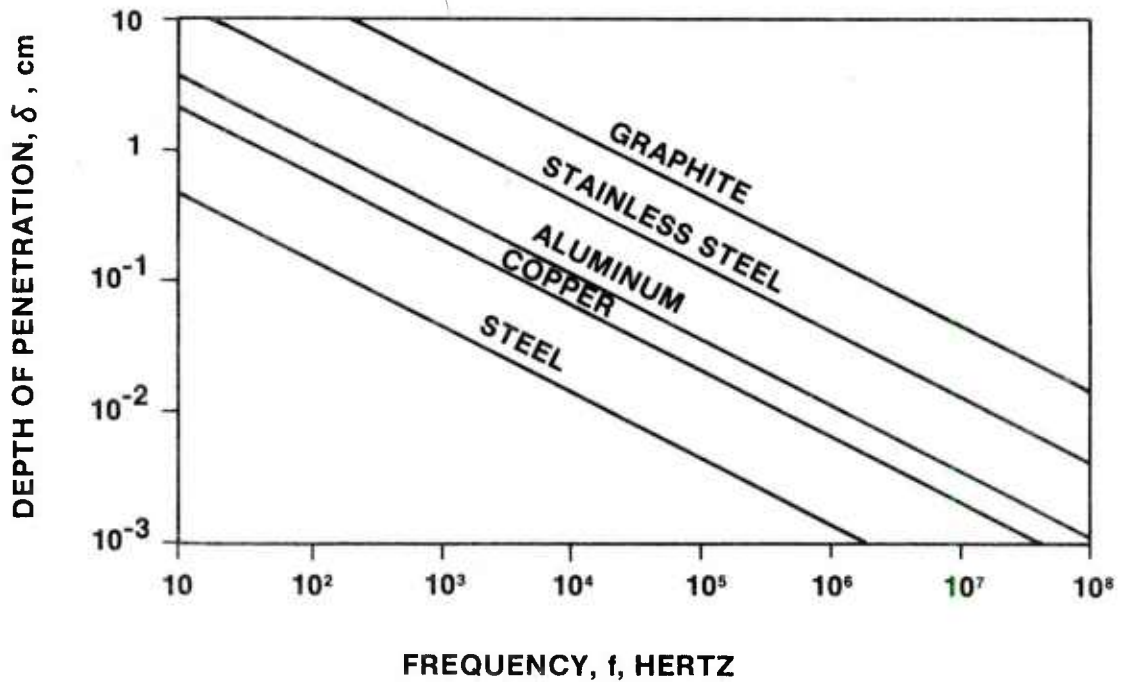


Figure 12. Depth of penetration in plane conductors [17].

An apparent change occurs in the impedance of a test coil when it is placed near a conducting test specimen. This change can best be illustrated by means of an impedance diagram. Such a diagram for a long nonferromagnetic cylindrical rod encircled by a solenoidal coil is shown in *Figure 13*. The impedance is given as two components, a reactive component X and a resistive component R , each one normalized by (ωL_0) , the inductance without a specimen. The parameter $g = \sqrt{\omega\sigma\mu}$ incorporates the effects of frequency, conductivity and permeability. It is the reciprocal of the skin depth δ . Curves are shown for several values of the filling ratio, ν , where $\nu = a^2/b^2$ and a/b is the ratio of the cylindrical specimen diameter to the coil diameter. The dashed curves show how the impedance changes when specimens of the same conductivity but different diameters are placed in the coil. When the specimen conductivity, as measured by g , increases the reactive component decreases while the resistivity component increases to a maximum and then decreases. *Figure 14* shows the impedance diagram for a ferromagnetic cylinder. Curves are given for various values of

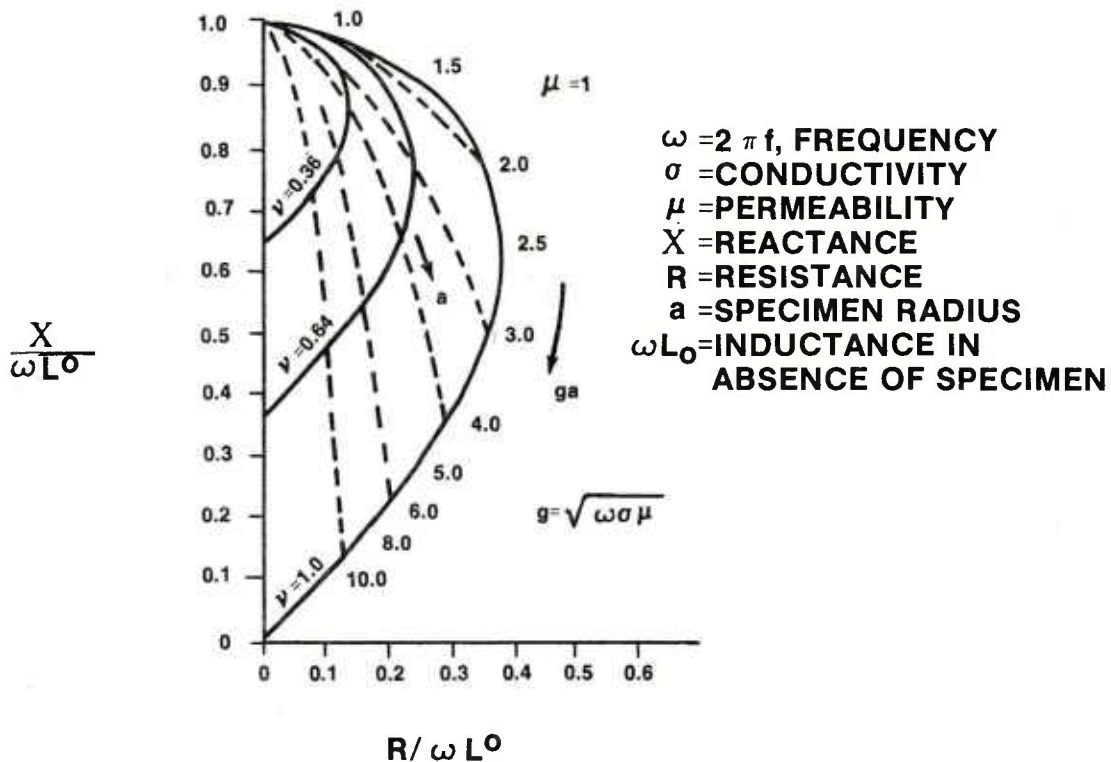


Figure 13. Coil impedance for variations in test frequency or conductivity and specimen radius for a nonferromagnetic cylinder encircled by a test coil [17].

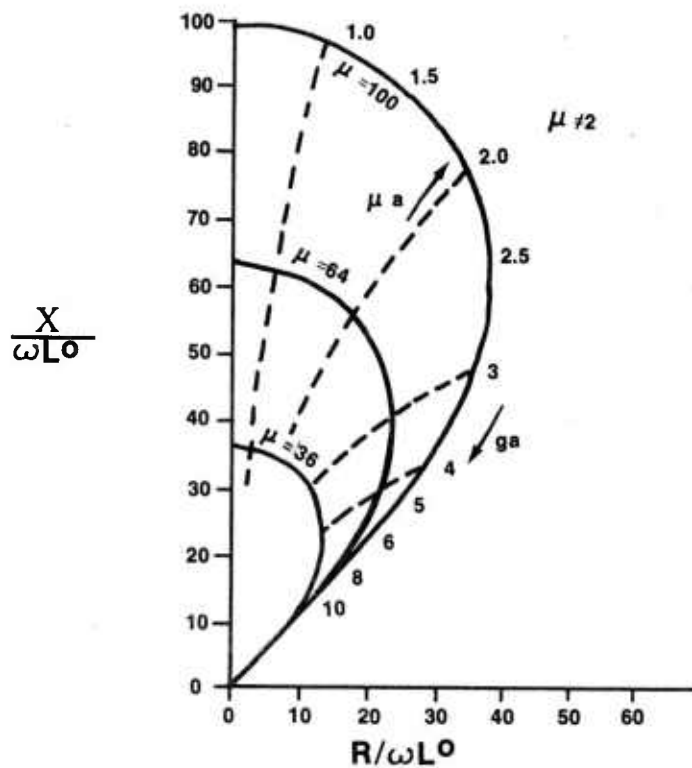


Figure 14. Coil impedance for variations in test frequency or conductivity and permeability or radius for a ferromagnetic cylinder encircled by a test coil [17].

specimen permeability μ , and the dashed curves show the effect of increasing the specimen diameter. The point to be made about *Figures 13 and 14* is that a change in either specimen dimension (diameter) or in conductivity or permeability will cause an impedance change — a change which can be measured by the proper circuits. Whether the change is produced by the difference in coil-specimen diameter (distance between coil and specimen is called lift-off) or a change in permeability may be difficult to determine. It is extremely difficult to predict analytically the phase plane effect of cracks; their effect is best determined empirically. The operator must know the phase plane signature of various flaws as the probe passes over them.

Various electrical circuits are used to sense the impedance changes produced in either the primary test coil or a second independent coil. The test coil can be included in a bridge circuit which contains a reference coil. The bridge is then balanced to a null position. A flaw passing underneath the test coil then produces a bridge imbalance and a measurable voltage

output. In other cases a filter arrangement is employed for which a voltage output can initially be tuned to zero for the test frequency. A flaw-induced impedance change then causes a voltage output.

Two identical secondary coils can be employed as shown in *Figure 15*. The primary coil produces the eddy currents. The eddy currents in turn generate a field which is sensed by the secondary coils but since the two secondary coils are identical no voltage output occurs. When a flaw appears under one of the secondary hoops then symmetry is lost and a voltage output, V_{out} , then occurs.

In another technique an independent device known as a Hall-effect device is inserted between the test coil and the specimen. This is not discussed here; Reference [17] contains a brief explanation of the method.

Test probes have a number of configurations depending upon the intended function — whether meant to inspect the inside of a hole, the outside of a tube, or some other surface.

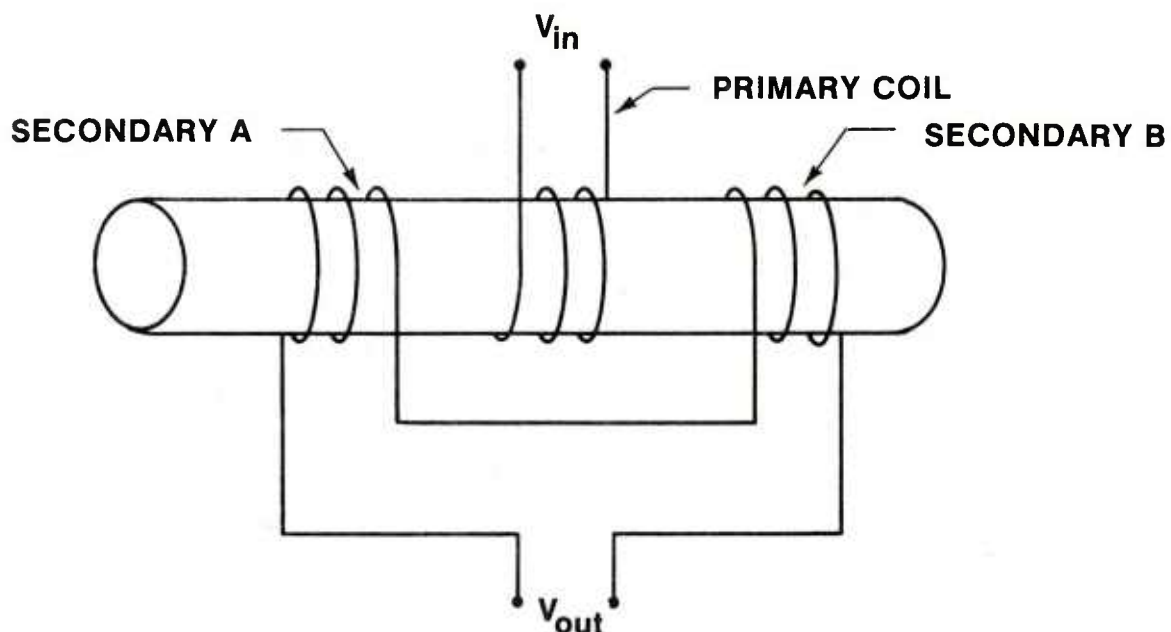


Figure 15. Two identical secondary coils in series used to detect difference in test material from A to B.

Figure 16 shows the coil arrangements for some typical probes. The gap coil *Figure 16(a)* produces a localized eddy current field and is used to detect small flaws. Encircling coils *Figure 16(b)* may be circular or otherwise shaped to fit the cross section of the test article. The probe coils *Figure 16(c)* can be held against a surface or inserted inside holes.

Coils are referred to as absolute or differential. Differential, in this case means that a test coil is compared to a second coil in series with the first. If the two coils and test conditions are identical no voltage output occurs. The second coil may be installed on a standard test specimen known to be free of defects. This arrangement compares a standard specimen to a test specimen. The two coils may be wound coaxially as the bobbin coils in *Figure 17*. In this case one section of the test specimen is compared to an adjacent section.

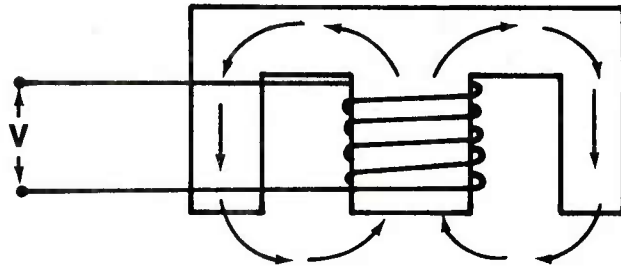
The design of a multifrequency eddy-current inspection method was recently discussed by Flora, et. al. [44]. The technique is designed to detect cracks under steel and titanium (Ti) fastener heads in airplanes.

D. Ultrasonics

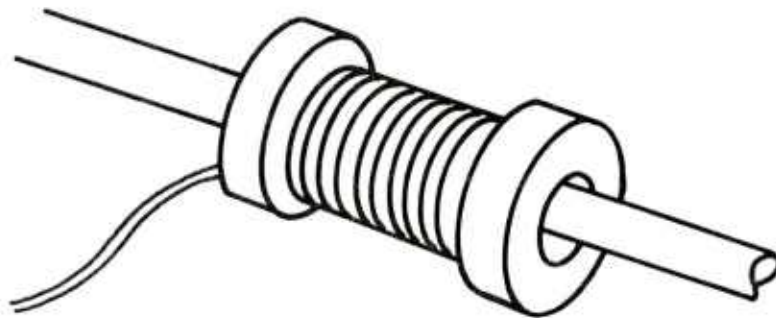
Ultrasonics refers to the use of ultrasound for flaw detection. Ultrasound is sound with a frequency greater than the human ear can hear, about 20 kHz. The frequency used in practical ultrasonics, however, is considerably higher, in the MHz, rather than the kHz, range. The idea of using sound to detect the quality of an item is an old one, as noted in Section I, dating back to the days of the ancients, when the ring of a sword blade was an indication of its quality. Practical ultrasonics was developed fairly recently, however. The principle of operation is simple. It relies upon the reflection of a generated sound wave from free surfaces and flaw boundaries.

Ultrasound can be caused to travel long distances — as much as several feet — in specimens without appreciable attenuation. Because of this, ultrasonics is the best method for detecting subsurface flaws deeply embedded in thick sections. Radiography, in inspecting for subsurface flaws, is limited to thicknesses of only a few inches, but ultrasound can continue to propagate through several feet. Moreover a very tight crack with only a 0.00005 inch wide opening will be sufficient to reflect the sound waves and provide an indication. Moreover, the inspection can be carried out from one side of the specimen, an obvious advantage, especially for in-service components.

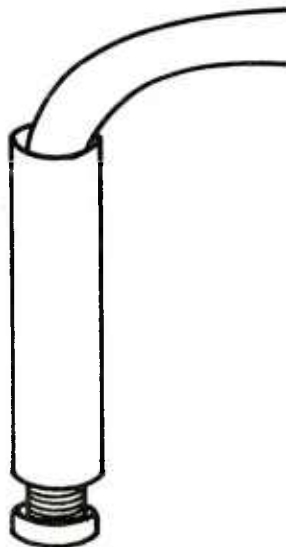
The ultrasound waves are generated by piezoelectric crystals. These are crystals which change their dimensions when a voltage is imposed on them. If an alternating voltage is



(a) Gap coil.

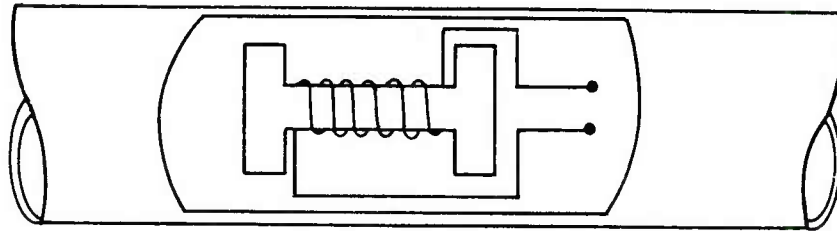


(b) Encircling coil.

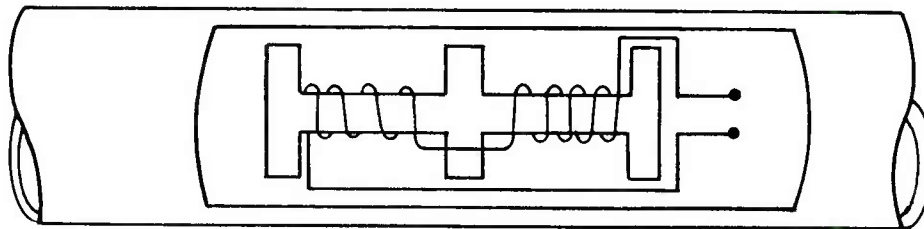


(c) Hand-held probe coil.

Figure 16. Types of coils.



(a) *Absolute bobbin coil.*



(b) *Differential bobbin coil.*

Figure 17. Example of absolute (a) and differential (b) bobbin coil.

applied to two of the crystal faces the crystal will expand and contract in step with the voltage. If the crystal is held in contact with a specimen while the alternating voltage of a selected frequency is applied then sound waves of the same frequency will be driven into the specimen. Conversely, the piezoelectric crystals have the property that if mechanical tension or compression is applied to them then a voltage proportional to the pressure will be produced. Thus when a sound wave, a propagation of alternating tension and compression — impinges on the crystal an alternating voltage will be produced. This makes it possible for a piezoelectric crystal to receive sound waves, as well as to transmit them.

Quartz crystals have been the most commonly used crystals for ultrasonics. The ceramic material, barium titanate, and the material lithium sulfate are also commonly used in transducers. Typical frequencies for ultrasonics are, say, $2\frac{1}{2}$ MHz or 5 MHz. The corresponding wavelengths in steel for these two frequencies are on the order of 0.086 inch and .043 inch, respectively.

The high-frequency sound will not travel in air; even a small air gap between the piezoelectric crystal and the specimen would prevent the passage of waves from the crystal to the specimen and vice versa. A coupling fluid such as water, glycerine and water, or oil is used to solve this problem. This is done two ways: by simply wetting a spot on the specimen between the probe and specimen or by immersing the whole specimen and probe in a tank of fluid and carrying out the inspection while the specimen remains immersed.

The pulse-echo and through-transmission techniques are both used in inspection. The two methods are indicated in *Figure 18*. In the pulse-echo method the same crystal is used to both transmit and receive the wave. This method requires access to only one side of the specimen and is used more than the transmission method. The transmission method (pitch-catch method) requires two probes, one to transmit (pitch) on one side of the specimen and one to receive (catch) on the other side as shown in *Figure 18*.

In inspecting a specimen, three scanning modes are used, denoted by A-scan, B-scan, and C-scan. In the A-scan method (*Figure 19*) the vertical axis of a cathode-ray tube (CRT) records the initial sound pulse as well as the pulse reflected from a defect or back surface of the specimen. The horizontal axis records the time from the initial pulse to the arrival of the echoes from the various free surfaces. Since the sound travels at a definite speed in the specimen the distance along the horizontal axis of the CRT also represents distance. Thus, the distance on the CRT from the initial pulse to the pulse for the specimen backside represents the thickness of the specimen and the distance on the CRT from the initial pulse to the defect pulse indicates the location of the defect in the specimen.

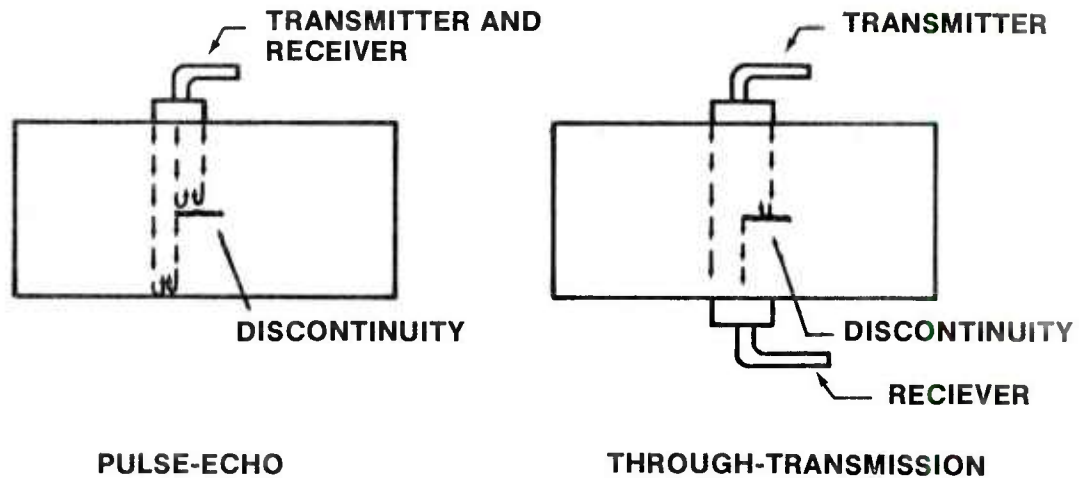
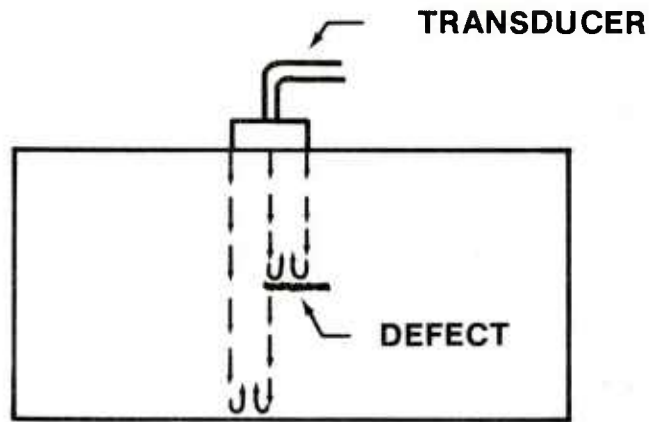


Figure 18. The pulse-echo and through-transmission methods.

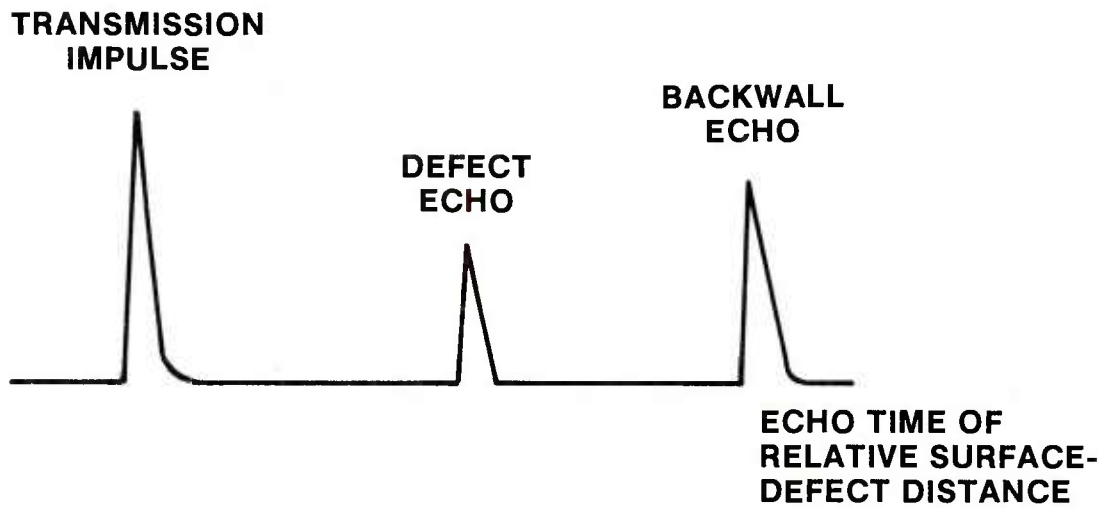
In the B-scan method *Figure 20* the vertical CRT axis represents the distance (time) from the inspection surface to the reflecting surfaces. The reception of the pulse itself is registered as a mark on the CRT and the horizontal sweep of the CRT is adjusted to move in step with the scanning motion of the probe. Thus a cross section view of the specimen, showing the front and back surfaces, and location of the flaws is obtained.

The C-scan is illustrated in *Figure 21*. The probe scans back and forth on the surface of the specimen. The beam of the CRT scans in step with the probe. The trigger level of the CRT is set to register brightness (or the reverse may be used) when a flaw-indicating pulse is received. Hence a plain view of the specimen showing the projected shape of the flaws is obtained. No depth information for the flaws is obtained, however.

To understand ultrasonic testing it is necessary to understand the basic behavior of stress waves in solids. A number of wave types are possible, depending upon how they are polarized and how they propagate.

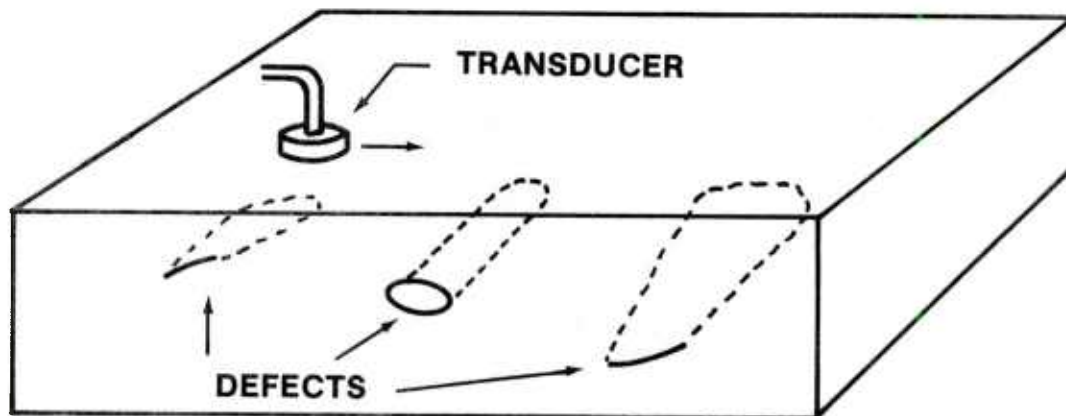


(a)

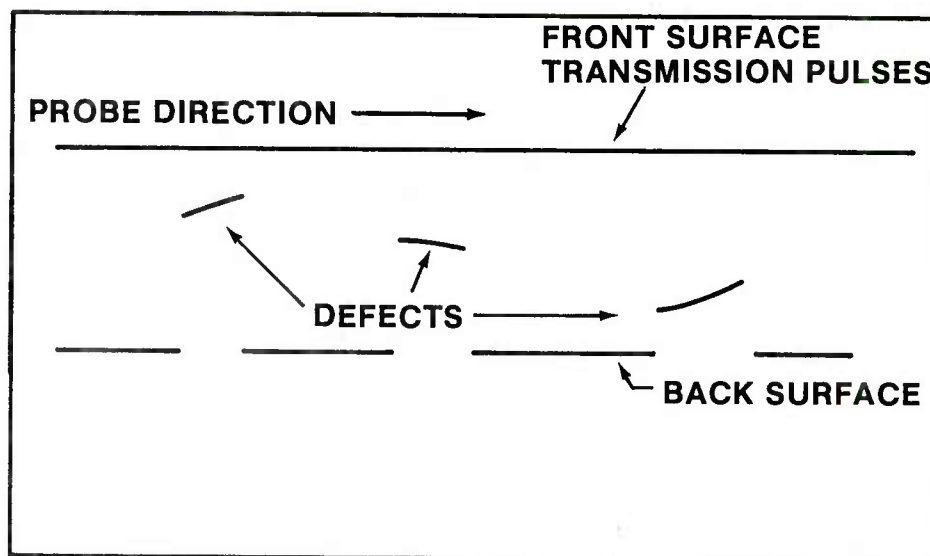


(b)

Figure 19. An example of the A-scan method.

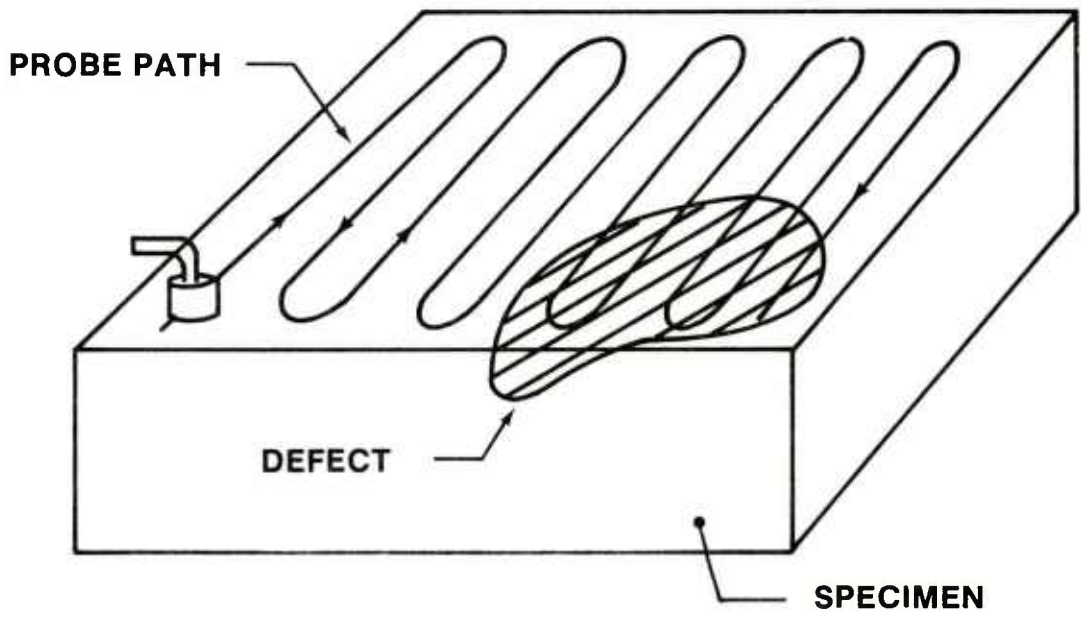


(a)

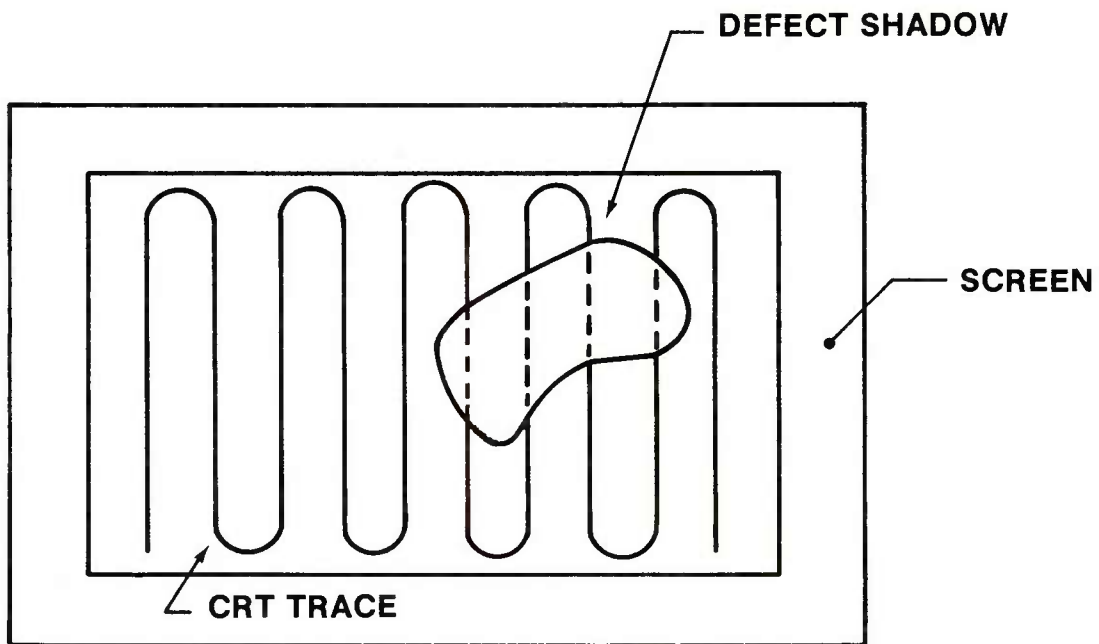


(b)

Figure 20. The B-scan method.



(a)



(b)

Figure 21. The C-scan method.

Longitudinal waves are a propagation of tension and/or compression. The material's particle motion is parallel to the direction of propagation. The wave causes no shearing stress only normal stresses. These normal stresses produce a change in volume per unit original volume referred to as dilatation. The waves are sometimes called dilatation waves. Their velocity of propagation in steel is in the neighborhood of 18,000 ft/sec. Shear waves are characterized by a propagation of shearing stresses but no normal stresses, and therefore no dilatation. The particle motion is transverse to the direction of propagation. Shear waves are slower than longitudinal waves, 0.5 to 0.7 times as fast depending upon the material. The two waves are illustrated in *Figure 22*. Rayleigh waves travel on the surface of a body in a manner analogous to water waves. The particle motion is both longitudinal and transverse. It occurs in a plane perpendicular to the surface and parallel to the direction of propagation. The Rayleigh surface wave produces a mixture of shearing and normal stresses. The velocity of the Rayleigh wave is less than for shear or longitudinal waves; for metals it is about 0.9 times the shear wave velocity. Waves which propagate in materials having thicknesses comparable to the wave length are called Lamb waves; Lamb wave particle motion is very complex and many modes are possible, some symmetric and some unsymmetric with respect to the midplane of the plate. Many other types of waves occur in solids but their importance to NDI is minor and so they are not discussed here. Most probe crystals are designed to transmit and receive longitudinal waves.

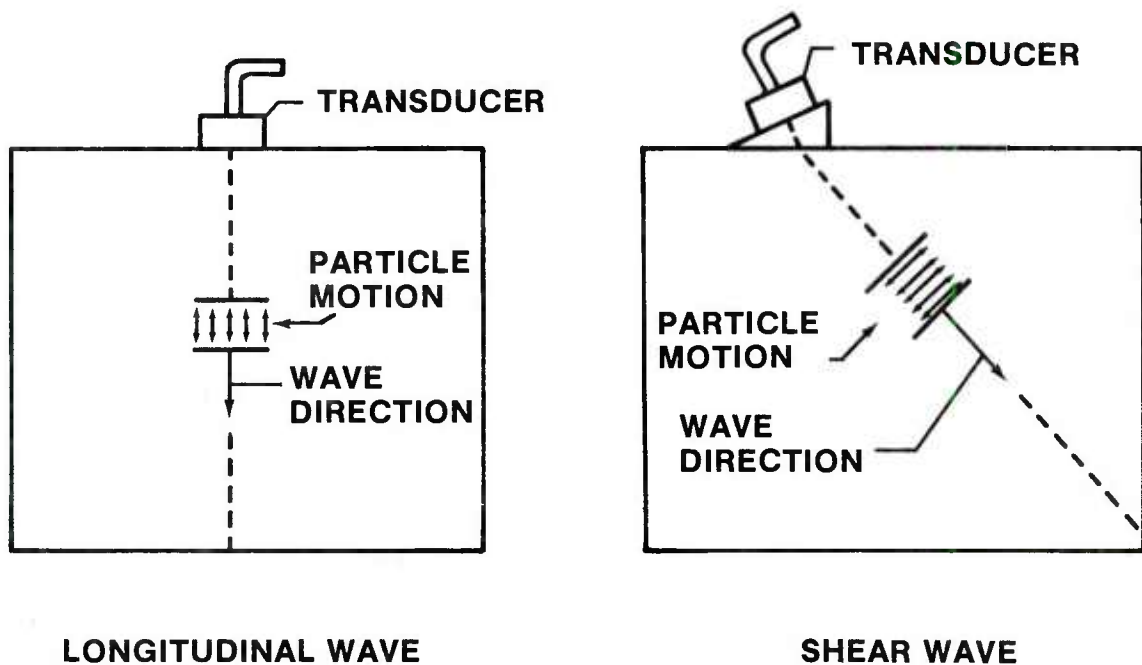


Figure 22. Longitudinal and shear waves.

The velocities of propagation of longitudinal waves, V_L , and transverse waves, V_T are given by the expressions below:

- Longitudinal:

1. Slender rod whose transverse dimensions are much less than the wavelength

$$V_L = \sqrt{\frac{E}{\rho}} \quad (2)$$

2. In an extended medium having dimensions much greater than the wavelength

$$V_L = \sqrt{\frac{E(1-\nu)}{\rho(1+\nu)(1-2\nu)}} \quad (3)$$

- Transverse:

$$V_T = \sqrt{\frac{G}{\rho}} = \sqrt{\frac{E}{\rho(1+\nu)2}} \quad (4)$$

where

- E = modulus of elasticity
- ρ = density
- ν = Poisson's ratio
- G = modulus of rigidity

Table 4 gives the longitudinal and shear wave velocities for a number of common materials.

A number of things occur when a wave strikes an interface between two materials. *Figure 23* shows in general what happens when a longitudinal wave strikes an interface:

- A longitudinal wave will be reflected.
- A longitudinal wave will be transmitted (refracted) into the second material.
- A shear wave will be both reflected and transmitted.

TABLE 4. EXAMPLE WAVE VELOCITIES IN TYPICAL MATERIALS [14]

Material	Longitudinal Wave Velocity, V_L, ips x 10⁵	Shear Wave Velocity, V_T, ips x 10⁵	Surface Wave Velocity, V_S, ips x 10⁵
Aluminum	2.46	1.22	1.10
Beryllium	5.04	3.43	3.10
Brass	1.85	0.84	0.76
Copper	1.82	0.84	0.76
Lead	0.77	0.25	0.23
Magnesium	2.27	1.20	1.08
Nickel	2.37	1.18	1.06
Stainless Steel	2.26	1.22	1.10
Tin	1.33	0.66	0.59
Tungsten	2.04	1.13	1.04
Glass	2.22	1.29	1.16
Lucite	1.05	0.43	0.39
Water	0.59

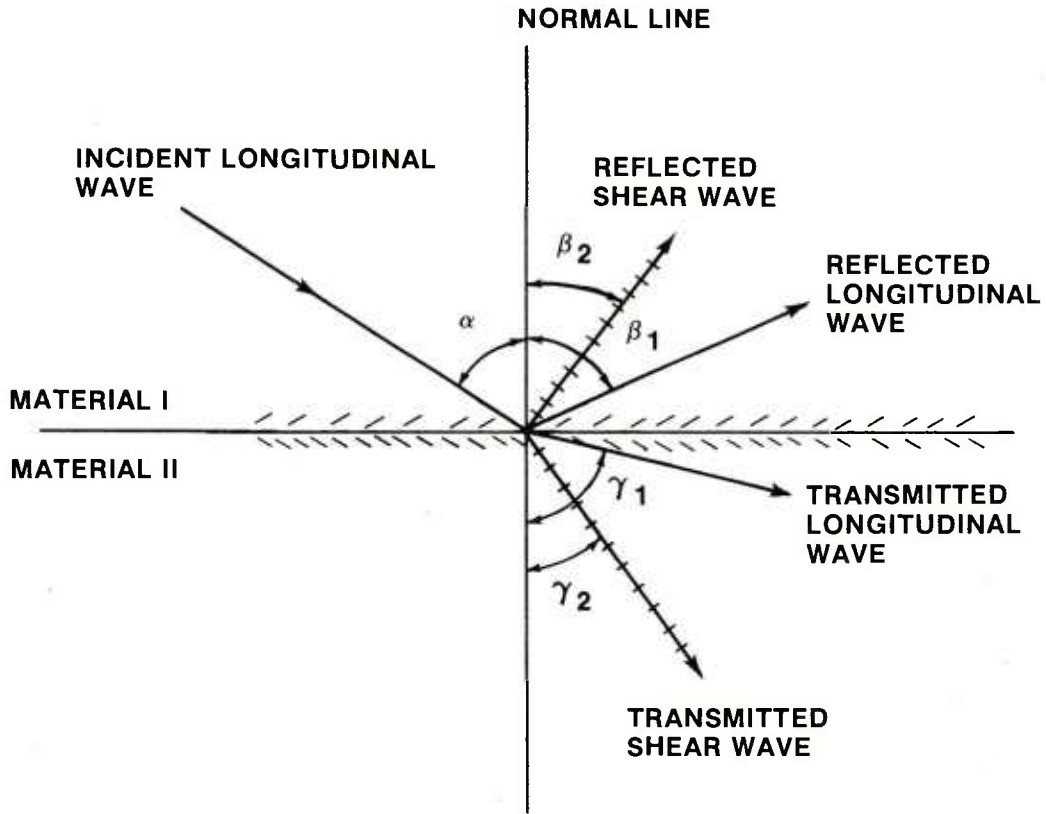


Figure 23. Incidence of longitudinal wave on interface between two materials showing the partial mode conversion.

- It can be seen that a mode conversion occurs, i.e. a longitudinal wave impinging on the interface generates or causes a shear wave.

Whether all events depicted in *Figure 23* happen or not depends upon the wave speeds in the two materials and the angle of impingement α . For example *Figure 24* shows what happens at a solid-air interface. The longitudinal wave will be reflected as both a shear wave and a longitudinal wave. However, if the angle of impingement is 90 degrees the reflection will be a longitudinal wave only. The reflection and transmission angles $\beta_1, \beta_2, \gamma_1$ and γ_2 indicated in *Figure 23* can be calculated for two materials [13,14,15]. Consider a plexiglas-steel interface shown in *Figure 25*. It can be shown [15] that if the angle α lies between 29° and 61° only a shear wave will be transmitted. This fact provides a method for generating a shear wave in a specimen. The scheme is shown in *Figure 26*. A section of plexiglass or some other suitable material cut to a wedge shape at the required angle is included between the crystal and the steel so that only a shear wave is transmitted. Such a probe is called an angle probe.

The ultrasonic beam travels in a straight line and spreads as it travels from the origin. The cone produced by the spreading can be characterized by θ the solid angle at the apex, *Figure 27*. The angle θ can be calculated by [14,15]

$$\sin \frac{\theta}{2} = 1.08 \frac{\lambda}{D} \quad (5)$$

where λ is the wavelength and D is the crystal diameter. It can be seen that as the wavelength becomes smaller (higher frequencies) or the crystal diameter larger the beam becomes more compact, and thus more directive. A 1-inch diameter crystal is more directive than a 1/2-inch diameter crystal. If the frequency were decreased until the wave length approached the crystal diameter then the energy would be transmitted out in all directions. *Figure 27* shows the beam spread in steel for various frequencies and crystal sizes. Equation (5) only applies in the far zone which begins at a certain minimum distance ℓ_0 from the origin. The length of the so-called near zone depends upon the wavelength (frequency) and crystal diameter. Namely [15].

$$\ell_0 = 0.25 (D^2/\lambda) \quad (6)$$

Beyond the distance ℓ_0 the beam intensity decreases inversely as the square of the distance, r , from the origin; that is, intensity is proportional to $1/r^2$.

Many applications examples are given by several publications [13,14,15,16] where only a few are illustrated here to give the general idea. *Figure 28* shows some typical contact test

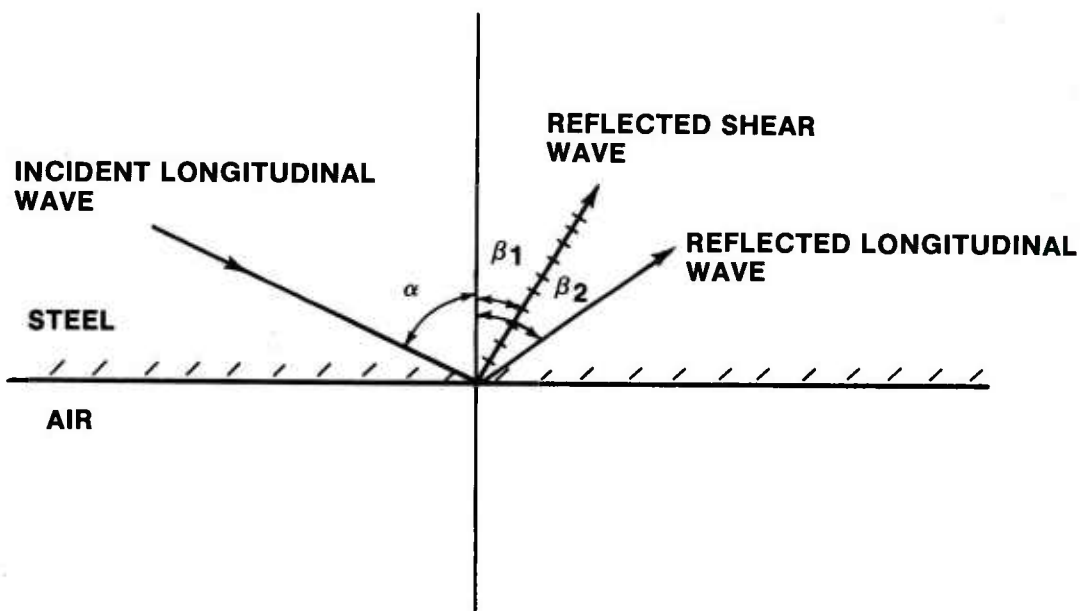


Figure 24. Mode conversion and reflection at a steel — air interface.

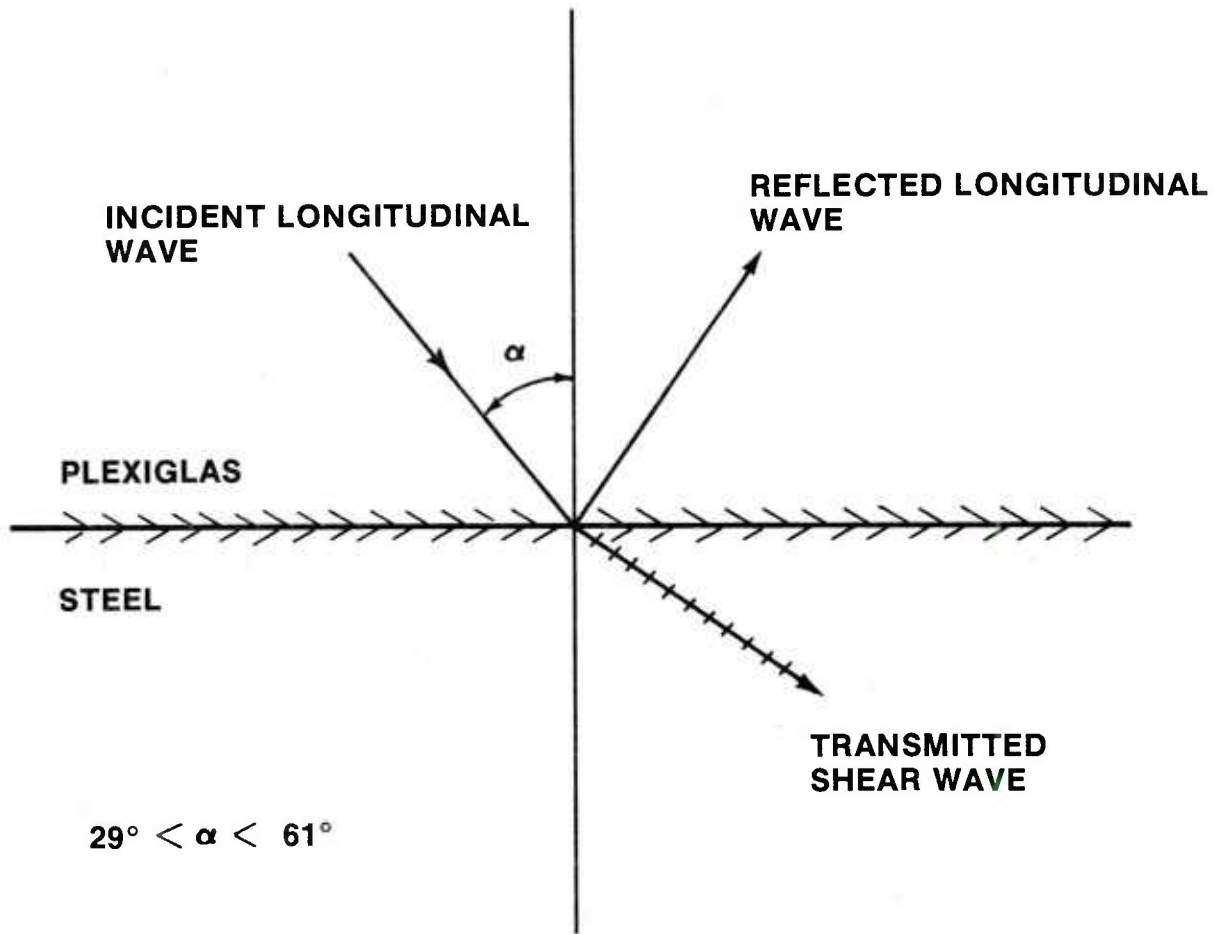


Figure 25. Mode conversion at plexiglas-steel interface for angle of incidence in range 29 to 61 degrees.

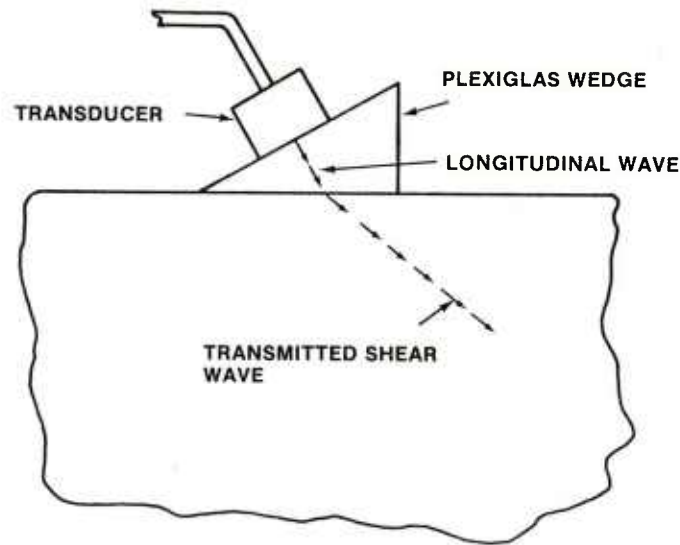


Figure 26. The angle probe.

flaw indications using the pulse echo method. At (a) the initial pulse is followed by an echo from the crack or nonmetallic inclusion followed by an echo from the back of the test piece. At (b) the initial pulse is followed by an echo from the crack. The long crack in this case blocks the beam from the back surface so that no back surface reflection occurs. *Figure 29* shows an immersion test for the bond surface between a porous bearing box and a bearing bush [15]. The trace for a good bond is shown at A. Following the initial pulse an echo P results from the front surface of the bearing bush. A record echo Z occurs from the bush-bearing bond interface. No reflection occurs from the back side of the bearing box because of its porous nature absorbing the wave. The trace at B shows the multiple reflections $Z_1, Z_2, Z_3 \dots$ etc. occurring from the disbond.

Angle probes are used in the inspection of welded seams and shouldered axles and seams. *Figure 30* shows some example inspections. It can be seen that the angle beam reaches the crack surface which would be inaccessible to a longitudinal beam. *Figure 31* shows the angle probe inspection scheme for a weld seam. The distance ℓ is known as the skip distance. The probe is moved back and forth by this distance so as to cover the entire depth of the weld.

Surface waves are used to inspect curved surfaces for surface discontinuities. The surface waves follow the surface contour, passing around corners, fillets, etc. *Figure 32* shows

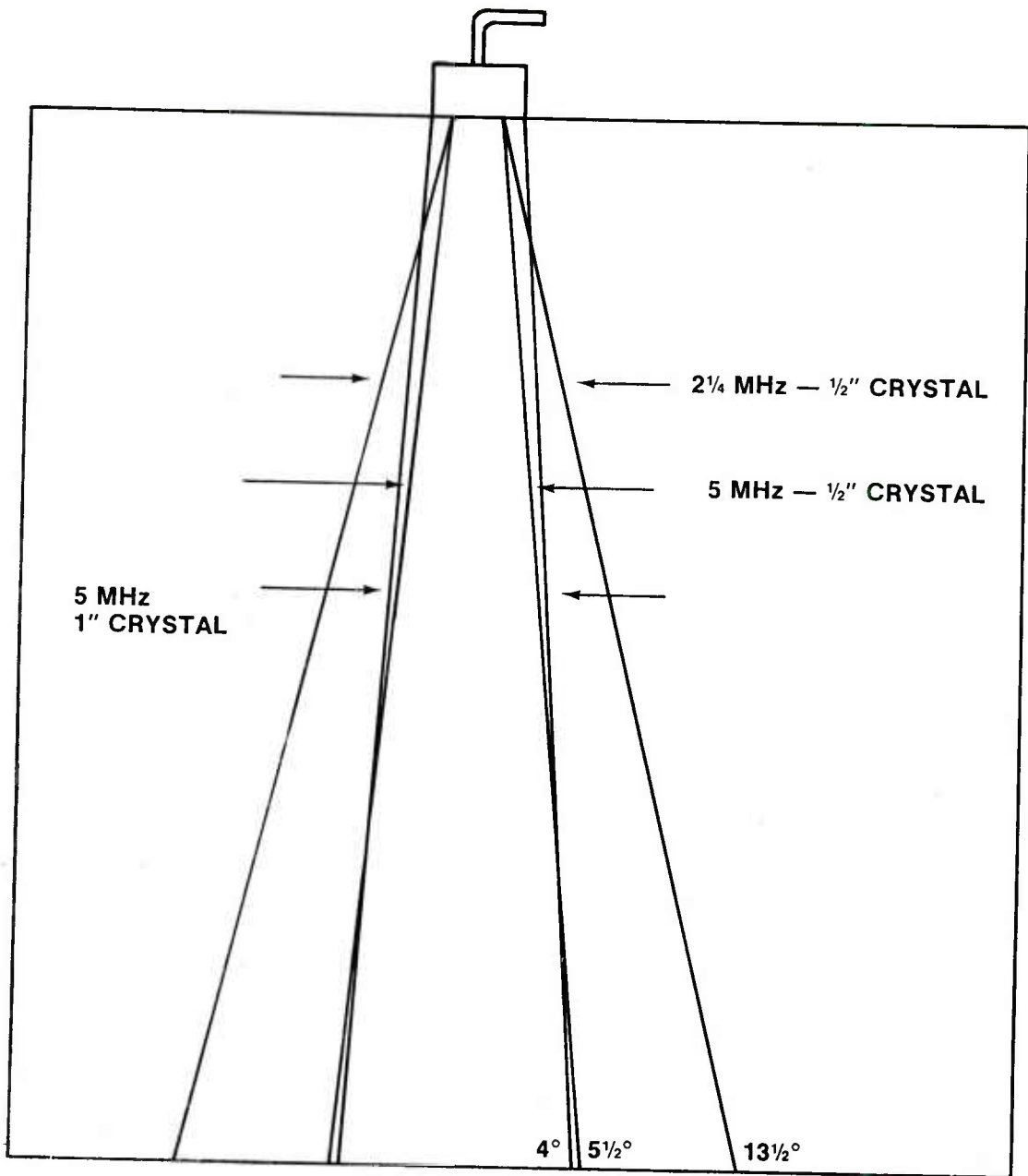
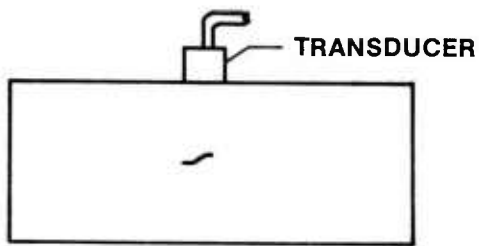
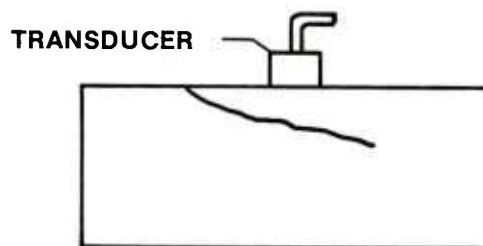


Figure 27. Beam spread as influenced by frequency and transducer crystal size.



**SMALL CRACK OR
NONMETALLIC
INCLUSION**



**LONG CRACK OR
SEAM**

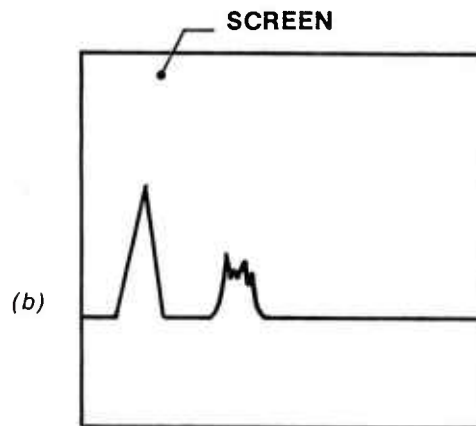
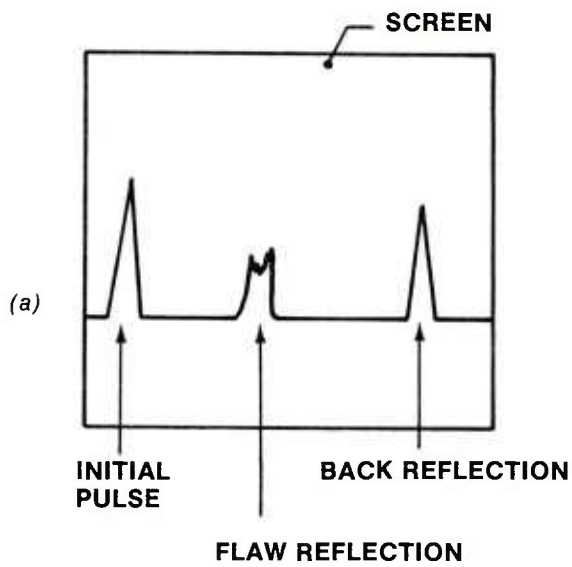


Figure 28. Example contact test indications.

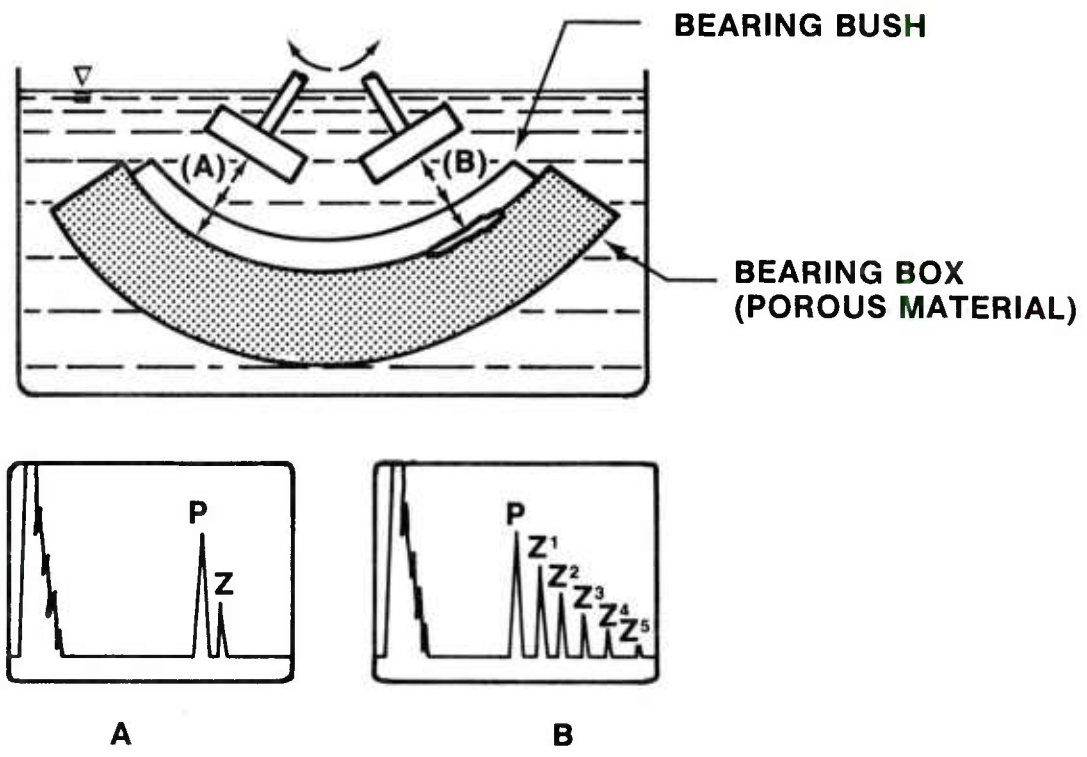


Figure 29. Immersion testing for disband of bearing bush and box [15].

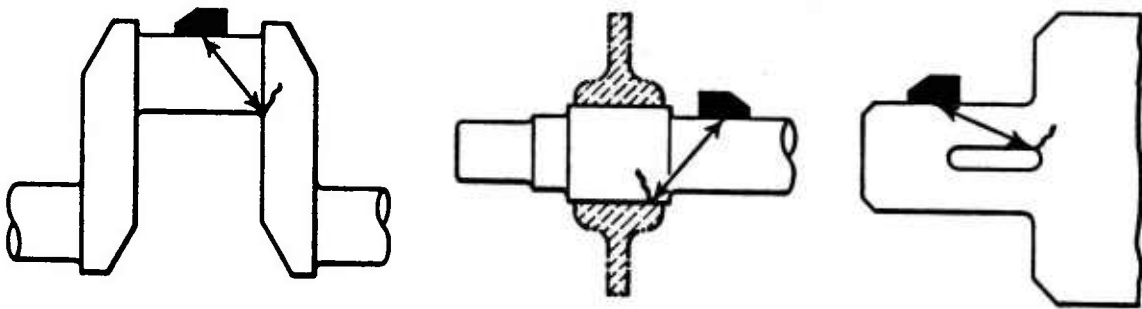
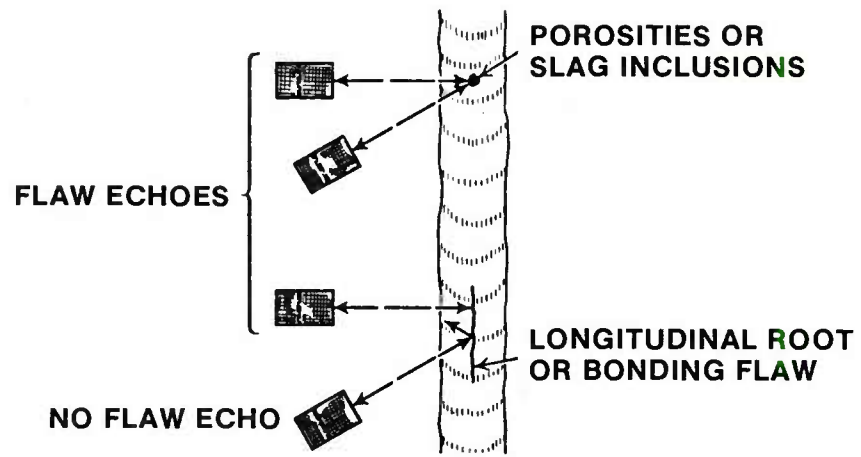
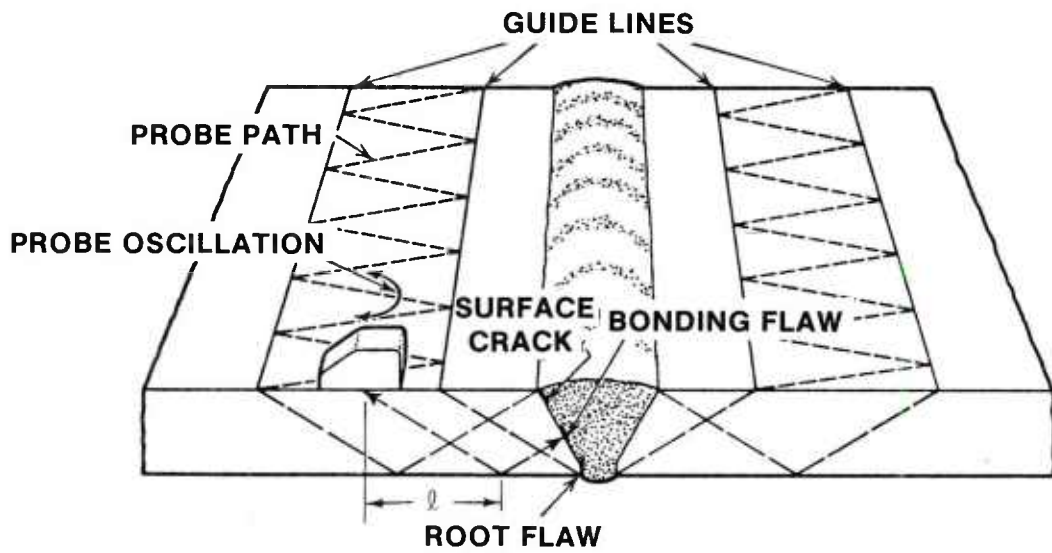


Figure 30. An angle probe [15].



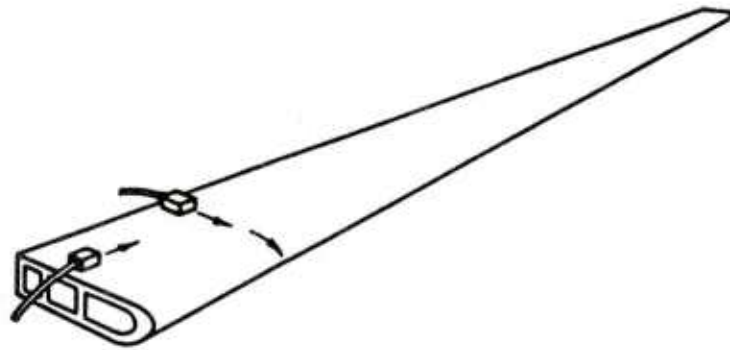
(a)



λ = SKIP DISTANCE

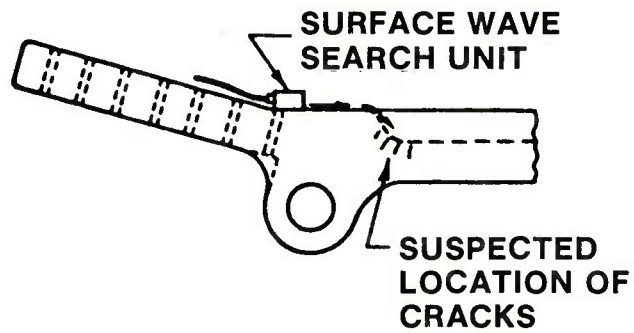
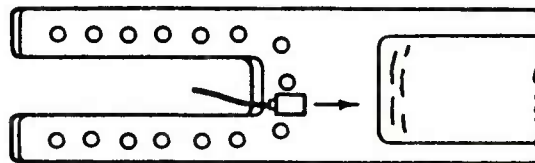
(b)

Figure 31. Angle probe, pulse-echo inspection of weld scan showing: (a) principle of detection, and (b) probe movement [15].



HOLLOW EXTRUSION

(a)



(b)

Figure 32. Surface wave applications showing: (a) inspection of a hollow extrusion and (b) surface crack search in a fitting [14].

two examples given by McGonnagle [14]. In (a) the hollow extrusion is inspected in two directions to locate randomly oriented flaws. Since the surface wave follows the curvature it can locate flaws on the extrusion side opposite the transducer. The illustration (b) shows how cracks in a depression were investigated by the surface wave.

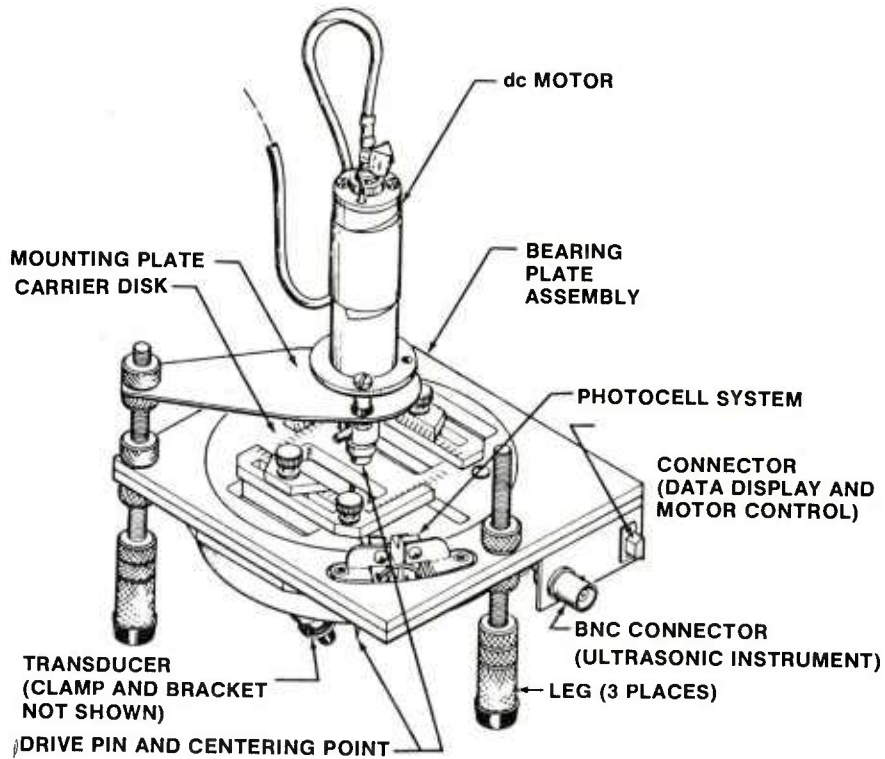
In-service inspection of aircraft sometimes requires the inspection of thousands of fastener holes for cracks. The inspection needs to be done with the fasteners installed since to remove them is expensive, time consuming and may even cause additional flaws. Responding to the need for a better inspection technique, the Boeing Company designed, built and evaluated an ultrasonic scanner [45]. *Figure 33(a)* shows a sketch of the scanner. The scanner contains two transducers positioned on either side of the hole and fastener as shown in *Figure 33(b)*. Once the scanner is centered over the fastener, the transducer assembly then can be rotated clockwise and counter clockwise to inspect all around the hole for cracks. The scanner is highly portable, weighing only 2.5 lbs.

E. Radiography

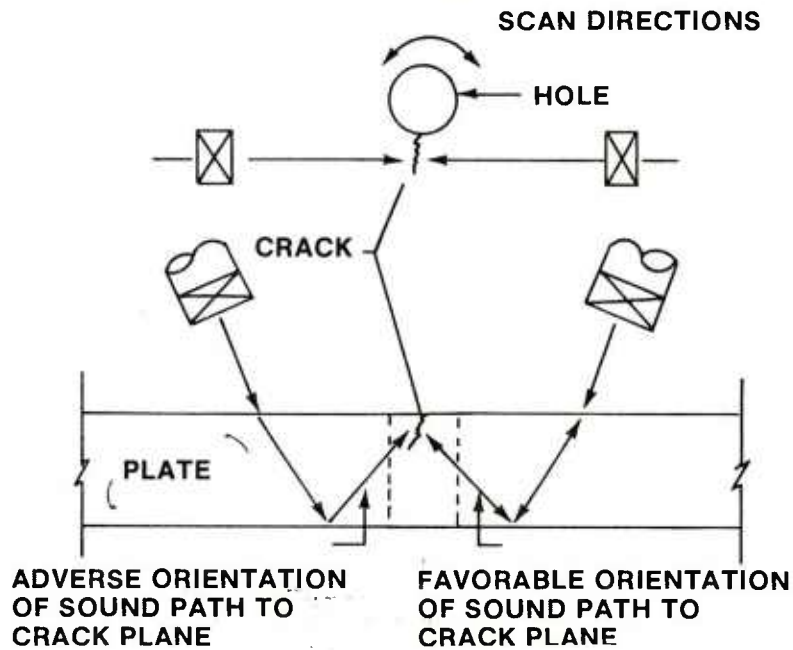
Radiography is one of the oldest NDE techniques; it was pioneered for industrial use at Watertown Arsenal by Dr. H. H. Lester [12]. The method employs x-rays and gamma rays. The two radiations are essentially the same but from different origins; x-rays result from an impressed voltage on a vacuum tube and gamma rays are spontaneously produced by the decay of radioactive elements. The wavelengths are very short, measured in angstroms (\AA) ($1 \text{\AA} = 1 \times 10^{-8} \text{ cm}$). Roughly speaking, the wavelengths are in the range 5-0.0004 \AA for x-rays and 0.1-0.005 \AA for gamma rays. For comparison, visible light has the range 4000-7500 \AA (0.000016-0.000030 inch).

A radiograph is basically a two-dimensional picture of the distribution of X or gamma ray intensity after passing through a test object. The basic radiographic process is shown in *Figure 34*. A test object is radiated with the penetrating energy. The recording film is placed behind the object. Regions in the test object which are thinner or which contain voids absorb lesser radiation and thus are outlined by causing a greater exposure on the film.

X-rays are produced when high velocity electrons are rapidly decelerated by striking a target. *Figure 35* illustrates a hooded-anode x-ray tube used to accomplish this. Electrons are driven from the cathode or negative pole by high voltage towards the anode or positive pole. They are suddenly stopped there and their kinetic energy is converted into radiation energy of the x-ray beam. While there are several types of x-ray tubes, the one shown in *Figure 35* is a



(a) Sketch of scanner for inspecting fastener holes [45].



(b) Ultrasonic scanning of a fastener hole with two transducers used because of possible adverse crack orientation.

Figure 33. The Boeing ultrasonic fastener hole scanner.

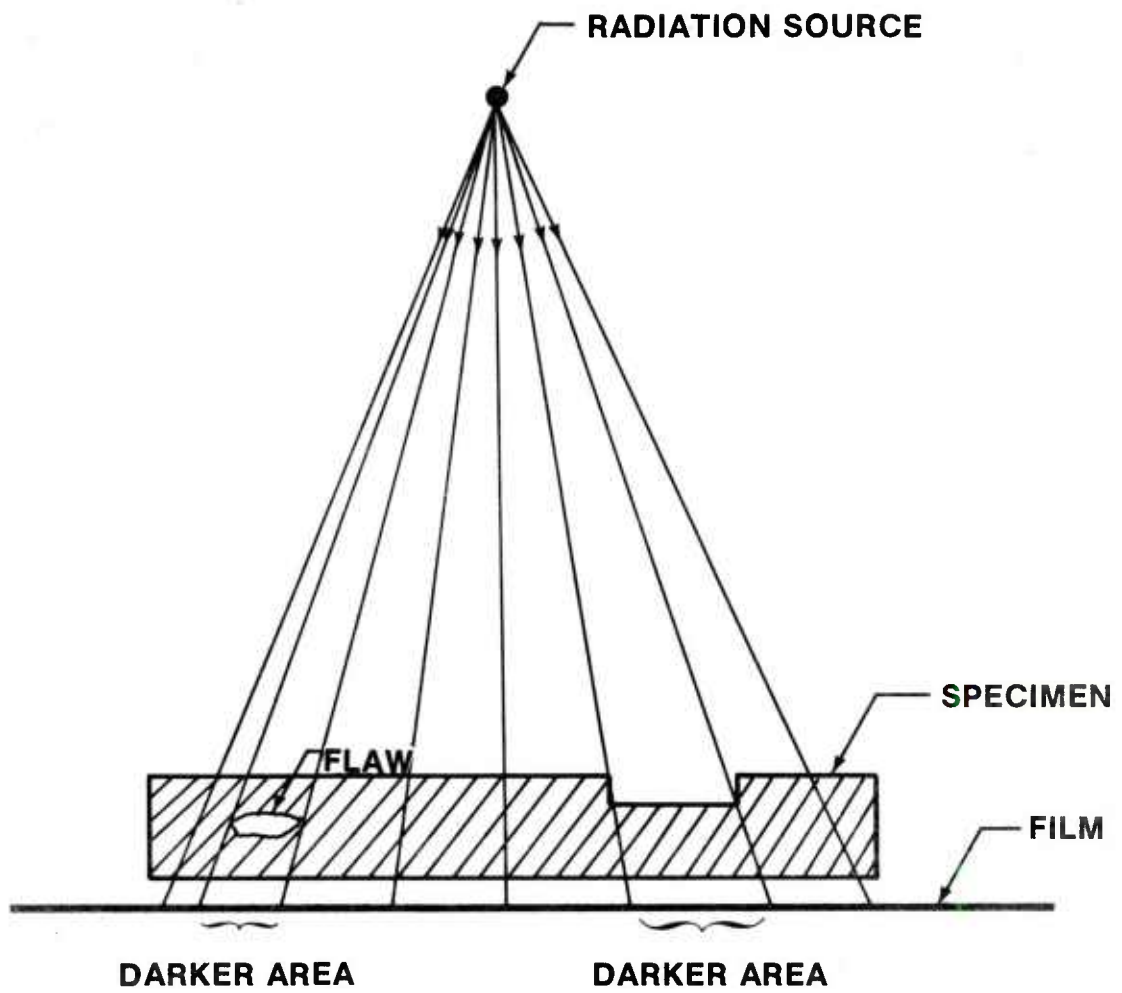


Figure 34. The basic radiographic setup.

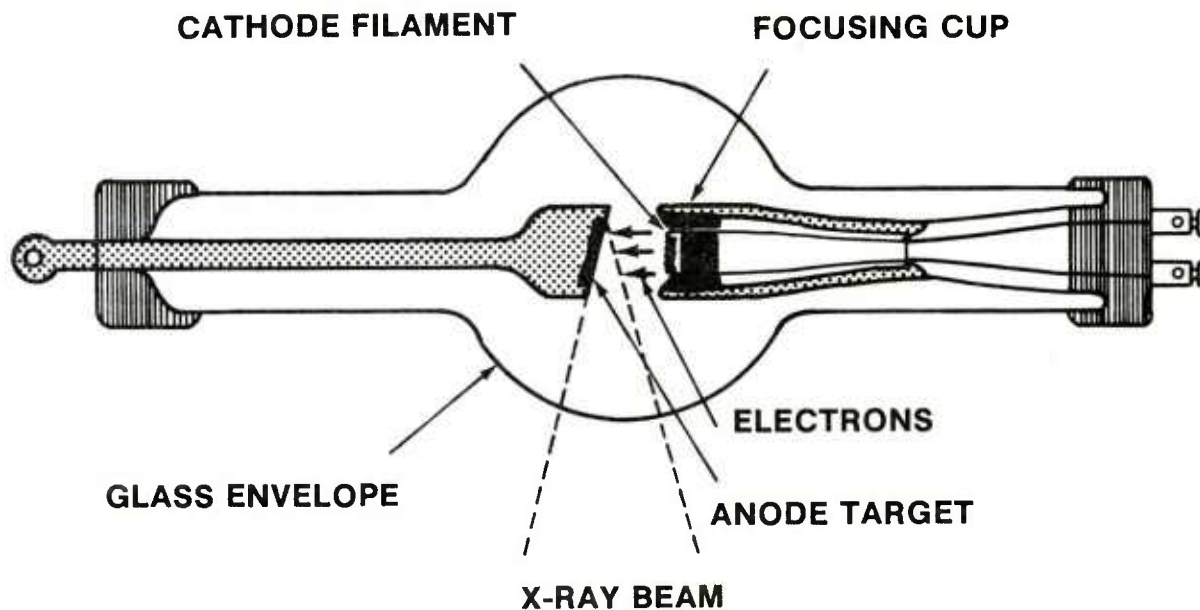


Figure 35. Basic x-ray tube.

bipolar tube in which each electrode is at high voltage with respect to earth. An incandescent filament is surrounded by a cloud of electrons. The high voltage applied to the terminals drives these electrons towards the tungsten target. There the electrons are stopped, and their energy converted into x-rays. Only a small fraction of the energy of the electrons is converted into x-ray energy; the rest is used in heating the target. To prevent melting from the heat, the tungsten target is welded to copper which can readily conduct the heat away. The copper is cooled by water. Typically, high voltages are required. The Watertown unit of 1922 operated at 200 kilovolts (kV) with a current of 5 milliamps (in A). As the technology progressed units with 1000 kV became available. Then with the development of the Van de Graaff generator and betatron, multimillion-volt units were developed. X-ray units of up to 100 million volts are now available; these are called linear accelerators. *Table 5* [17] shows some typical radiographic applications for various tube voltage levels.

Gamma rays, except for their source of production and wavelength, are an electromagnetic radiation identical to x-rays. Gamma rays are produced by the decay of certain radioactive isotopes. Two useful characterizing properties of the isotopes for radiography are the half life and the gamma ray energy. The half life of an isotope is the time required for the radioactivity to decay to one-half of its initial strength. The energy of the

TABLE 5. TYPICAL APPLICATIONS VERSUS TUBE VOLTAGE [17]

Voltage Rating	Typical Applications
50 kV	Wood, plastics, textiles, leather, and grain. Diffraction and microradiography.
100 kV	Light metals and alloys. Fluoroscopy of food stuffs, plastic parts and assemblies, and small light alloy castings.
150 kV	Heavy sections of light metals and alloys, and of thin sections of steel or copper alloys. Fluoroscopy of light metals.
250 kV	Heavier sections of steel or copper (Fluoroscopy is not generally used at this voltage.)
1 to 2 MeV	Radiography of very heavy ferrous and nonferrous sections.

gamma rays is measured in kilo-electron-volts (keV) or in millions of electron volts, which corresponds with the maximum energy of x-rays generated by an electronic x-ray tube energized at the stated potential. Most of the x-rays generated by a tube are at about 40 percent of the maximum energy and so gamma rays are similar to x-rays at about twice the energy. In other words the penetrating ability of cobalt-60 having an energy of 1.2 mega-electron-volt (MeV) is similar to the penetrating ability of x-rays produced by a 3.0 MeV generator. *Table 6* shows the energy and half life for four commonly used isotopes.

Gamma rays cannot be turned off, controlled, or directed. Obviously, very strict State and Federal standards govern handling and storage. A gamma ray source is stored in a shielded container designed to permit radiation-safe storage and remote handling. The equipment used for handling and safe storage during radiography is normally referred to as a camera. *Figure 36* illustrates a camera. The isotope, when not in use, is kept in the heavily-shielded pig. The isotope can be remotely cranked out along the flexible tube to the tube's end then placed where the exposure is to be made. Lights on the control unit indicate the location of the source.

TABLE 6. CHARACTERISTICS OF FOUR ISOTOPES USED FOR RADIOGRAPHY

Isotope	Energy meV	Half-Life	Comments
Cobalt-60	1.2	5.3 years	For radiography of steel, copper and brass and other medium weight metals 1 to 8 inches thick. Thick source shielding required.
Cesium-137	0.66	33 years	For steel 1 to 2.5 inches thick. Superior rate of decay (very slow). In soluble powder form requiring special safety precautions.
Iridium-192	0.38	74 days	For steel and similar metals 0.25 to 3.0 inches thick. Easily shielded source of small physical size (small focal spot).
Thulium-170	0.084	127 days	For thin metals. Small amount of shielding required. Good portability.

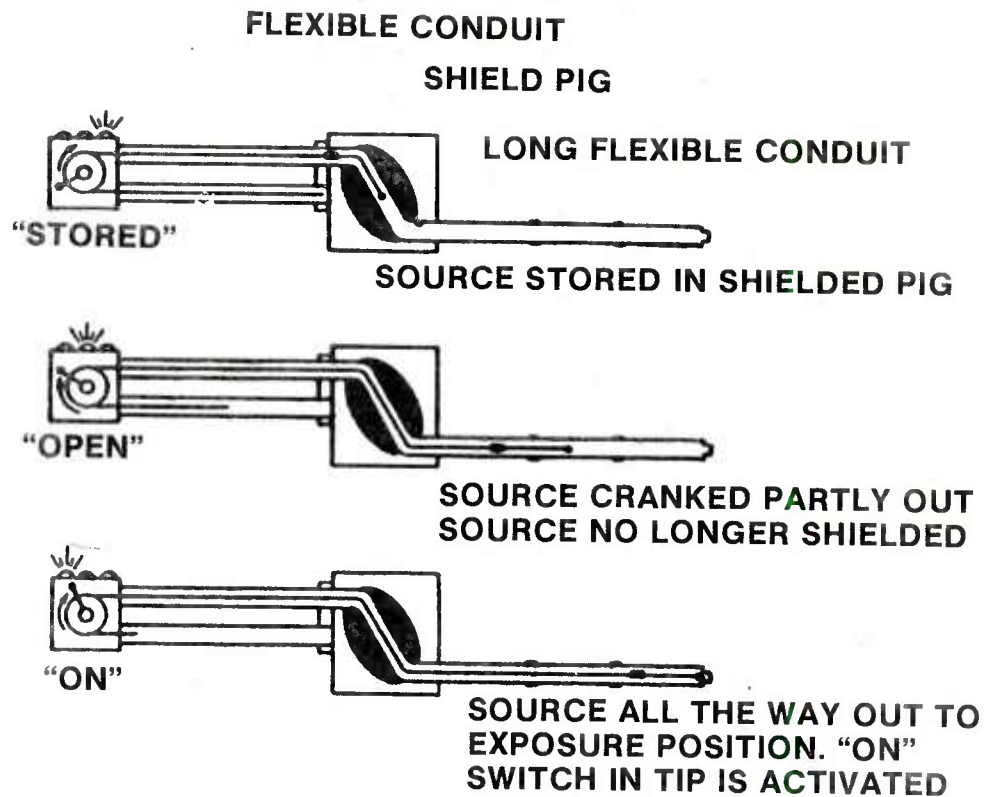


Figure 36. Arrangement and operation of typical isotope camera.

X-ray film is very similar to ordinary photographic film except that it is sensitive to the x and gamma ray wavelengths. It consists of a transparent cellulose derivative coated with an emulsion either on one or both sides. The emulsion contains silver halide grains which are sensitized by the radiation. When subsequently subjected to a chemical developer the silver grains turn to a black metallic silver. The aggregation of black silver grains on the transparent film constitutes the image. The film must necessarily provide high contrast, otherwise a small change in the subject, a small amount of absent material due to a flaw, would not be visible. Thus the film must enhance the contrast. The film is supplied in three grades of grain size: coarse, fine, and very fine. The fine grain, as in ordinary photography, provides the highest quality and highest contrast but requires more exposure. The coarse grain film is most easily exposed but does not provide the quality of the finer grain film. Film is sold in two forms: sheet film of various standard sizes, and roll film of various widths and very long lengths. The latter is convenient for radiographing circumferential areas.

A film's exposure is measured by its density, a quantitative measure of the blackening of the film following exposure and development. The density is controlled by the product, I_t , of

the radiation intensity, I , and exposure time, t . For x-rays, the intensity is directly proportional to the tube voltage, if the source-film-distance remains constant. As the distance from the source increases the intensity decreases inversely proportional to the distance squared — the inverse square law. If the distance is doubled the intensity decreases to one-fourth its previous value. Since the product, It , controls the exposure if the intensity is decreased to one-half then the exposure time must be doubled. In other words either the intensity (tube voltage or source-film distance) or exposure time can be changed at will; so long as the product It remains constant the exposure density will remain constant. There is reciprocity between intensity and exposure time. When the radiation strikes the film less than one percent of the energy is absorbed by the film. Sometimes fluorescent or lead screens in front of and behind the film are used to convert the energy into a form which can be absorbed by the film. When screens are used the reciprocity law fails. The film emulsion, which is sensitive not only to the amount but also the brightness of the fluorescent light, causes this failure.

A number of factors can affect the sharpness of a radiograph. *Figure 37* shows how specimen edge unsharpness (penumbra) are affected by source size and the ratio of source-specimen distance and film-specimen distance. It can be seen that to make the image of the specimen edge sharp (penumbra small) the source needs to be small and at a great distance

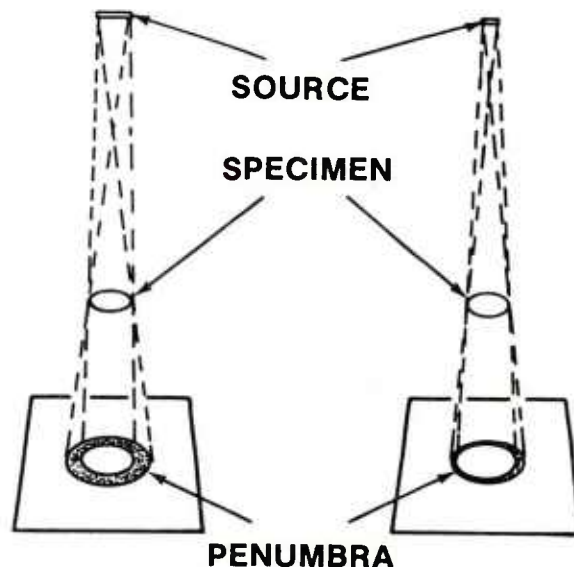


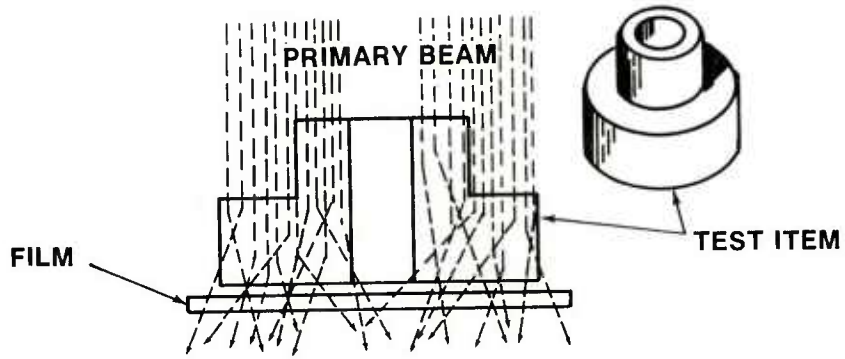
Figure 37. Penumbra caused by finite source size and finite specimen-film distance.

from the specimen while the film needs to be near the specimen. This ideal case can rarely be attained: x-ray tubes and gamma ray sources have a characteristic source size; increasing the source-specimen distance requires longer exposure time; the film cannot be placed in contact with certain parts of complex specimens.

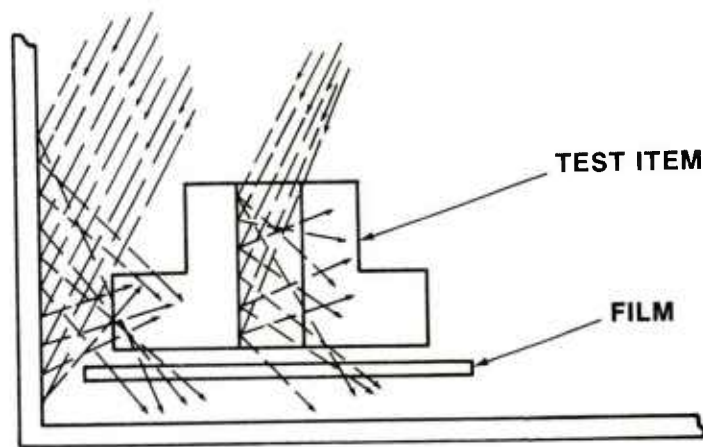
Scattering of the rays obscures specimen edges and blurs the image outline. *Figure 38* shows the three kinds of scatter which occur. Internal scatter is produced by rays scattering from internal surfaces. It tends to be uniform over a specimen of uniform thickness. Side scatter is scattering from walls, adjacent objects, or portions of the object itself. Back scatter is the scattering of rays from objects behind the test specimen. Scattering in general produces an undesirable loss in contrast.

Image distortion occurs in a number of ways as illustrated in *Figure 39*. If the plane of the specimen (or at least the plane of interest in the specimen) is not parallel to the film, if the plane of the specimen is not perpendicular to the rays, or if the film is not perpendicular to the rays image distortion will result. Sometimes due to physical limitations the specimen plane of interest cannot be perpendicular to the rays. If so the image distortion must be kept in mind when viewing the radiograph to avoid misinterpretation. *Figure 40* shows an example of this effect on the image location of two flaws in a specimen when viewed at four specimen-ray angles. At A the flaws 1 and 2 appear in the proper position; at B their respective images have moved closer together; at C one flaw marks the other; and at D the relative positions of the two flaws are interchanged. In positioning a specimen for radiographic crack inspection, the plane of the expected crack must be kept in mind. As shown in *Figure 41*, if the crack plane is parallel to the rays, (A) then the crack can be seen whereas if the crack plane is perpendicular to the rays (B) then nothing can be seen on the radiograph.

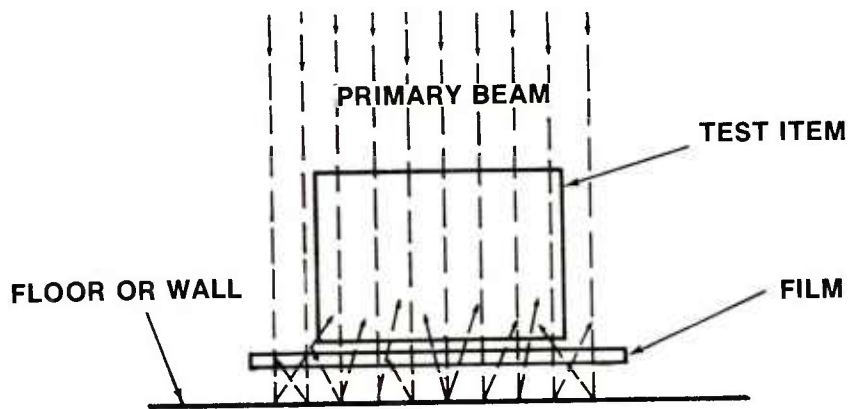
In a given radiograph one needs knowledge of the smallest change in specimen thickness which can be seen. If a void in a specimen constitutes only a one percent change in thickness and if the sensitivity of the radiograph is such that only a two percent change can be seen then the void would not be detected. A penetrameter is a device whose image on the radiograph is used to measure the radiographic quality level or sensitivity. The standard penetrameter is a rectangular piece of metal with three drilled holes of given diameter, *Figure 42*. It is composed of material radiographically identical to the material being radiographed. The penetrameter is normally placed on the surface of the test object facing the radiation, or if this is not possible it is placed on the film. If the outline of the penetrameter can be seen on the film and if the penetrameter is 2 percent of the specimen thickness then the radiographic sensitivity is at least 2 percent. Each penetrameter is identified by an I.D. number that gives the maximum thickness of the specimen for which the penetrameter is normally used. The



(a) Internal scatter.



(b) Side scatter.



(c) Back scatter.

Figure 38. Three kinds of radiation scattering.

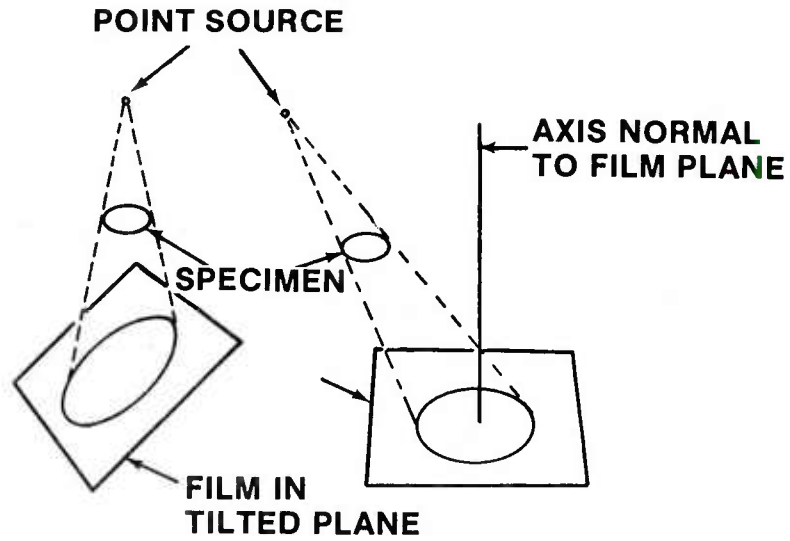


Figure 39. Image distortion due to source-specimen-film misalignment.

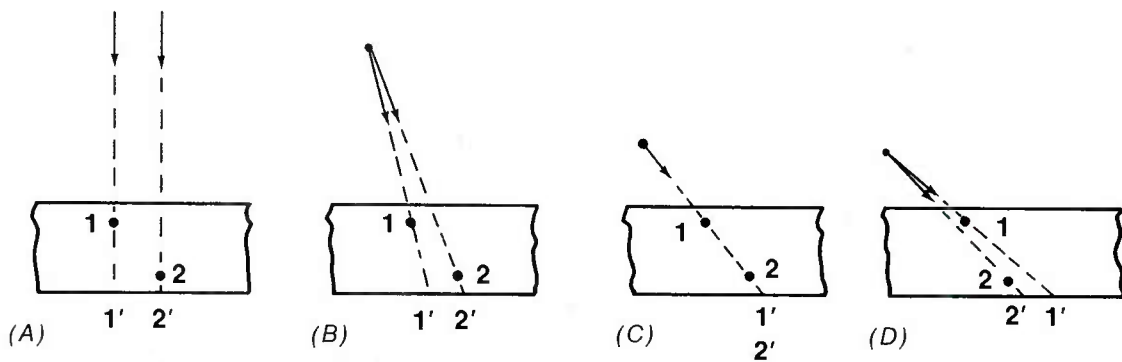


Figure 40. Influence of ray divergence on recorded flaw location.

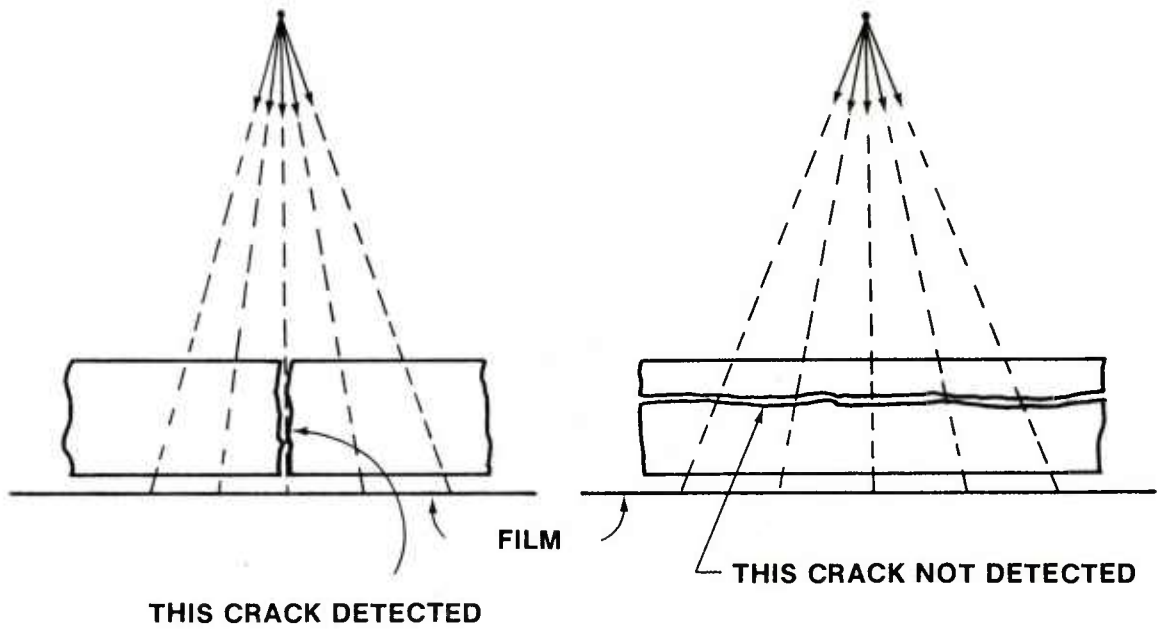


Figure 41. Influence of relative crack and ray orientation on detection sensitivity.

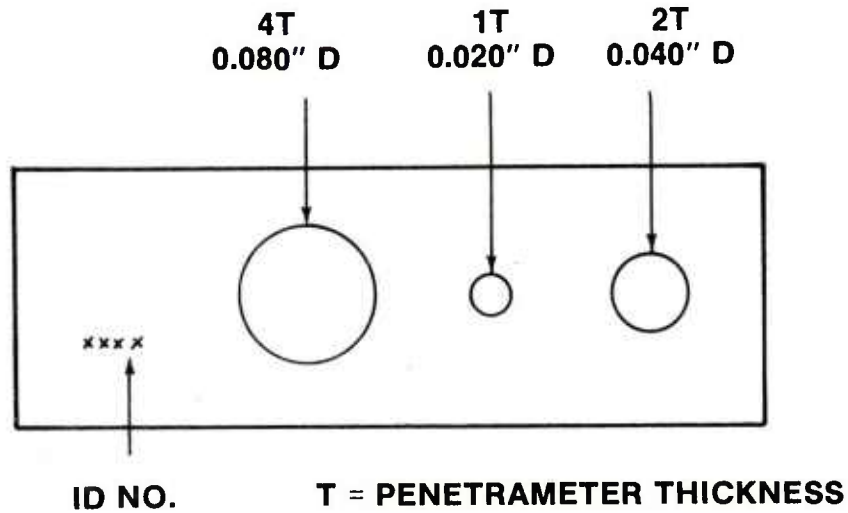


Figure 42. Standard penetrameter for a 1-inch thick specimen.

standard thickness is 2 percent. Holes of diameters one, two, and four times the thickness of the penetrometer are specified by ASTM. The penetrometer provides three ideal defects — ideal because the hole edges are sharp and well defined. Real flaws are irregular in shape and have rounded or tapered edges which provide a gradual change in thickness. Hence a real flaw with the same diameter as the smallest penetrometer hole may still not be seen. A number of different types of penetrometers have been designed for special purposes such as penetrometers containing small wires for radiography of electronic components.

Parts of the test specimen are sometimes covered with an absorbent material during exposure. This is known as masking. Masking reduces the exposure in the masked area and reduces the scatter. Masking materials are lead, barium clay, and metallic shot.

Fluoroscopy and television imaging provide two ways to view the x-ray image in real time, eliminating in some cases, the need to permanently record the image on film. In fluoroscopy, the film is essentially replaced by a fluorescent screen. The image on the screen is then viewed indirectly through an optical system to prevent eye exposure to radiation. Television viewing provides for remote viewing of the image, and permanent records can be obtained by photographing the television screen.

IV. ADVANCED NDE METHODS

A number of advanced methods are very briefly discussed here. These methods are advanced in the sense that they are, in general, somewhat newer than the five commonly-used methods discussed in Section 3; they are somewhat less familiar to the NDE community and less widely used; and they are still undergoing highly active development to make them more amenable for general inspection use. Some of these methods — neutron radiography and holographic interferometry, for example — are already experiencing considerable application and their importance and use is expected to increase in the future.

A. Neutron Radiography

Neutron (n) radiography uses the penetrating ability of a neutron beam to obtain information about the internal features of an object. The method was born in the early 60's. One of its first applications was to inspect radioactive nuclear fuel rods. With the development of sources for the neutron beams the method has grown rapidly and in 1975 was the subject of a symposium sponsored by ASTM, and the National Bureau of Standards [46]. Similar to x-radiography, the method provides a picture of internal features. Unlike x-radiography, however, the penetrating properties of the neutron beam are practically the reverse of the x-ray

beam. That is, the neutron beam very readily passes through heavy metal sections which would absorb x-rays; on the other hand the neutron beam is absorbed by hydrogenous materials through which the x-ray beam would readily pass. This makes the two methods particularly complimentary; an inspection problem for which x-radiography is unsatisfactory may be ideally suited to neutron radiography. Neutron radiography can be used to inspect dense materials such as lead and uranium. It can be used to reveal details of plastic, oil or water surrounded by steel or lead. According to Barton [47], details of 0.5 mm of hydrogenous material have been revealed in the middle of 30 cm of lead. Even materials of similar atomic number and density can be contrasted by using neutrons.

There are three types of sources of neutrons for neutron radiography:

- Nuclear reactors.
- Particle accelerators.
- Radioactive isotopes.

A reactor for neutron radiography is expensive, estimated from \$500 thousand to \$1 million in 1975 dollars [48]. Some commercial neutron radiography services do have reactors, which they use commercially to inspect specimens shipped to them by customers. Particle accelerator sources typically employ a Van de Graaff generator to bombard a suitable target (beryllium) with positive ions. Again, such a source is expensive. In the case of isotope sources, the most promising and commonly used isotope is californium — 252. Radiographs made by reactor sources, because of their higher source intensity, are generally superior to radiographs made by means of the other two sources.

Four neutron energy ranges are: cold, thermal, epithermal and fast neutrons. The thermal range provides the most pronounced differences between neutrons and x-rays, and hence is the one used in neutron inspection. Thermal neutrons are characterized by wavelengths of from 0.5 to 3 Å. Thermal neutrons are generated by surrounding a fast neutron source by a moderating material, such as paraffin, water, or graphite, which slows the particles down to the thermal range.

Figure 43 illustrates the arrangement for thermal neutron radiography. Imaging is accomplished by the direct exposure method, and the transfer method. In the direct method the film together with either one of two intensifying screens is behind the specimen in the

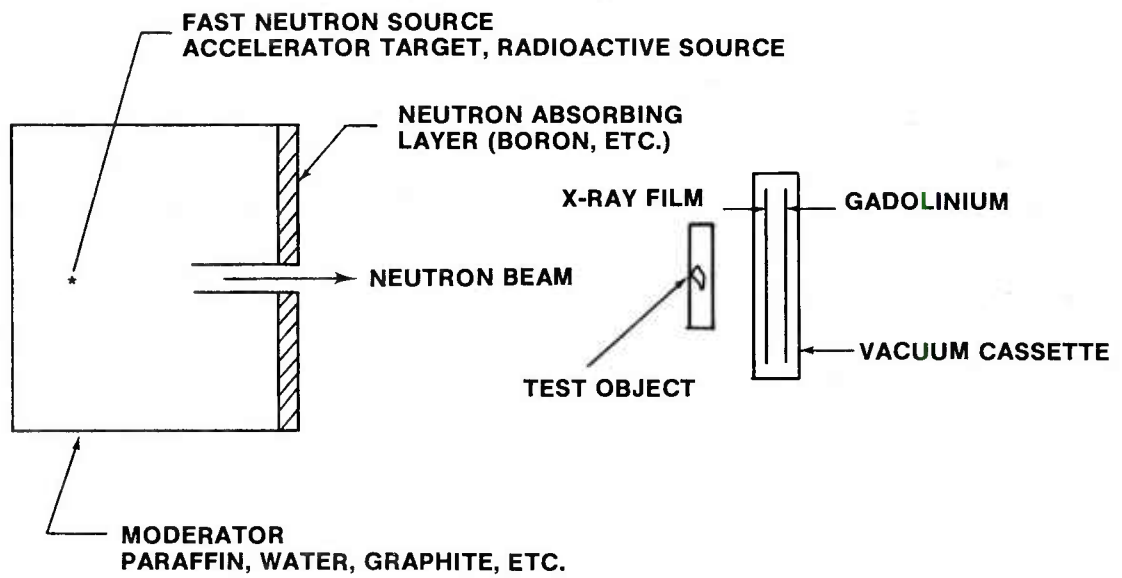


Figure 43. Typical arrangement for thermal neutron radiography — direct method of imaging shown.

neutron stream. The film is x-ray film and the screens are normally made of gadolinium (Gd). The direct method is illustrated in *Figure 43*. In the transfer method a metal foil (indium (In) or dysprosium (Dy)) instead of film is placed in the neutron stream. The foil becomes radioactive under neutron bombardment. The pattern of radioactivity in the metal foil is then transferred to the film in a film cassette. This method prevents fogging of the x-ray film by extraneous gamma radiation in the neutron beam or from a radioactive test object itself. Numerous examples of applications are given in Reference [46]. The method is most useful for inspecting nonmetallic features concealed behind metal. Its corrosive detection capability is reported to be superior to all other NDT methods even when the corrosion is hidden behind metallic structures several inches thick [49]. It has been used to inspect for residual ceramic core in hollow air-cooled turbine blades [50] and the adhesive bond on aluminum honeycomb aircraft panels [51]. Many neutron radiographs reported in the literature are remarkable for their sharpness and clarity [52]. Inspections of complicated assemblies containing both metallic and nonmetallic components are most effectively carried out by using both neutron- and x-radiography. In an example shown in [52] explosive bolts were inspected by both methods. The neutron radiograph clearly showed the explosive pellets the Silastic fill, the plastic cap and the coating on the aluminum caps, while the x-radiograph showed the metallic components and the lead-based explosives. Neutron radiography is rapidly increasing in use. NASA, Navy and Air Force specifications now include neutron radiography [47].

B. Acoustic Emission

Acoustic emission uses the elastic energy spontaneously generated in the form of a stress wave by either flaw growth or plastic deformation within a test body. Sensors in the form of accelerometers are placed on the surface of the test object. As the test load is increased if any flaw begins to propagate it sends out stress waves which the sensors receive. By using several sensors, the flaw can be located by triangulation similar to the way that earthquakes are located. As an NDE method, the technique is unique in that the material flaw when propagating transmits its own signal with the sensor acting as a receiver. The method has been undergoing development since the early 60's and it continues to be an area of active research and development. Hartbower [53] recently provided a summary of the method together with an extensive literature review. A brief summary of the method was also provided by Dunegan [54]. Although the method is still undergoing development, available instrumentation systems are so sensitive that it is already possible to detect each stage of the failure process starting with deformation, crack propagation, and, finally, the onset of unstable crack propagation. The elastic energy travels as elastic waves from the flaw to the surface where they generate transducer signals. There are two emission types [53]: one is a low energy continuous emission where the amplitude increases with the load; the second type occurs in discrete bursts of

considerably larger amplitude. The second type is linked to the appearance and growth of macroflaws such as cracks. The frequencies associated with these waves range from audible clicks (less than 20 kHz) up to 50 MHz. The amplitude of the signal is such that amplification by factors of 10^4 to 10^7 are required. This high amplification leads to electrical and mechanical noise which must be filtered.

Acoustical emission has been applied to a variety of problems including:

- Measurement of fatigue crack growth rate
- Detection of stress-corrosion cracking and hydrogen embrittlement
- Strain-aging embrittlement
- To monitor welding operations for weld cracking
- As a precursor to crack instability

Some of these applications were demonstration programs, others involved monitoring in-service structural components. For example, airplane wing structures have been monitored by acoustical emission [55]. During proof tests acoustical emission is used to monitor subcritical flaw growth. If the acoustical emission indicates the likelihood of a flaw instability, the proof test can be halted and the flaw repaired, thus preventing an expensive proof test failure.

Some metals exhibit a behavior known as the Kaiser effect. After such a metal has been loaded to a given level and the load stopped the acoustical activity eventually ceases. If the load on the structure is then relaxed and reapplied no further acoustical emission will occur until the previous load level is reached or exceeded. This effect provides a possible way to determine the maximum load to which a structural component has been previously subjected.

As a general rule an acoustical emission detection system is composed of one or more transducers with associated preamplifiers, high pass and low pass filters, and amplifier and a recording system. What may be considered as a typical acoustic emission monitoring system is shown in *Figure 44*. When triangulation is to be performed, multiple channels are required interfaced with a small computer. Triangulation to locate a flaw is carried out essentially by drawing illuminating circles with radii equal to the difference in stress wave arrival times as measured by two transducers multiplied by the wave speed. Typically two signal counting methods are used: (1) the total stress waves emitted (TSWE) also referred to as total emission

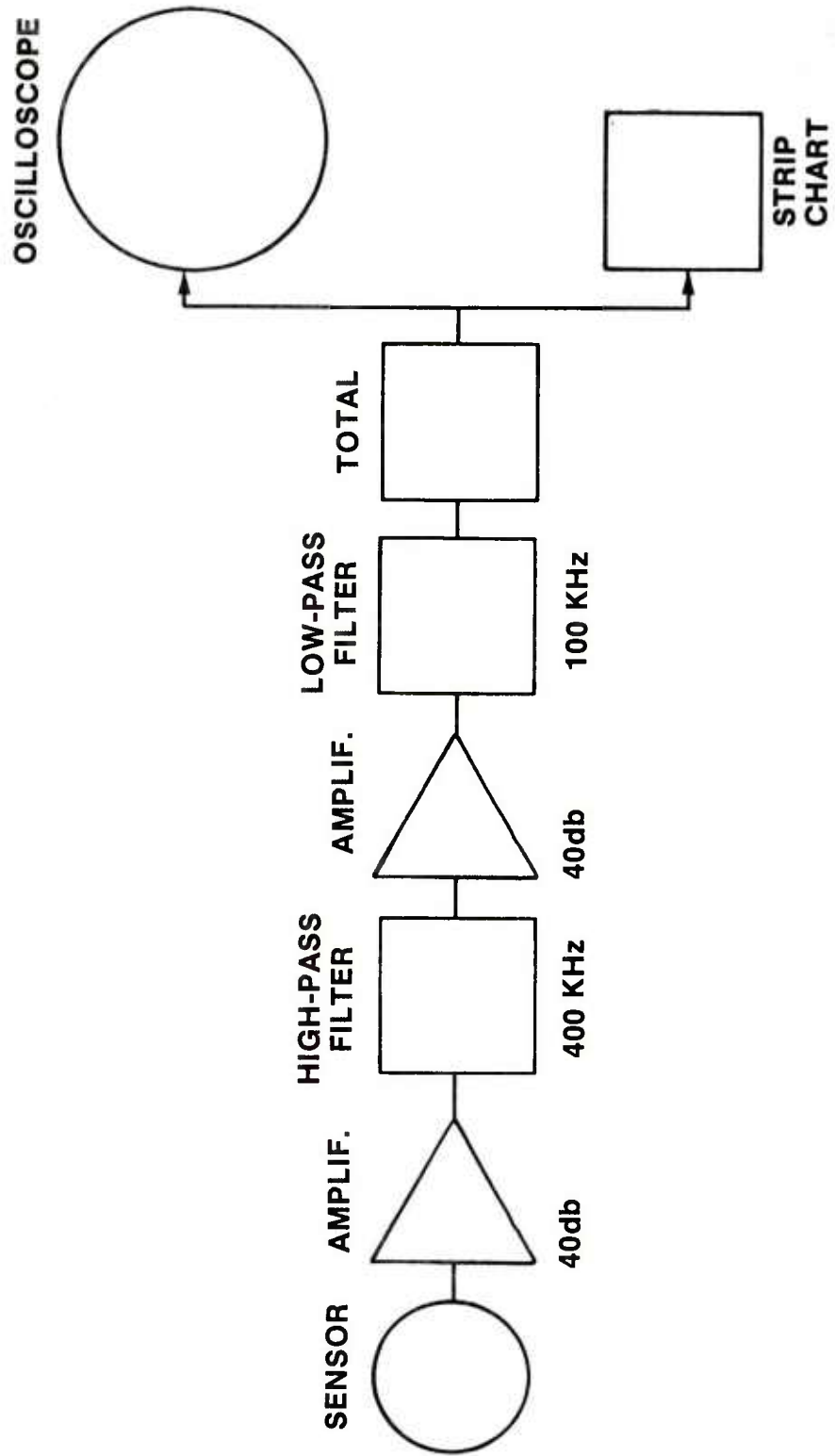


Figure 44. Acoustical emission monitoring system showing some typical filter and amplifier values.

count, pulse count, emission summation, number of emissions, and cumulative count and (2) emission rate referred to as burst rate, pulse rate, count rate, stress-wave-emission rate, etc.

Many developmental tests have been conducted to correlate the stress wave count with test component stress, stress intensity factor, and crack growth rate. *Figure 45(a)*[56] shows an example of the emission rate plotted alongside tensile stress in an aluminum bar. *Figure 45(b)* shows the accumulative stress wave count for the same bar. It can be seen that the acoustical emission increases rapidly preceding the yield point and decreased rapidly thereafter.

An application of acoustical emission for detecting fatigue crack growth is illustrated by *Figure 46*, where low-cycle, high-intensity fatigue shows how the TSWE rapidly increases as the specimen approaches its failure cycle. Thus a rapid increase in TSWE can presage a fatigue failure. The maximum stress-intensity-factor, K_{MAX} , can be correlated with TSWE. *Figure 47* shows one such correlation. A near linear relationship is observed between K_{MAX} and TSWE. Fatigue crack growth rate $\frac{dN}{dt}$ has been correlated with acoustical emission. *Figure 48* shows how the fatigue crack growth rate can be predicted from ΣSWE for two conditions of D6aC steel.

Hydrogen embrittlement cracking was studied by Dunegan [54]. He related the acoustical emission rate dN/dt to the stress intensity factor K . *Figure 49* shows the emission rate as a function of the stress intensity factor. From the tests the following pulse rate stress intensity factor relation was determined.

$$\frac{dN}{dt} = 6.66 \times 10^{-5} (K^{5-7.05}) \quad (7)$$

This shows a direct relationship between $\frac{dN}{dt}$ and K . This relation would no doubt be different for different materials, presumably, however, an equation such as (7) can be found for many subject materials. The advantage of an equation such as (7) is that from measuring a given pulse rate $\frac{dN}{dt}$, one can readily predict the stress intensity factor and thus judge how near the specimen is to unstable fracture. *Figure 50* shows an example of how the summation of acoustical emissions may be related to K . Curves such as *Figure 50* suggest that the ΣSWE - K relationship should be of the form

$$N = AK^m \quad (8)$$

where m is a constant for a given material and thickness [57]. For the example in *Figure 50* $m = 4$ — i.e., there is a fourth power equation for N and K . Other studies have indicated values,

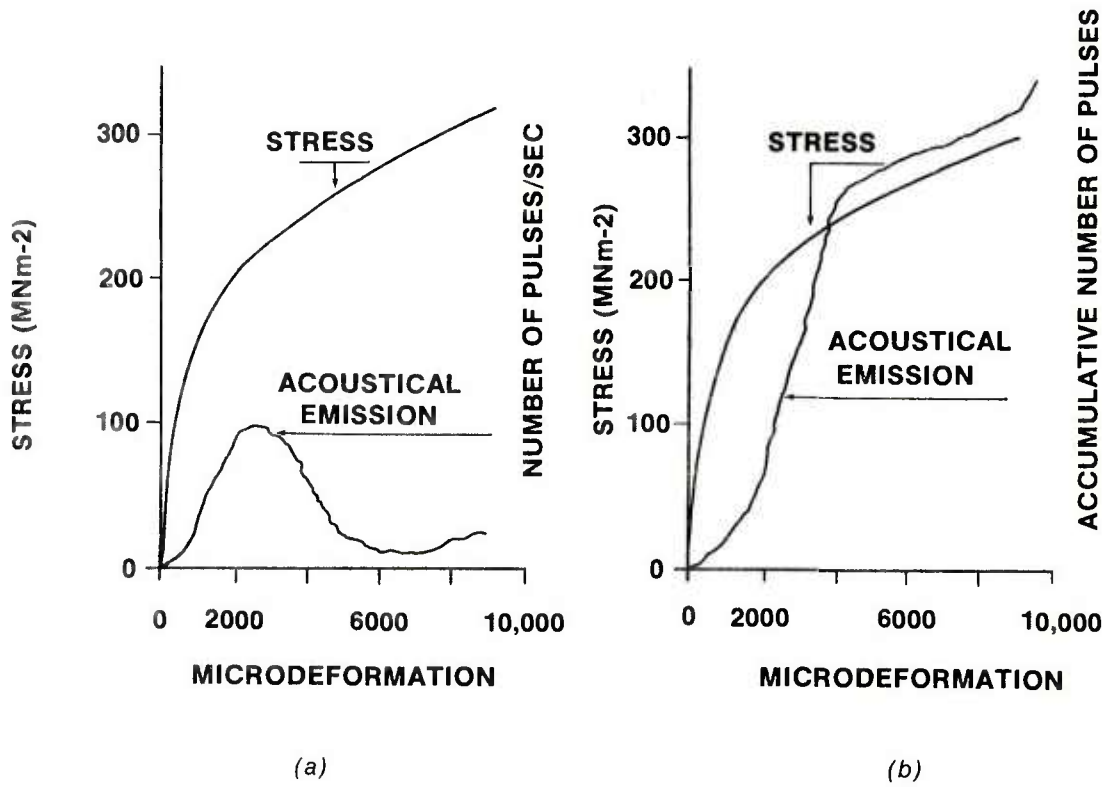


Figure 45. Acoustical emission activity as a function of specimen stress in terms of: (a) pulse rate, and (b) accumulated counts [56].

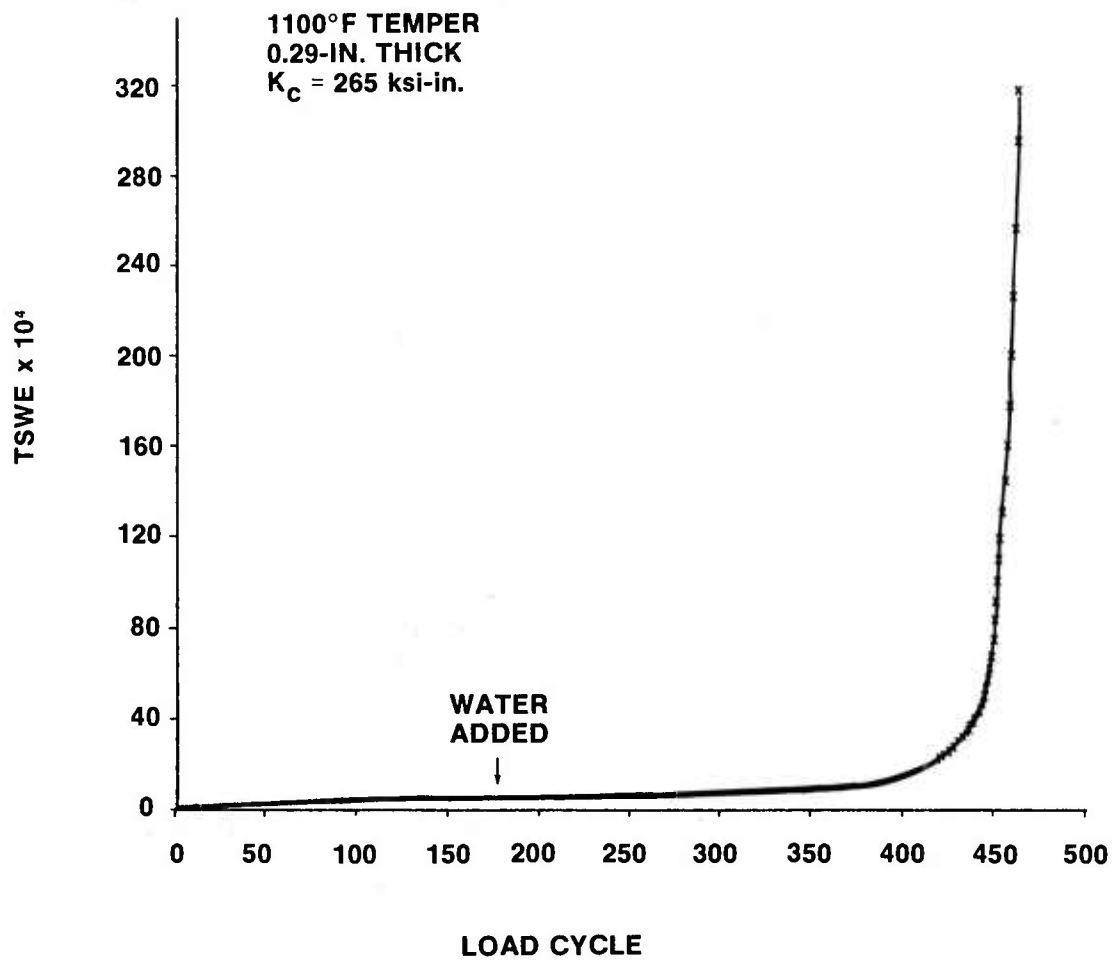


Figure 46. Fatigue corrosion test showing how the acoustical emission count can serve as a precursor of unstable crack propagation [53].

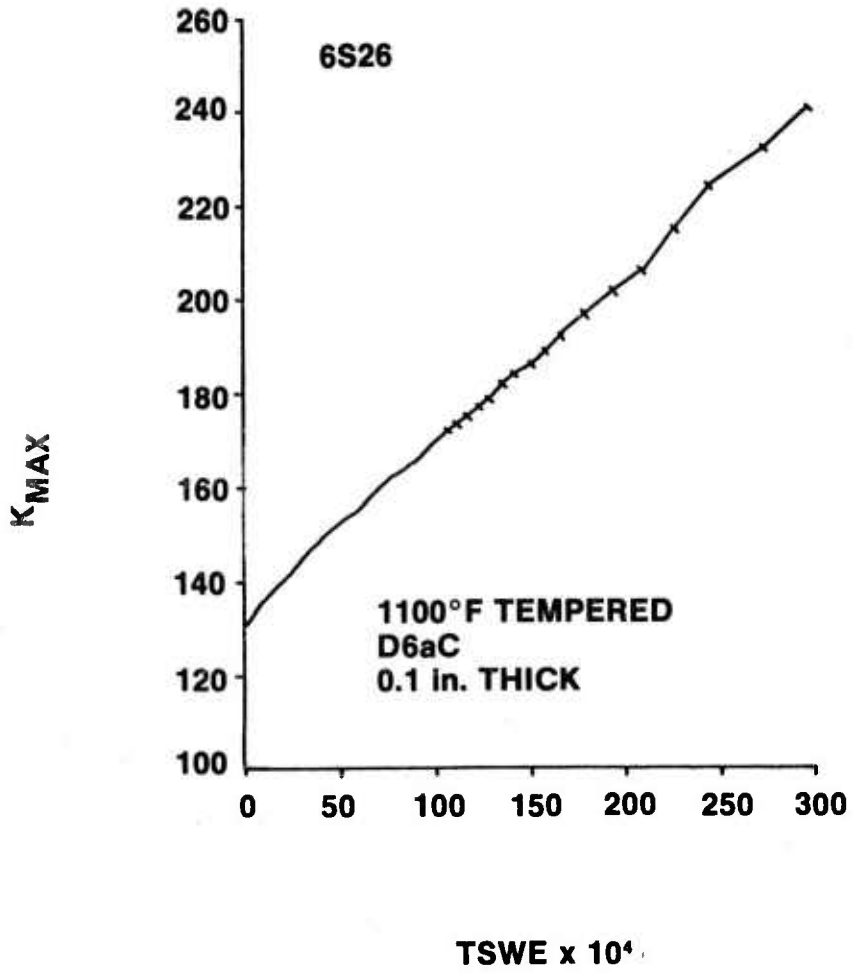


Figure 47. Total stress waves emitted correlated with K_{MAX} from a fatigue cracking test [53].

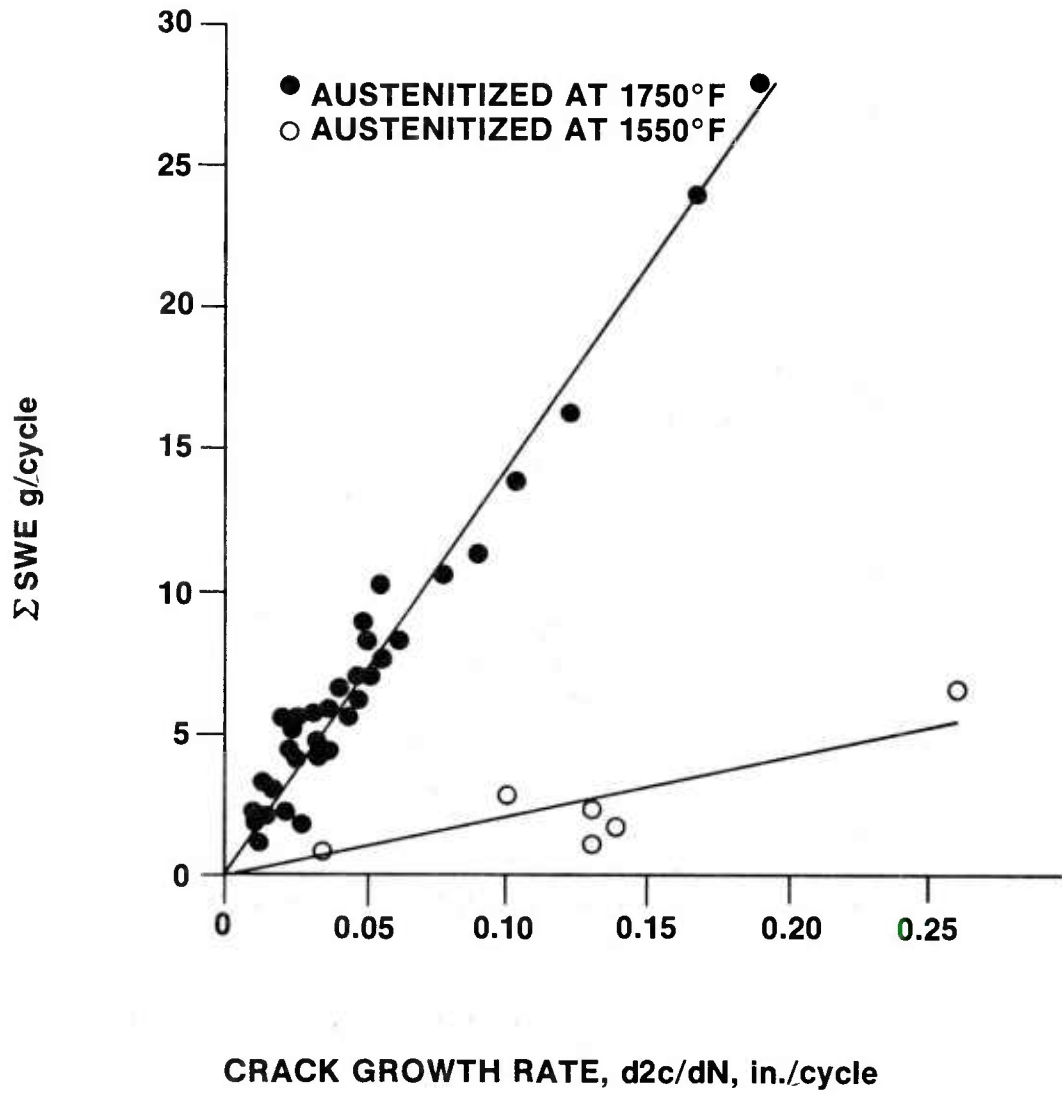
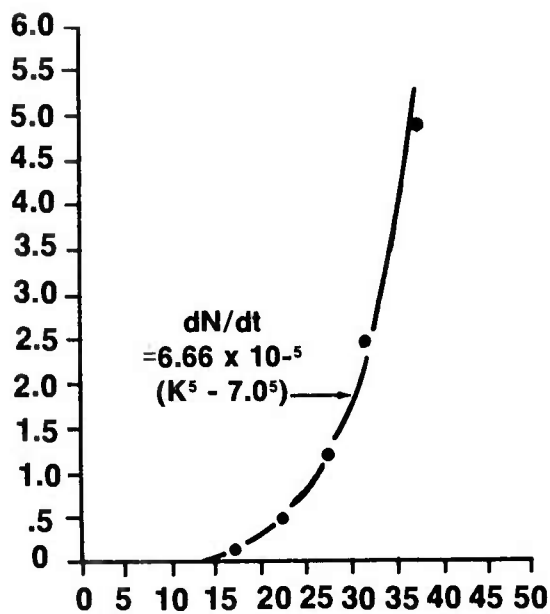


Figure 48. Relationship between fatigue crack growth rate and stress wave emission for two conditions of D6aC steel [53].

ACOUSTICAL EMISSION RATE (dN/dt) — 10^3 counts/min



STRESS INTENSITY FACTOR K — ksi-in.

Figure 49. Relationship between acoustical emission rate and the stress intensity factor for a high strength steel undergoing hydrogen embrittlement cracking [54].

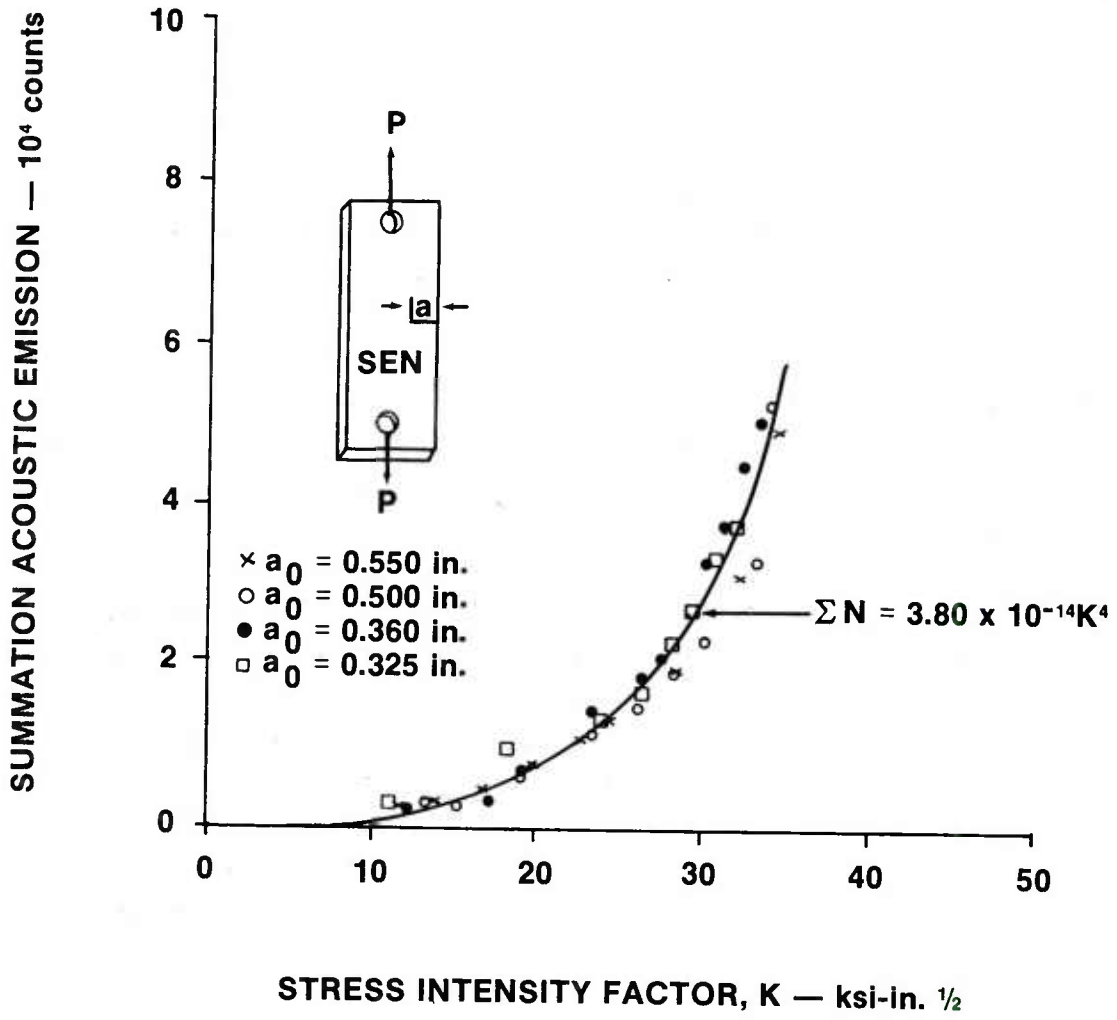


Figure 50. The relationship between acoustical emission and stress intensity factor [54].

however, of between 6 and 8 for m [53], and Hartbower has observed a direct proportionality (i.e., $m = 1$) between N and K . Thus further work is required to determine the precise relationship between N and K . The relationship between N and K may be affected by considerations such as trigger levels [53]. The importance of a relationship between N and K lies in the possibility of estimating flaw sizes and failure load based on in-service acoustical emission monitoring of a flawed structure. It appears though that more development is necessary before acoustical emission is capable of determining quantitatively the size or stress intensity level of a flaw.

C. Liquid Crystal

Liquid crystal technology has been extensively developed by Brown [58,59] at the US Army Missile Command. Only a summary of the method is included here. More thoroughly detailed information, and excellent discussions of the method are included in [58] and [59].

Liquid crystals are compounds that for certain temperature ranges exhibit some of the properties of liquids while retaining some of the properties of solids; they flow much like a liquid but retain some of the molecular order of solids. While there are three classes — smectic, nematic, and cholesteric — only the cholesteric is of interest in NDE technology. The cholesteric crystal has three optical properties: birefringence, optical rotation, and scattering of white light. It is this last property which makes the liquid crystals useful as a visual inspection technique. The scattering causes reflection of different wavelengths, giving iridescent colors. The observed color is a function of the temperature. As the liquid crystals go from a solid to a liquid state or vice versa they go through a spectrum of color changes. Each color corresponds to a specific temperature of the material. Since the liquid crystals have the ability to reflect colors dependent upon their temperature they present a visual picture of temperature discontinuities. Around flaws such as cracks and disbonds in structures the normal heat flow and temperature are disturbed. This disturbance representing the location of the flaw is easily indicated by the liquid crystals.

Cholesteric compounds of various sensitivities are possible, ranging from as small as 3° C to as large as 30° C. By blending pure cholesteric compounds [58]. Brown has developed blends which go through the entire spectrum of colors in 0.1° C or less. Temperatures at which color changes begin can be below room temperature to above 150° C.

Two methods are used to apply the liquid crystal to a test object: (1) a solution application, and (2) a film application. In the solution application the liquid crystal is sprayed

or brushed onto the structure. In the film method the liquid crystals are encapsulated in a thin Mylar film which is spread over the surface of the test object. The film is reusable.

Figure 51 illustrates a solution application to a test component. The test object is cleaned with an organic solvent. Using a water soluble paint a dark background is then painted onto the surface to improve visibility. The liquid crystals mixed with a solvent, are sprayed or brushed onto the surface and the solvent is allowed to dry. The test object is then heated through the appropriate temperature range (simultaneous heating from one side while cooling from the other is optimum [58]). The defect is outlined by an area of different color which can be marked or photographed. After the inspection, the liquid crystals are removed by a solvent and the dark paint by water.

The film application is shown in *Figure 52*. The Mylar film containing the liquid crystals is draped over the test object and both are put inside a vacuum bag. Drawing a vacuum insures close contact of the liquid crystal film on the test object. Heat is applied to the object by placing it on a heating blanket or near some suitable source of heat. The defect areas heat up more slowly than the rest causing the film to show a different color in those areas. After the inspection the vacuum is released and the film can be reused.

The method appears to work especially well when testing for disbonds and crushed core in honeycomb laminates. Brown [58] has applied the method with good success to the following structural components:

- Aluminum skins with high temperature phenolic honeycomb core.
- Glass cloth skins with glass fiber honeycomb core.
- Titanium skins with aluminum honeycomb core.
- Titanium skins with high temperature phenolic honeycomb core.
- Glass cloth laminates.

D. Holographic Interferometry

Holographic interferometry is a relatively new technique for recording surface displacements of test objects using two optical interference holograms. *Figure 53* illustrates the technique of making holographic interferograms [60]. The method involves illuminating

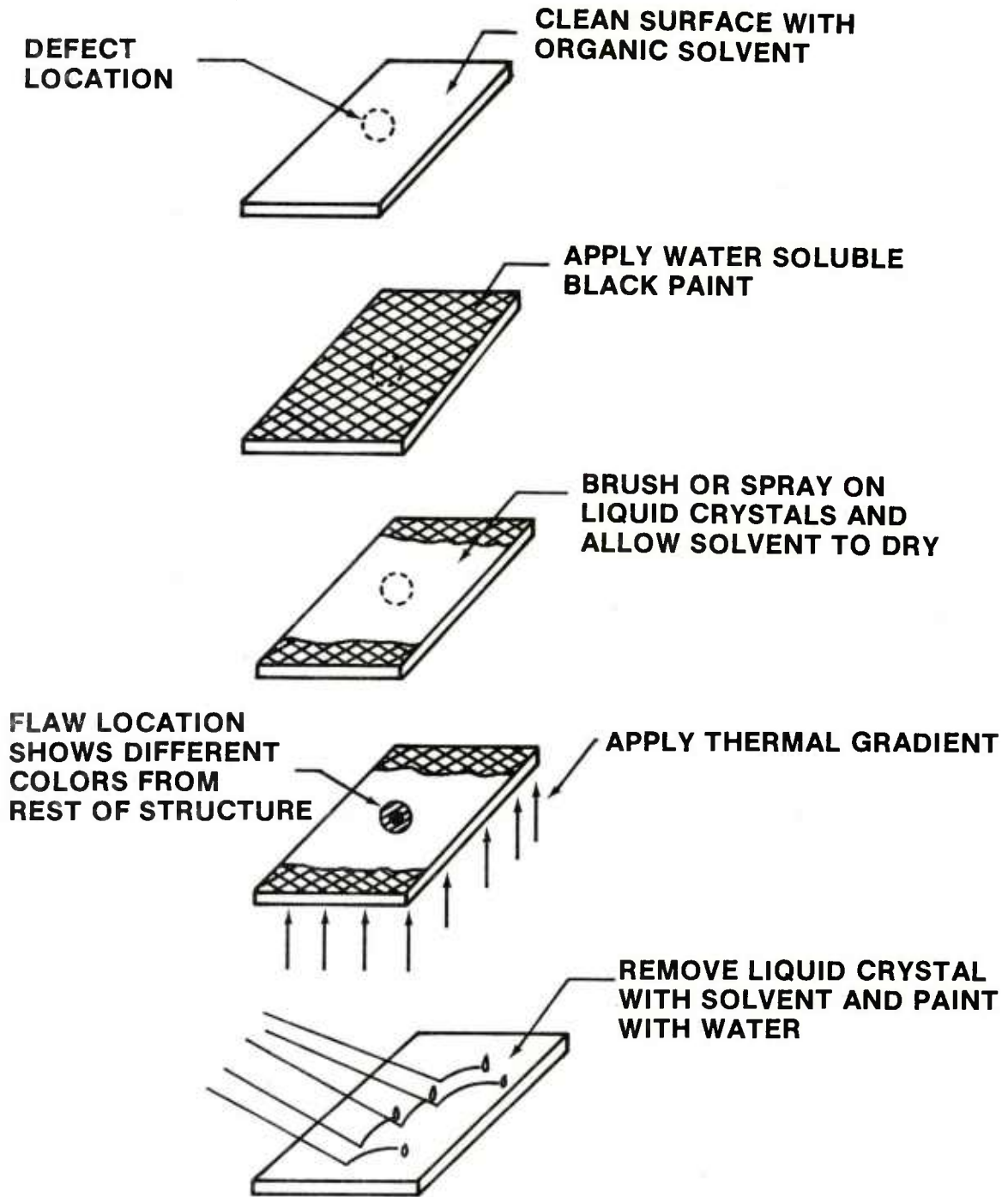


Figure 51. Steps in the liquid crystal solution application.

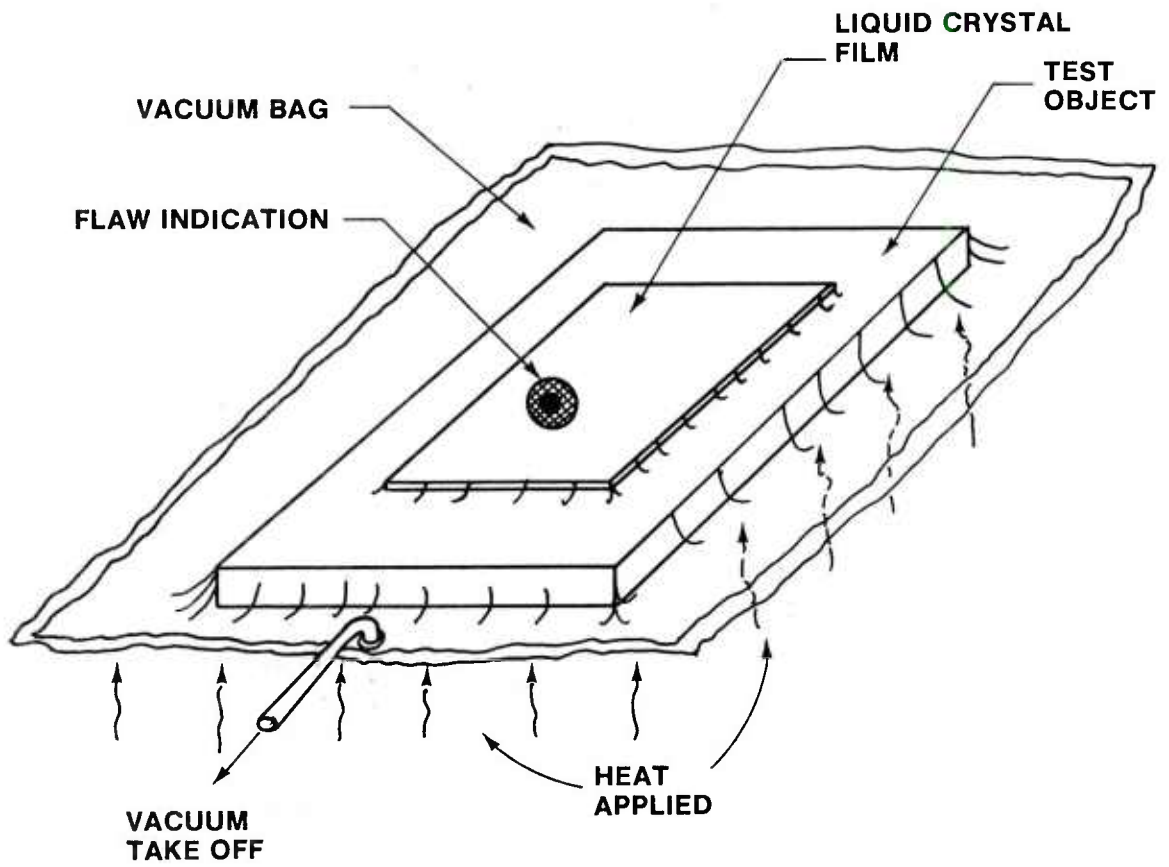
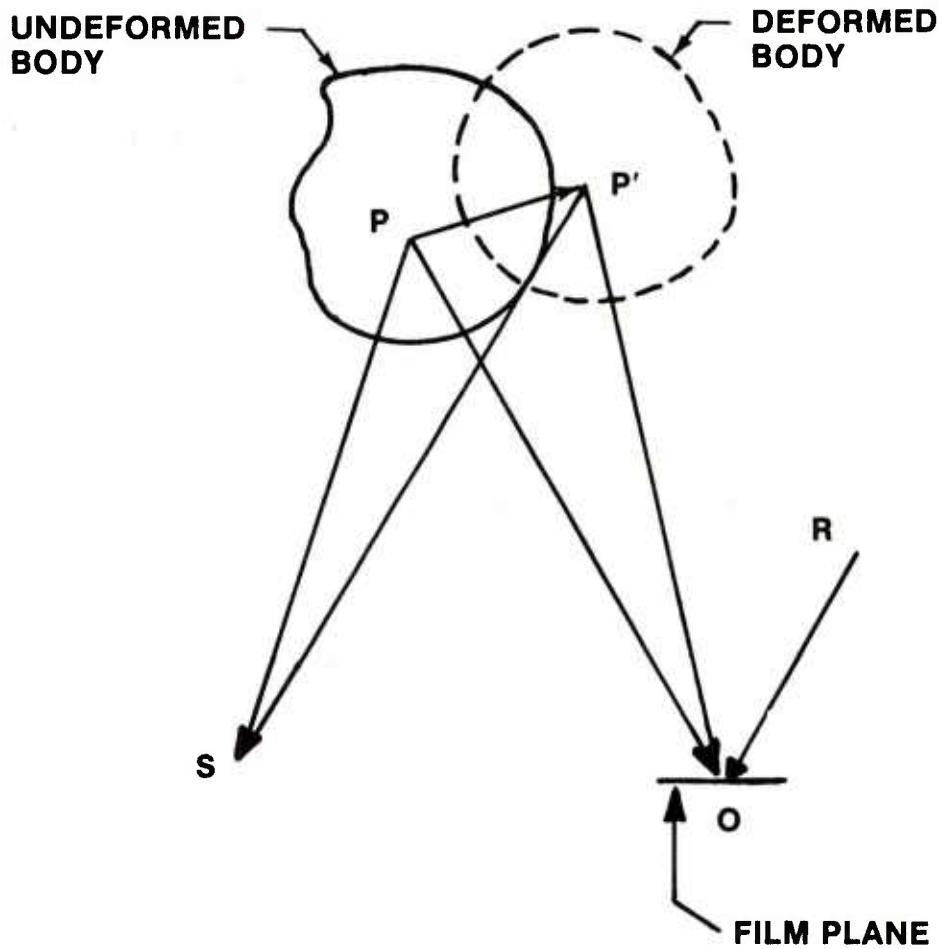


Figure 52. Liquid crystal film test.



**(S) COHERENT LIGHT SOURCE, (O) OBSERVATION POINT,
(R) REFERENCE COHERENT LIGHT SOURCE.**

Figure 53. Typical optical geometry for making holographic Interferograms.

an undeformed body with spatially coherent light; e.g. laser light. A photographic film located at the point O receives diffuse light reflected from a point P on the object as well as coherent light illumination from a source located at R. The film in effect records the phase and amplitude information of the object wave from the undeformed body when the coherent sources of light are turned on. If the film is exposed, photographically processed and replaced back in the film plane as when first exposed then a three dimensional image of the undeformed body may be viewed. This is done by removing the undeformed object and illuminating the film with the reference wave. An image of the object will appear exactly where it originally was if viewed through the hologram in the direction of the original object.

To make a holographic interferogram the following steps are usually taken [61]. First a hologram of the undeformed object is made as before. Second the object is deformed and a second hologram of the deformed body is made by double exposure of the original hologram. The double exposure hologram is then processed photographically and replaced back in the film plane. The body is removed and the hologram is viewed as before. Fringes will appear on the image of the body much like those in *Figure 54*, which is a double exposure holographic interferogram of a composite tube with an embedded circular teflon tape flaw in the filament windings. The flaw may be observed at the center of the tube as a circular region of concentric fringes.

Each fringe is assigned a fringe order when interpreting the interferogram quantitatively. Although interpretation of the data is difficult it may be done. Displacement information of the deformed body is obtained by relating each fringe order to a change in the optical path length from \overline{SPO} in the undeformed body to $\overline{SP'O}$ in the deformed body. Normally three views of the deformed body are required to separate displacement information.

There are several interesting points to be made about holographic interferometry. Displacement data on the order of the wavelength of light can be obtained. Due to the extreme sensitivity of the optical technique vibration isolation is required to make useful interferograms. Not only can the technique be used for static deflection analysis but dynamic vibration analysis as well. Current NDT applications include tire inspection, vibration mode analysis, military component inspection and thermal stress field mapping.

E. Acoustical Holography

The detection of internal structural discontinuities in opaque objects is of serious NDT importance. Although neutron and x-ray radiography are of definite usefulness there

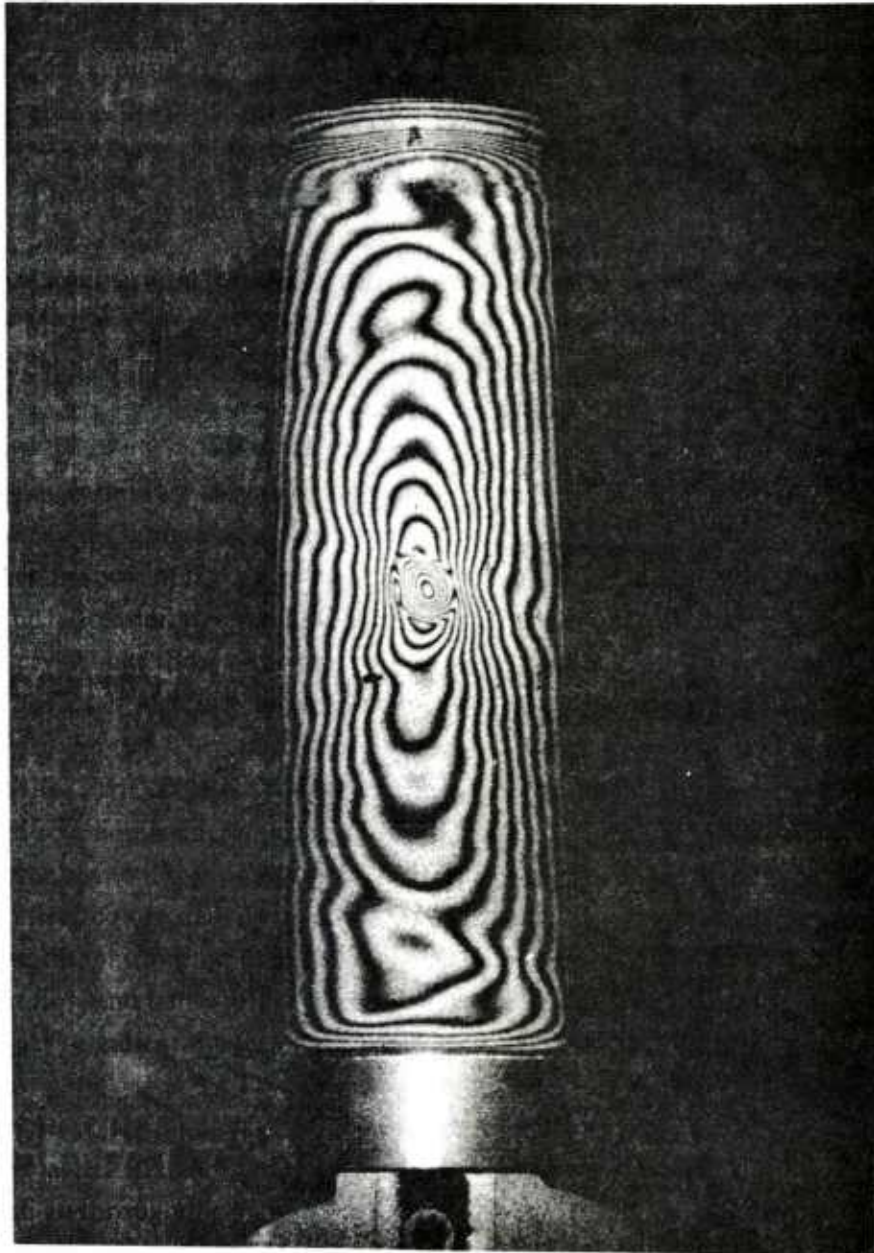


Figure 54. Holographic interferogram of composite tube with circular embedded teflon tape flaw at center of tube.

are many applications where they are either insensitive or dangerous to use. Acoustical holography which is similar to optical holography in many aspects has been developed to fill many of the places where radiographic techniques show less promise. In acoustical holography the coherent light source of optical holography is replaced with an ultrasonic sound wave which instead of reflecting from the object surface transmits through it. Subsurface structural anomalies modulate the sound wave as it travels through the object and may be detected.

Figure 55 illustrates a typical configuration for making acoustical holograms of objects to be NDT tested [62]. In the system shown, an object is placed in a main tank which consists of an acoustical couplant for aiding in the transmission of ultrasound. An object transducer generates continuous plane wave front longitudinal waves which propagate through the object. Acoustical lenses are used to correct aberrations in the transmitted acoustical waves. These waves are reflected to the surface of the acoustical couplant in a minitank using an acoustical reflector. The minitank is used to provide vibration isolation and often has a special liquid for supporting standing acoustical waves. A reference transducer also generates continuous plane wavefront longitudinal waves which are directed toward the minitank. This transducer is analogous to the reference beam used in optical holography. On the liquid surface of the minitank the two acoustical wave fronts interfere to produce an acoustical hologram by modulating the liquid surface.

The acoustical hologram is played back by a laser which illuminates the liquid surface of the minitank. The light reflected from the surface of the minitank is the optical reconstruction of the acoustical hologram and may be viewed by the eye, with photographic film or with video recording equipment. The main features of acoustical holography include real time imaging of flaws and the lack of damaging radiation effects.

F. Speckle Interferometry

Although much less sensitive than holographic interferometry, laser speckle interferometry is a technique growing in popularity for making deformation measurements [63]. Typical applications of the technique include measurements of displacements of loaded structures on the order of a few thousandths of an inch. The technique is largely limited to the measurement of surface deformation of opaque objects. *Figure 56* illustrates the basic method for making laser speckle interferograms. The optically diffuse surface of a structure to be tested is illuminated with coherent radiation. A grainy speckle effect may be imaged by the eye or film plane of a camera due to the interference of light from the structure. The speckle effect is enhanced even further when the structure has microscopic surface irregularities. If the optical

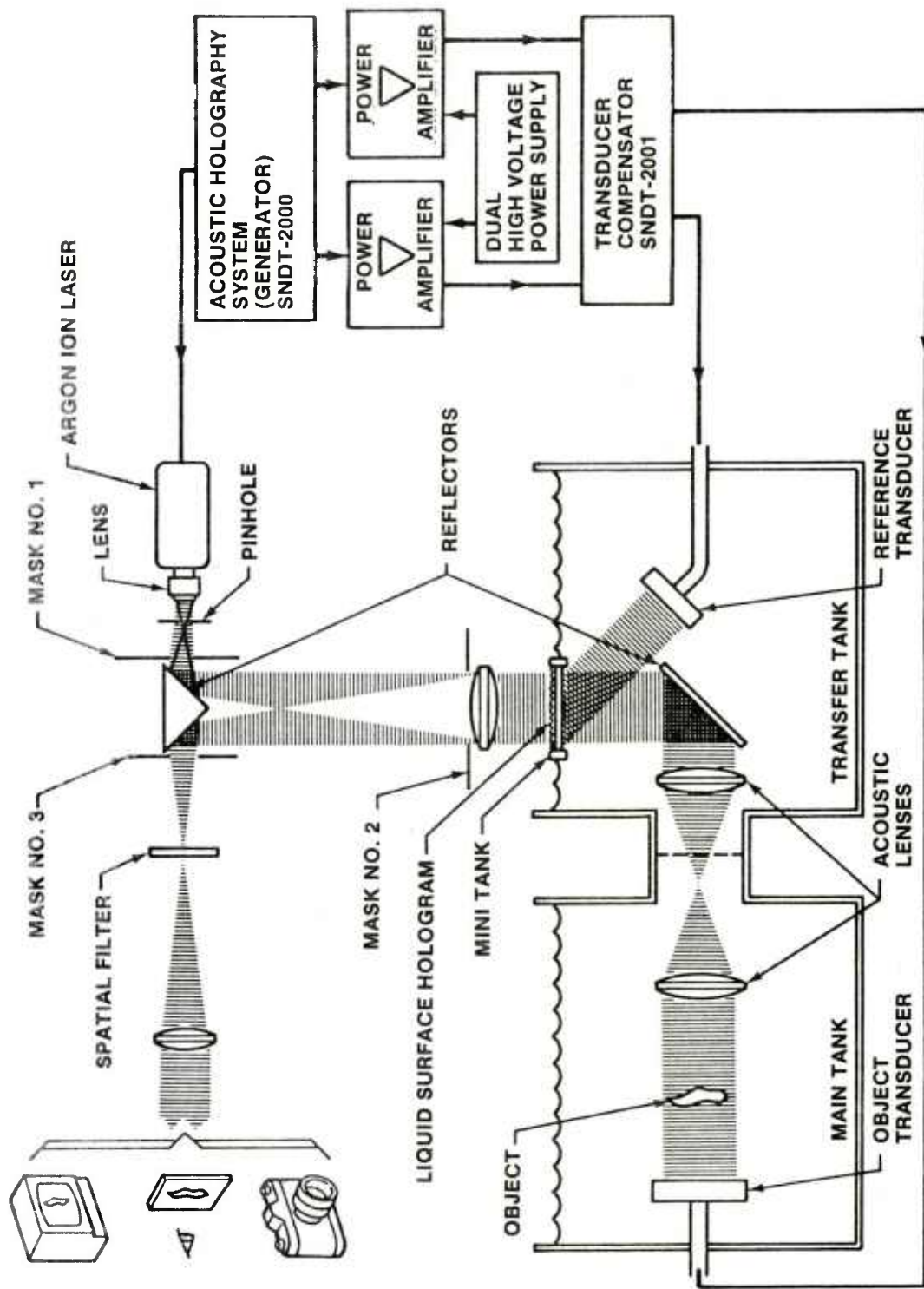
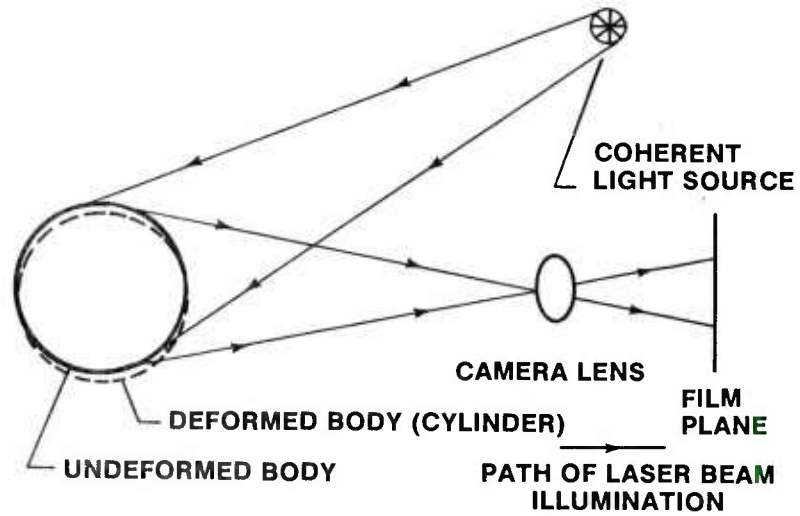


Figure 55. Typical acoustical holography NDT configuration.

(a) Formation process.



(b) Reconstruction process.

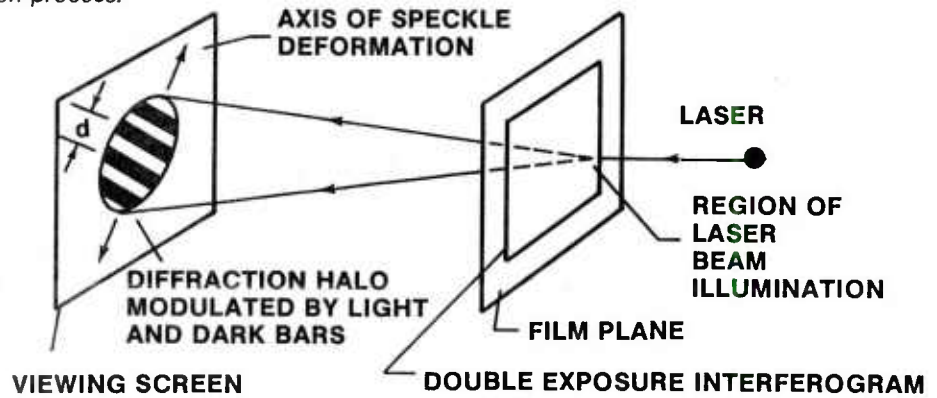


Figure 56. Typical optical configuration for making laser speckle interferograms.

configuration is fixed, the speckle pattern of the test object may be recorded on the film plane of a camera. Now, if the structure is deformed the speckle points shift with the deformation and a second exposure of the deformed speckle pattern may be made.

Speckle interferograms of a structure are normally made by photographing the speckle pattern in a deformed and undeformed configuration using a photographic double exposure. A beam of laser light is then passed through a region of the double exposure where the local deformation is desired. As the beam passes through the film the deformed and undeformed speckle recorded there diffract the laser light and cause an interference effect on a viewing screen. A diffraction halo modulated by light and dark bars of light is produced where the distance d between bars is inversely proportional to the distance between the undeformed and deformed speckle on the film plane. *Figure 57* illustrates the effect. A normal to the light and dark bar pattern indicates the axis of deformation of the speckle.

The laser speckle interferometry technique has been extended to translucent solids, vibrational analysis and temperature induced displacement fields. The technique is generally limited to in-plane displacement measurements without large rotations of speckle in the film plane of the camera.

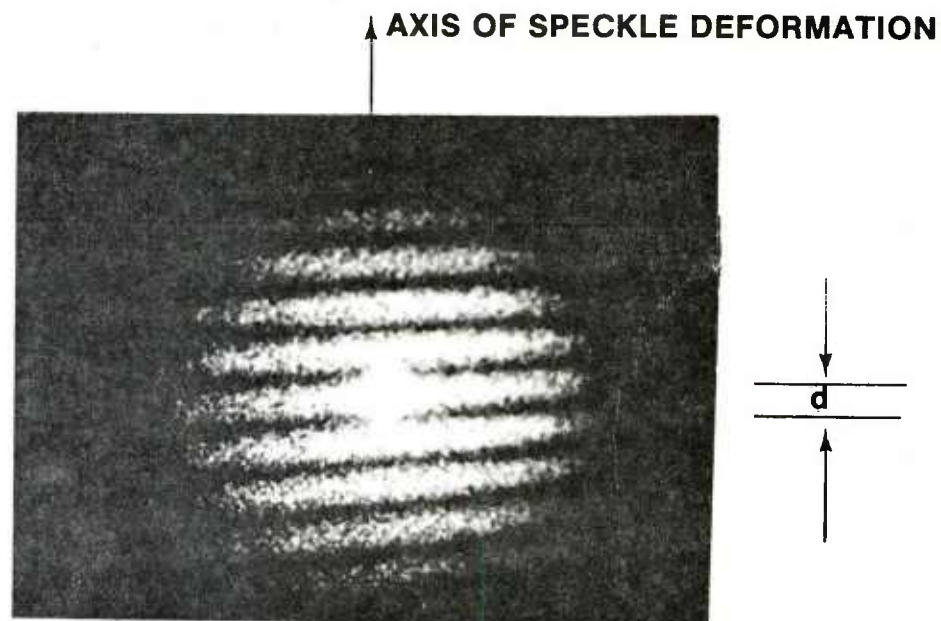


Figure 57. Typical reconstructed diffraction halo modulated by light and dark bars of light.

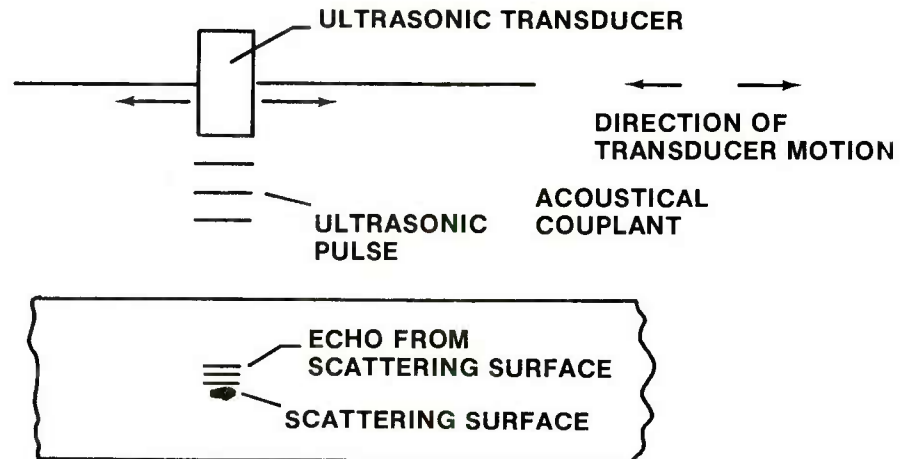
G. Acoustical Speckle Interferometry

When the surface of an object is irradiated with ultrasound small surface irregularities, often in the microscopic regime, they reflect and transmit the ultrasound [64]. These irregularities may be recorded with a receiving transducer to give a mapping of the surface over some small region. If the surface is displaced, the displacement can be determined by examining the displacement of the mapping function.

One of the more important aspects of ultrasound in interferometric measuring is that it has the capability to penetrate into an object. If a scattering region exists within a structure then its displacement can often be predicted. *Figure 58* illustrates two possible configurations for mapping the random ultrasonic interference effects from a structure. In the pulse-echo mode, usually a 1.0-4.0 microsecond pulse of ultrasound from 1.0-10.0 MHz is sent from the transducer to the structure. When the ultrasound encounters the structure-acoustical couplant interface, a portion of the energy is reflected from the interface and the rest is transmitted into the material. If an anomaly exists below the surface, a reflected echo is produced from this scattering surface. In pulse-echo scanning the return echo from the interface and scattering surface is gated, amplified and digitized to produce a map of the echo return amplitude from any layer below or at the interface between the structure and acoustical couplant. The map over a plane region is made by moving the transducer.

Continuous mode scanning utilizes a separate transmitter and receiver transducer. The echo return from some level below or at the surface of the structure is recorded by properly orienting the receiver transducer. As the transmitter and receiver transducers are moved across the surface of the test object their orientation with respect to one another remains fixed. *Figure 59* shows an example of continuous wave scan of a reflecting-scattering layer. In the upper portion of the figure, a pair of transducers are oriented for receiving the return echo from the scattering layer which is homogeneous except for a small inclusion. The transducers are scanned from x' to $x' + x''$ and the return echo amplitude is plotted as a function of x . Graph (a) shows a decrease in the signal amplitude $A(x)$ at x''' due to the presence of the inclusion. This random variation in the echo return is referred to as acoustical speckle. After scanning the undeformed solid, the transducer pair is returned to its starting position at $x = x'$. The solid has now displaced an amount Δx under same load condition and the transducers scan the same scattering layer and the result is shown in Graph (b) as the $A'(x)$ return echo. From the $A(x)$ and $A'(x)$ echoes which are numerically correlated with a computer, Δx is determined.

(a) *Pulse-echo mode.*



(b) *Continuous wave mode.*

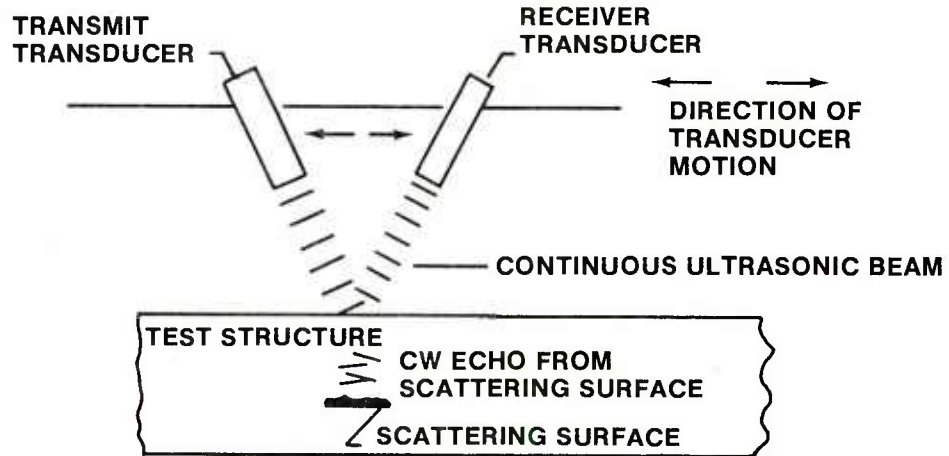


Figure 58. Typical configurations for acoustical speckle interferometry.

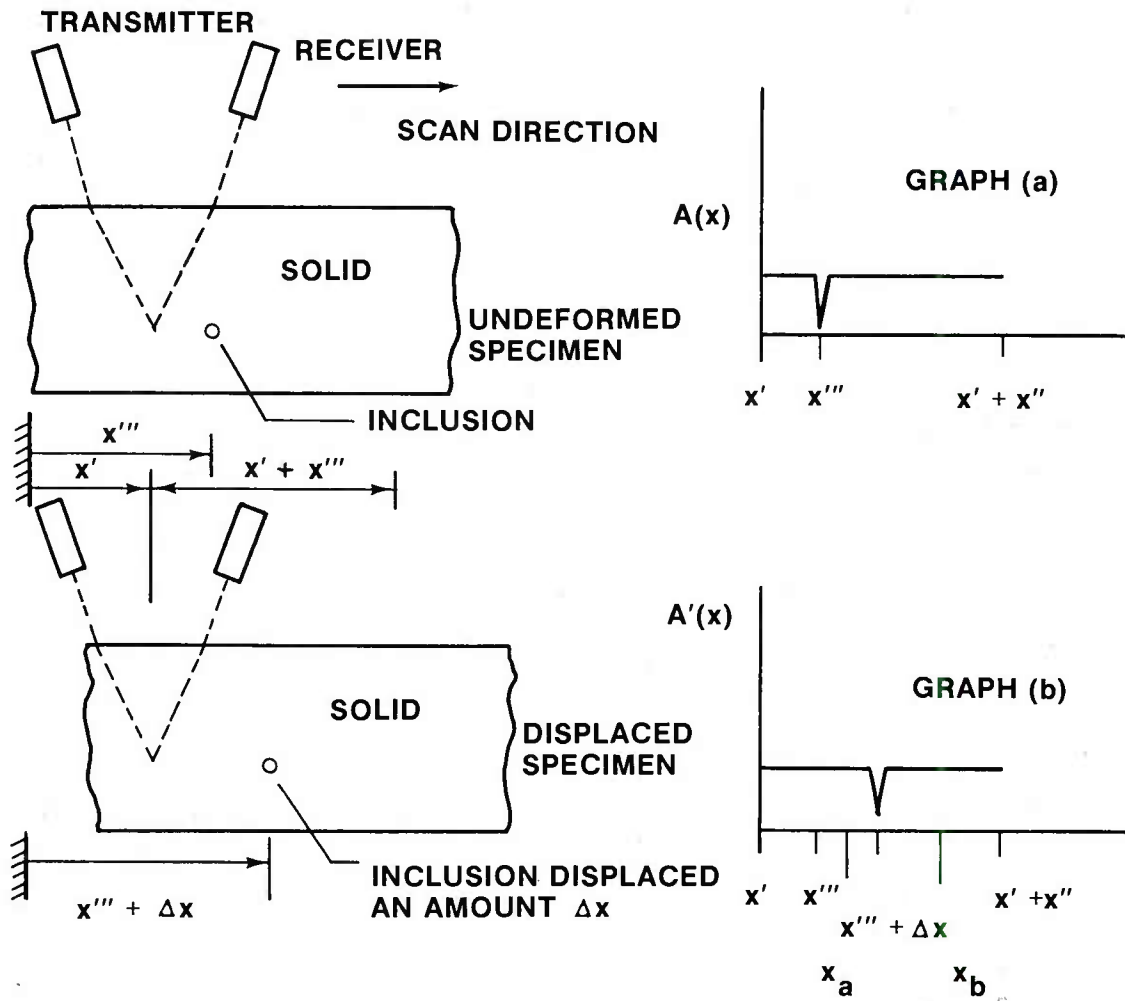


Figure 59. Echo-return correlation in acoustical speckle interferometry.

Acoustical speckle interferometry is currently under development and shows great promise for the future. It may now be used for finding the deformation, both surface and internal, of simply shaped geometrical objects.

V. THE SENSITIVITY AND RELIABILITY OF INSPECTION METHODS

From the viewpoint of fracture mechanics it is important to know the size of the largest flaw which will go undetected during the NDI of a structure. To calculate the fracture stress of a component the fracture mechanics specialist uses an equation of the form [1]

$$K_{IC} = \alpha \sigma_c (\pi a)^{1/2} \quad (9)$$

where K_{IC} is the fracture toughness of the material available from handbooks or from fracture toughness tests on the material; α is a parameter which depends upon the geometry of the specific component and the size, shape and location of the flaw, determined from stress analysis; σ_c is the desired fracture stress and a is the characteristic flaw length. In order to determine the fracture stress, σ_c the designer must either know or assume the size, shape, and location of the flaw. In addition, the designer in calculating crack growth rates and the time-to-fracture of a given flaw must again know the initial size of the flaw. He must insure that the flaw will not grow to critical length during the inspection interval.

These requirements have placed an increased burden upon NDE to quantify the shape-size of the smallest flaw which will be detected (or the largest flaw which will go undetected) during NDI. Moreover the smallest flaw which can be detected by a given method is not the smallest flaw which can be detected at a given confidence level with a given probability of detection. Therefore it is not sufficient to merely specify the smallest flaw which can be detected, one must also quantify the probability of detection at a given confidence level.

A. State-of-the-Art Detection Capabilities

Setting aside for the moment the question of NDE reliability it is instructive to consider the flaw detection capabilities for the five commonly used methods. This capability depends upon many things such as:

- The material.
- Geometric complexity of the component.
- Experience and training of the inspectors.

Thus the demonstrated capability in one situation may be quite different from that of another case. This must be borne in mind when reviewing stated capabilities for the given cases.

Figure 60 is originally from data [65] that has been cited many times before [21,23,36]. The graph shows the sensitivity ratio as a function of crack length. The sensitivity ratio \bar{p} is computed by,

$$\bar{p} = \frac{S}{N} \quad (10)$$

where N is the number of flawed components inspected and S is the number of successful flaw detections. The curves show that quite small flaws can be detected (less than 0.100 inch) but that the probability of detection decreases sharply as the flaw size decreases. The figure also indicates that radiography is not a suitable NDT technique for surface flaws.

Data of similar results [66] are shown in Figure 61 for surface flaws in thin (0.060 inch) aluminum specimens and Figure 62 for surface flaws in thick (0.225 inch) aluminum specimens. These figures both indicate good flaw detection capability for eddy current, penetrant and ultrasonics for surface flaws longer than say 0.10 inch, although sensitivity is greater for the flaws in the thin specimens. Radiography is not sensitive in either case.

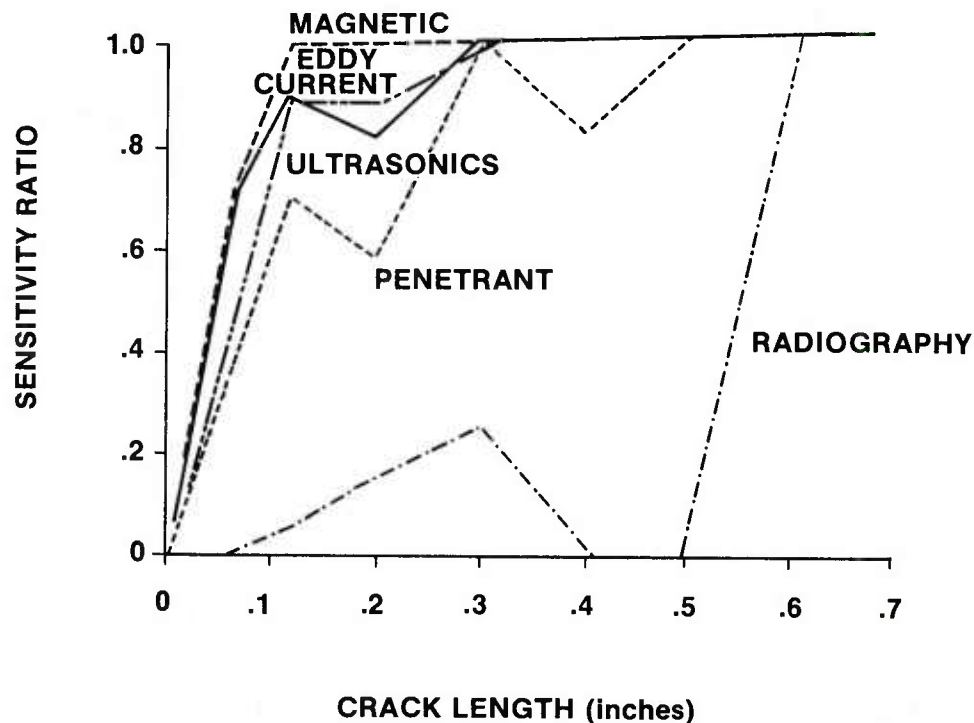


Figure 60. Sensitivity of five NDT methods to surface flaws [21,23,36,65].

NO. OF DETECTED FLAWS/TOTAL FLAWS

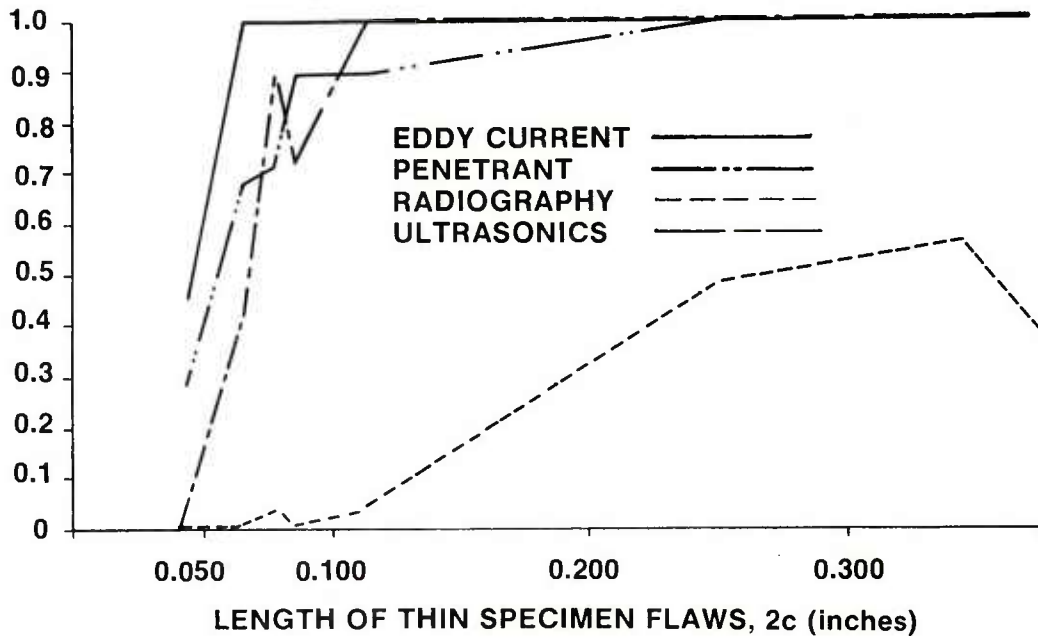


Figure 61. Inspection sensitivity for surface cracks in thin aluminum plates [66].

NO. OF DETECTED FLAWS/TOTAL FLAW

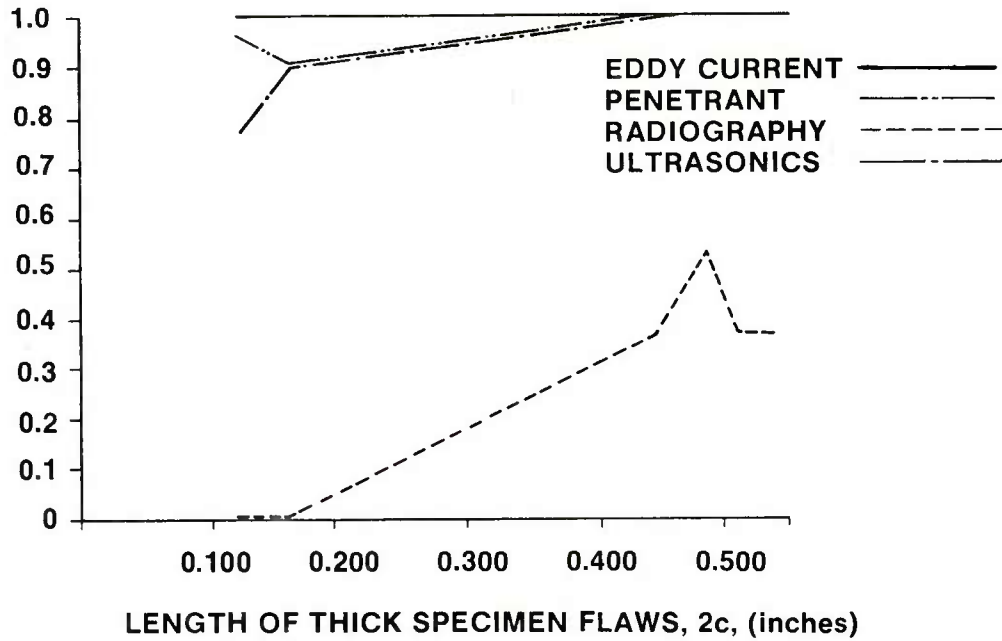


Figure 62. Inspection sensitivity for surface cracks in thick aluminum plates [66].

Anderson's study [66] included flaws of various aspect ratios, $a/2c$, where a is flaw depth and $2c$ is the surface flaw length. Only flaw length is indicated in *Figures 61* and *62*. The effect of surface finish was included by machining specimens having four grades of smoothness varying from a finish of 27-32 μ inch in the fine range to 225-230 μ inch in the rough range. Surface finish had no significant effect for any of the methods except for the penetrant method. The computed significance even for the penetrant was somewhat inconclusive due to contradictory results for the thin and thick specimens. Inspections were made before and after surface etch. No significant change in detection ability due to the surface etch was noted. Detection capability improved following proof test.

Detectable surface flaw sizes by penetrant inspection are shown in *Figure 63* [21,23,36,67]. It was hypothesized that the smallest detectable surface flaw would be given by the hyperbolic curve. This means that the shortest flaw which can be detected depends upon the flaw's depth or the flaw's $a/2c$ ratio Hagemaiier [36] indicates that the bilinear curve (actually a special case of the hyperbolic curve) is perhaps closer to the actual flaw detection limits. This indicates that the shortest flaw detectable by penetrant is about 0.20 inch although from inspection of *Figure 61* it can be seen that at a reduced probability flaws as short as 0.04 inch were detected by penetrant.

Figure 63 can be compared with *Figure 64* [30]. *Figure 64* shows estimated curves of design values for reliable detection of surface cracks. The curves give detectable threshold lengths or depths for each of several inspection methods, and provide an estimate of interaction between crack length and crack depth as it affects detectability. The curves originally were derived from Rockwell International B-1 Division qualification tests on NDE techniques for application to the B-1 program. The curves display a shape that appears to fall somewhere between the hyperbolic and bilinear curves of *Figure 63*.

The surface crack detection probability at a 95 percent confidence level (explained later) of four methods for 2219-T87 was studied by Rummel, et. al. [68,69]. Their data summarized in *Figure 65* indicates that the ultrasonic and eddy current methods are better than penetrant. X-ray is again shown to be very insensitive.

From data of Packman [28] the sensitivities of four methods are shown for finding surface cracks in 4330V steel specimens, *Figure 66*. In the crack length range 0.02-0.05 inch, detectable flaws at a 10-20 percent sensitivity are indicated.

The surface crack detection capability of four methods for finding surface flaws in titanium plates was studied by Lord [70]. Two of the methods, penetrant and surface wave

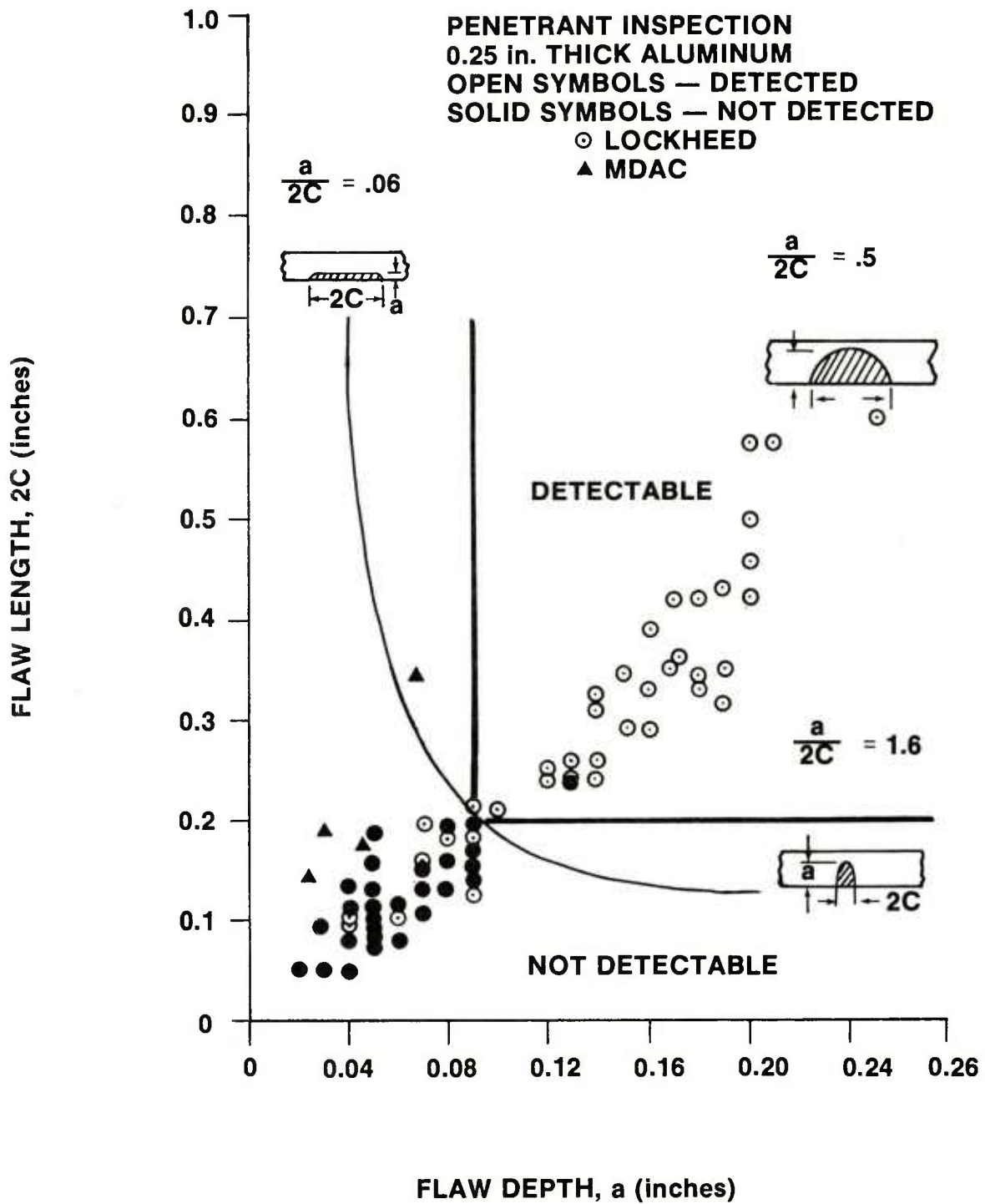


Figure 63. Detectable surface flaw size data [21,23,36,67].

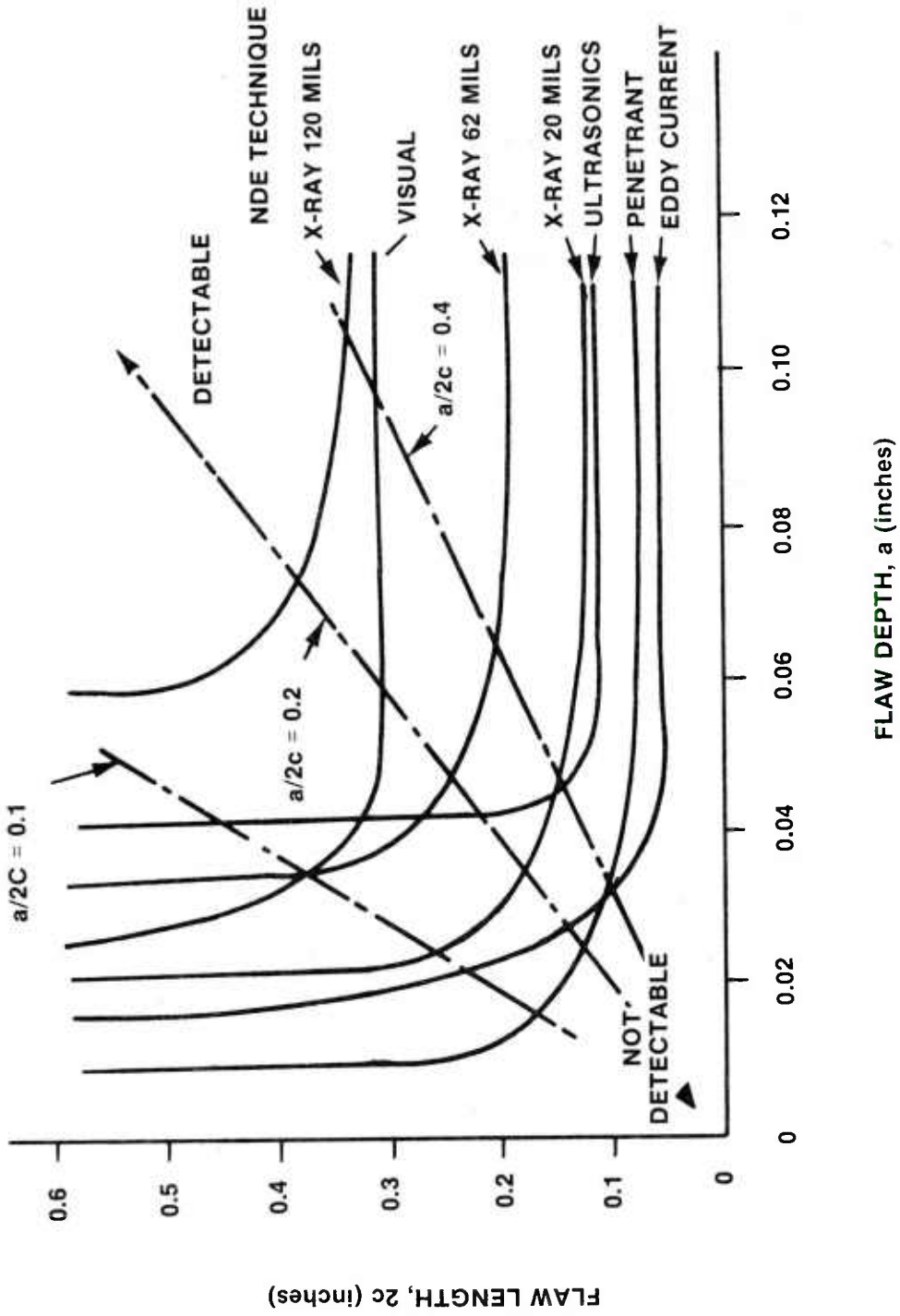


Figure 64. Estimated NDE capabilities for flaw detection for the B-1 program [30].

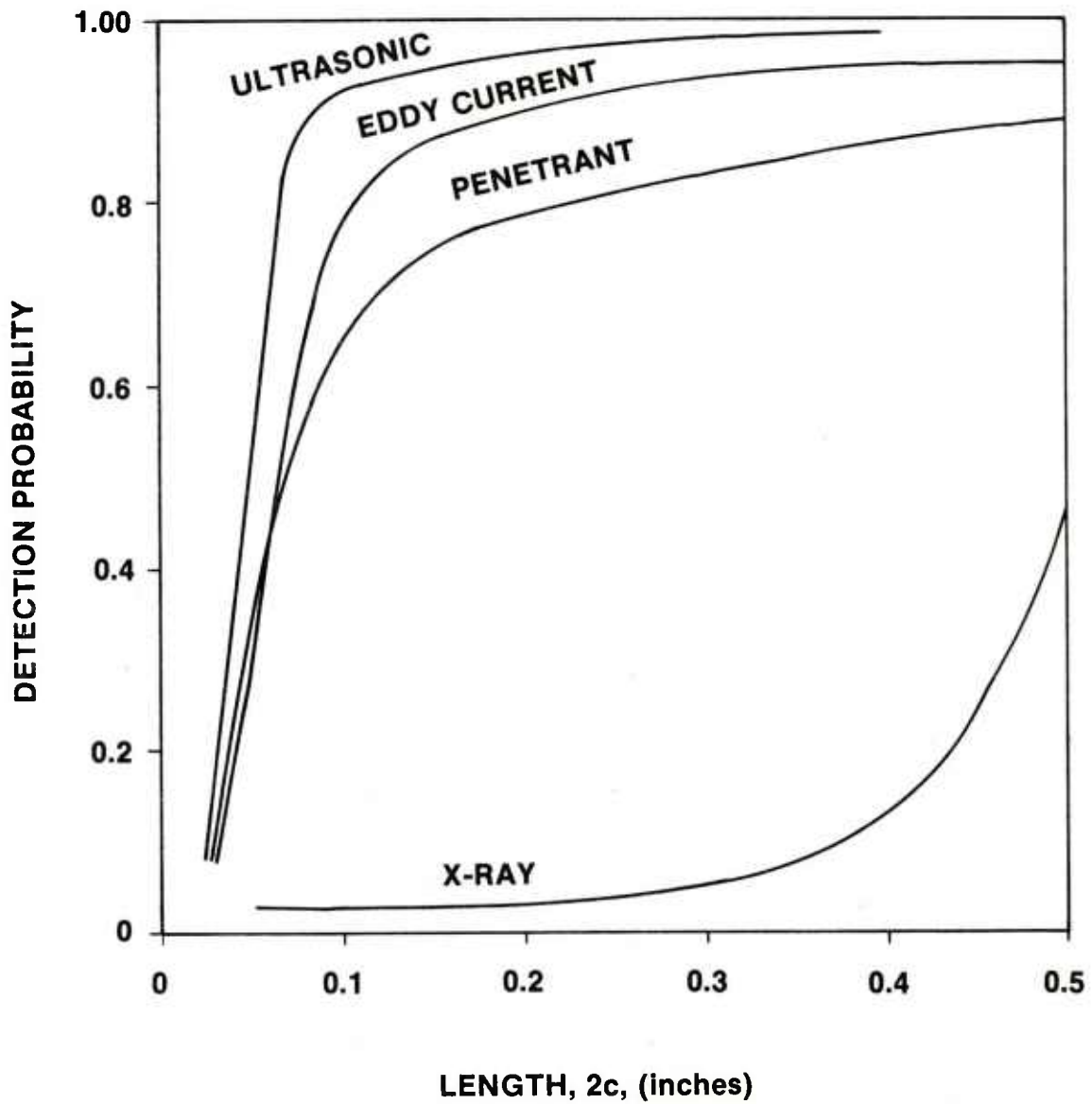


Figure 65. Crack detection probability for surface cracks in 2219-T87 aluminum at 95 percent confidence level [68,69].

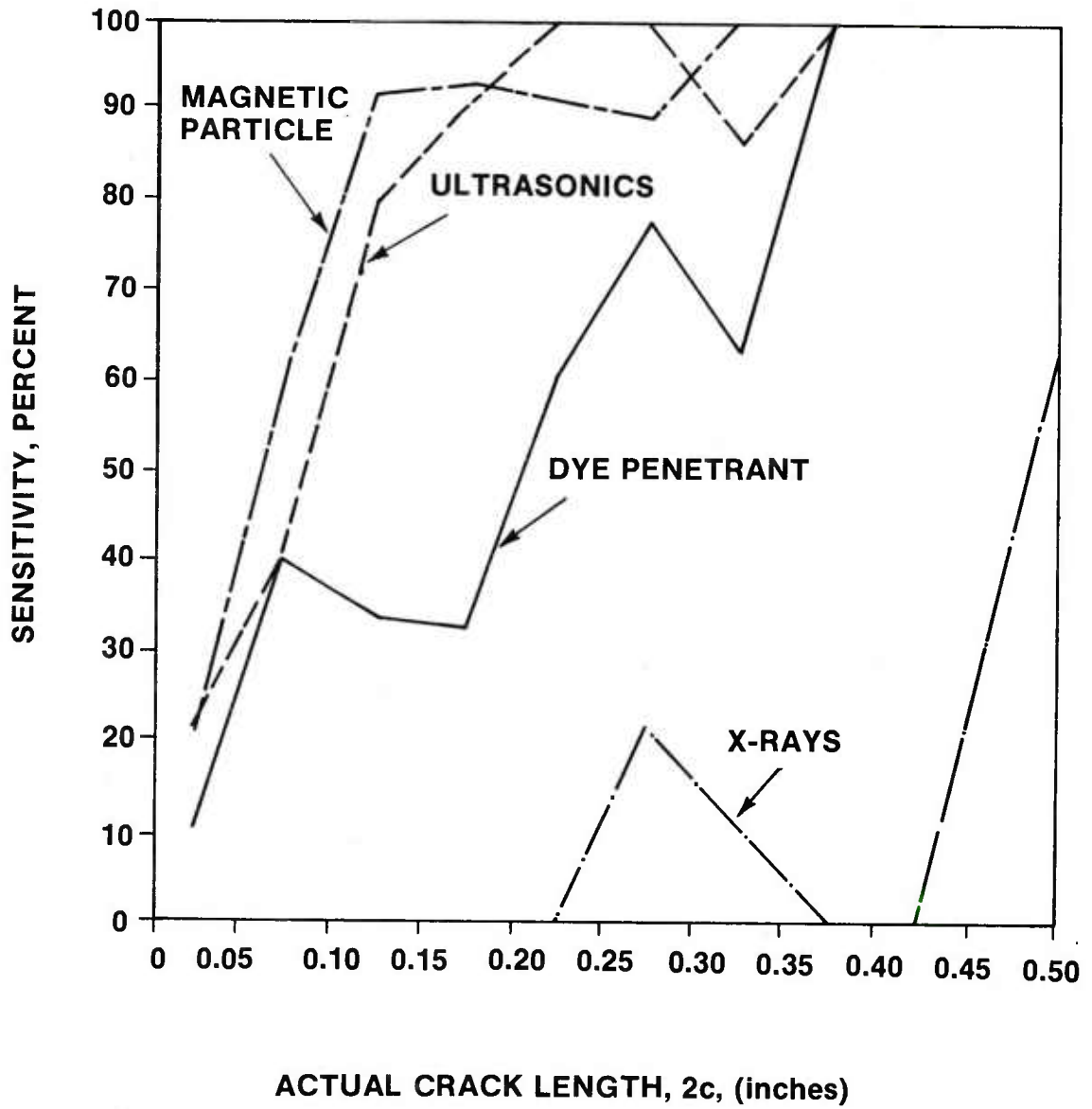


Figure 66. Sensitivity of four methods for finding surface fatigue cracks 4330V steel [28].

ultrasonics are shown in *Figure 67*. Radiography was found to be ineffective. Eddy current was used to inspect fatigue cracks in unfilled fastener holes. The method could detect cracks having depths of only 0.025 inch.

A number of examples have been given of NDT sensitivity; it is appropriate now to consider NDT accuracy in obtaining an estimate of the size of a detected flaw. Packman, et. al. [28] addressed this question by measuring the lengths of cracks in aluminum and steel cylinders. The accuracy, $A_{\text{NDT}}(C)$, of the NDT method in determining the flaw was calculated from

$$A_{\text{NDT}}(C) = 1 - \frac{|2C_{\text{NDT}(i)} - 2C_i|}{2C_i} \quad (11)$$

where $2C_i$ was the true flaw length and $2C_{\text{NDT}(i)}$ was the NDT estimate of the flaw length. The accuracy of the NDT measurements for a large number of specimens was calculated from

$$A_{\text{NDT}}(C) = \frac{1}{N_{\text{f}}(\text{NDT})} \sum_{i=1}^{i=N_{\text{f}}(\text{NDT})} \left(1 - \frac{|2C_{\text{NDT}(i)} - 2C_i|}{2C_i} \right) \quad (12)$$

where $N_{\text{f}}(\text{NDT})$ was the total number of flaws detected in a particular crack length grouping. The index $A_{\text{NDT}}(C)$ does not reflect the ability of the NDT method to detect a flaw but instead is only a measure of the accuracy of the flaw size estimates for those flaws detected. Obviously, when $A_{\text{NDT}}(C)$ approaches unity accuracy is high whereas when $A_{\text{NDT}}(C)$ approaches zero the accuracy is poor. Crack sizes were grouped into eleven size ranges starting with specimens containing no cracks and increasing in 0.050 inch increments to 0.50 inch. *Figure 68* shows the accuracy obtained in the aluminum and steel specimens. For both aluminum and steel the ultrasonic method was the most accurate for small cracks. For larger cracks the dye penetrant and magnetic particle methods were more accurate. Beyond a crack length of about 0.15 inch the accuracy for both materials was in the 0.70-0.90 range.

The capabilities and limitations of several NDT methods have been further discussed by Neuschaefer and Beal [71], for both metal alloy and bonded composite materials. Data collected from the literature are presented in tabular form showing the capabilities of individual NDT methods for various discontinuities and materials.

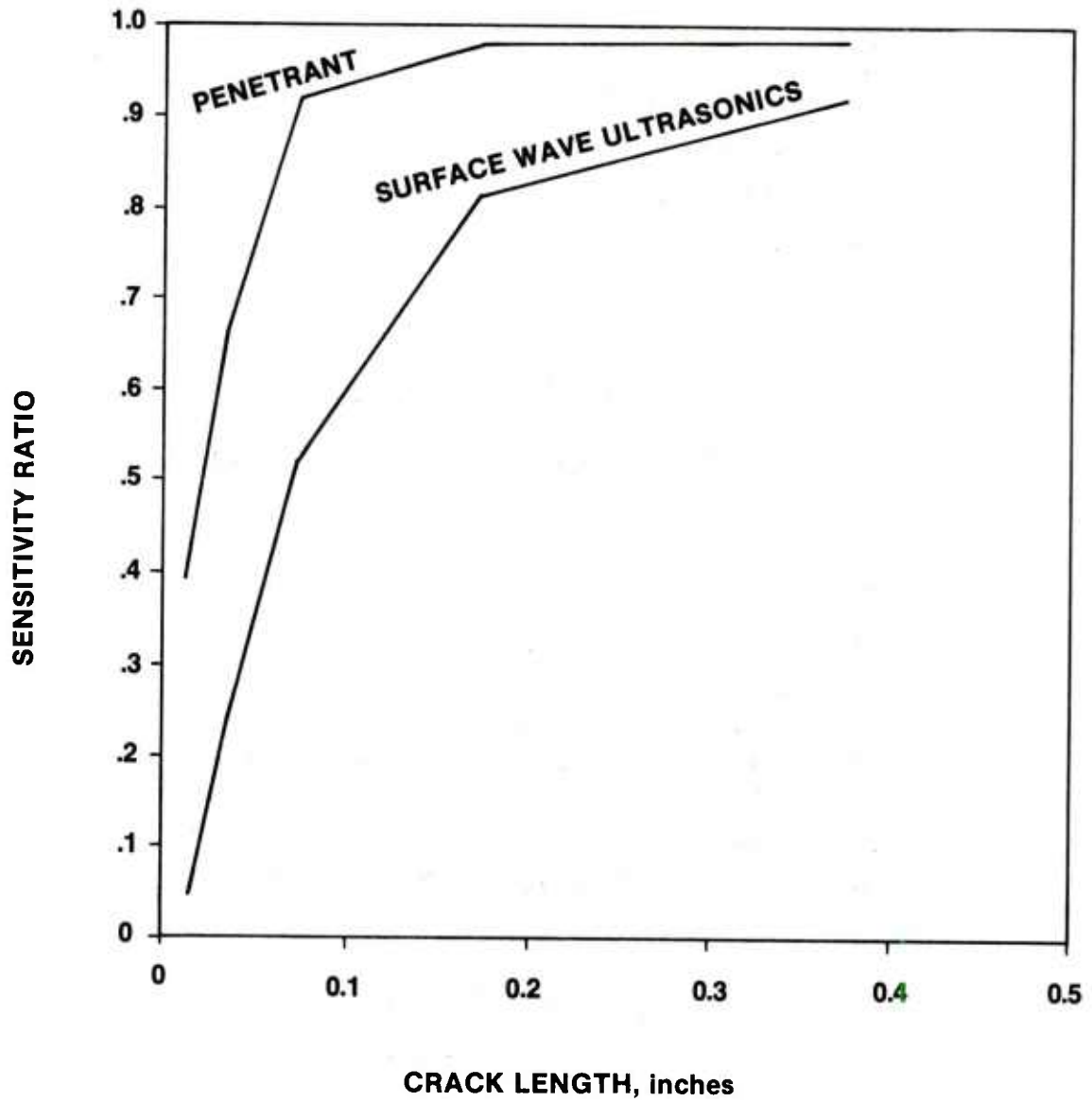


Figure 67. Production inspection capability of two methods for finding surface flaws in titanium plates [70].

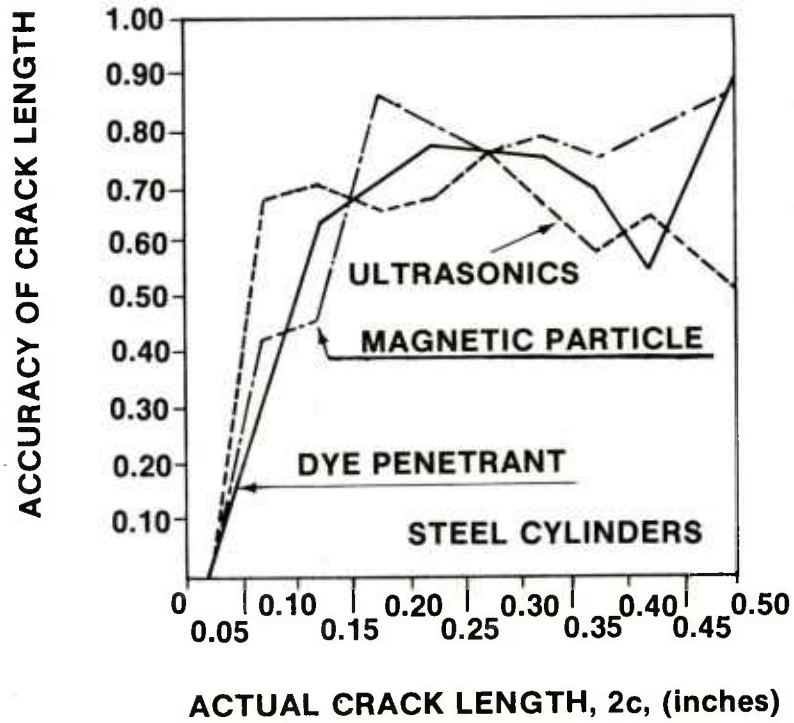
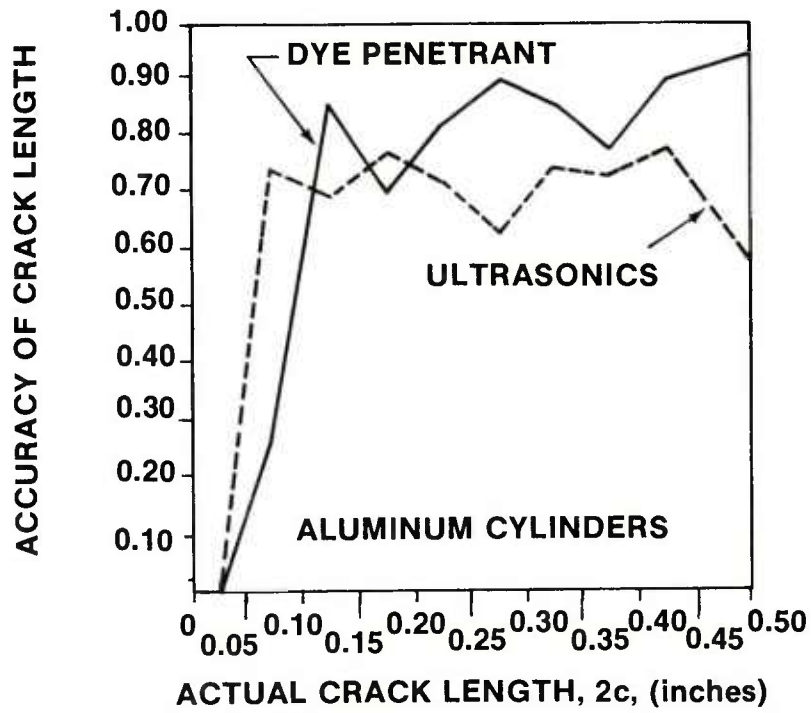


Figure 68. The accuracy of three NDT methods for cracks in aluminum and steel cylinders [28].

B. Reliability of Flaw Detection

Figures 60 through 68 give an indication of the flaw detection capabilities of several methods. It is important to understand that the smallest flaw which can be detected by a given method is not the smallest flaw which can be detected with a high degree of probability or reliability.

In the overall reliability, the influence of method sensitivity may be eclipsed by the adverse affect of other factors such as specimen geometry, conditions of light and temperature under which the inspection is conducted, inspector training and competence and even the mental attitude of the inspector. On the positive side, crack detection of some methods can be enhanced by certain actions. Cracks can be made more detectable by application of a load to hold the crack open; crack detection ability can be increased by a prior proof load [72]; multiple inspections can increase reliability [73]. Often the application of several NDI methods can improve detection reliability [30]. Still, as Forney [74] has pointed out it is one thing to consider the accuracy and sensitivity of a method under laboratory conditions but quite another thing to consider the accuracy of that method when applied by an inspector under field conditions. Flaw detection sensitivities in the laboratory may be measured in the thousandths of an inch while under field conditions $\frac{1}{4}$ to $\frac{1}{2}$ inch may be more reasonable.

The Air Force Material Laboratory conducted a survey to learn just how good inspection results were as practiced by a spectrum of aerospace companies [75]. Twenty-four actual parts containing real flaws were sent to eleven companies for magnetic particle inspection. The companies included airframe, landing gear, and engine manufacturers, as well as private testing laboratories. The flaws ranged from 20 mils to 1 inch long. The results, shown in *Figure 69*, were not as good as one might expect. Most of the companies found about half of the flaws. There were two notable exceptions: one company found about 93 percent of the flaws while another found only 19 percent. While this was not a closely controlled experiment in a statistical sense, it demonstrates a fairly low probability of flaw detection as practiced in the aerospace industry. To quantitatively determine the flaw detection reliability a demonstration program must be conducted. Many things can affect the reliability; therefore the inspection conditions simulated by the demonstration program must be duplicated precisely by the demonstration program. The same inspectors should be used. Specimens must be prepared which accurately simulate the production or in-service flaws. Flawed and unflawed specimens must be mixed and identified by serial numbers only so that inspectors will not know beforehand which specimens are flawed and which are not.

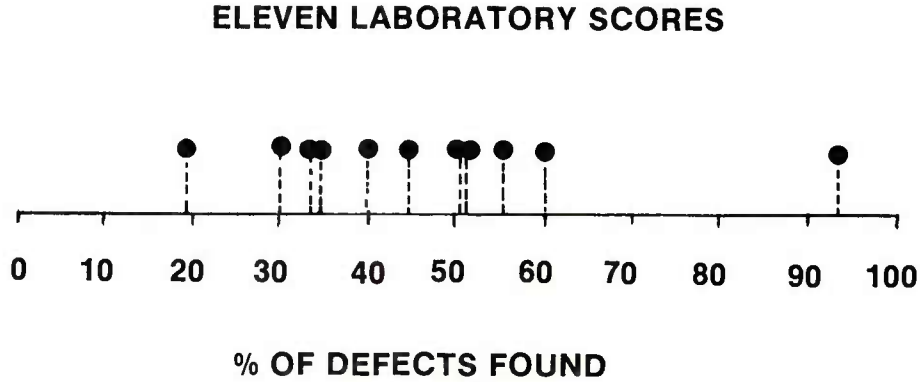


Figure 69. Round Robin test results of eleven laboratories [75].

From S successful crack detections from N -flawed specimens containing a given-sized crack the sensitivity ratio \bar{p} , Equation (10), provides a point estimate of the probability of crack detection. This is not, however, the true probability, p , of crack detection. To find the true probability an infinite number of tests N would be required, so p must remain unknown. The point estimate (sensitivity ratio) \bar{p} will approach p as N is increased. Since fabrication of flawed specimens is expensive, the number of inspections N must necessarily be limited to a practical value. To circumvent the problem of obtaining a good estimate of p a lower bound probability p_L , is computed – a value above which the true probability will lie, not always but at least a certain percentage, $100 G$, of the time. This percentage, $100 G$, is referred to as the confidence level. To assure that the true probability, p , lies above the computed lower bound probability, p_L , most of the time the confidence level, $100G$, should be near 100 percent. To understand how to compute $100G$ and p_L it is first necessary to understand the binomial distribution. The discussion here follows that of Packman, et. al. [76] and Yee, et. al. [77], who have thoroughly discussed the use of the binomial distribution in the statistical treatment of NDE experiments.

Suppose one has N specimen containing cracks. Suppose further that each specimen will be inspected independently so that the true probability, p , (albeit unknown) of finding the crack in each specimen is the same. Each inspection has only one of two possible results; either the crack will or will not be found. Such an event is known as a binomial event. Let S be the number of cracks found, i.e., the number of successful inspections. S has $N + 1$ possible values, i.e., $0, 1, 2, 3, \dots, N$. The probability P that S will equal one of the possible $N + 1$ values, n , is governed by the binomial distribution,

$$P(S=n) = \binom{N}{n} p^n q^{N-n}$$

where

(13)

$$\binom{N}{n} = \frac{N!}{n! (N-n)!}$$

p = the true probability of crack detection

q = $1-p$ is the true probability of missing the crack.

By Equation 13 one can select any possible value of n and determine the probability that S will equal that value of n . If Equation 13 is evaluated for all possible values of n and then summed the results will be unity, viz,

$$1 = \sum_{n=0}^{n=N} \binom{N}{n} p^n q^{N-n} \quad (14)$$

The probability of detecting n or more flaws can be found by summing all probabilities for $S \geq n$, i.e.

$$P(S \geq n) = \sum_{i=n}^{i=N} \binom{N}{i} p^i q^{N-i} \quad (15)$$

If a large number of inspections are conducted the point estimate, \bar{p} , of the detection probability will approach the true value, p . This takes a large number of specimens, each one

containing an identical hard-to-make crack. Instead it is more practical to compute a lower bound probability p_L which will be lower than p most of the time. The lower bound p_L is computed from results of inspection of a number of specimens, and one wishes to have a high degree of confidence that p is indeed larger than p_L . This confidence is measured by the confidence interval G (or $100G$ when expressed as a percentage) computed from

$$1 - G = \sum_{x=S}^N \binom{N}{x} p_L^x (1-p_L)^{N-x} \quad (16)$$

The confidence G is selected arbitrarily; it depends upon how certain one wishes to be that the true probability p indeed exceeds the lower bound p_L . For any given N and S the higher G the lower will be p_L .

What sample size N and how many crack detection successes S must one have in order to demonstrate a given probability of detection at a given confidence level? Suppose one wants a 90 percent detection probability at a 95 percent confidence level (90/95CL) as required by MIL A 83444 [24]. Substitution into (16) yields

$$1 - 0.95 = \sum_{K=S}^N \binom{N}{K} (.9)^K (.1)^{N-K} \quad (17)$$

to solve for N and S . This yields a set of values of N and S of 29 and 29, respectively. In other words, for a sample of 29 flawed specimens all 29 flaws must be detected without a miss. The next combination of N and S is 46 and 45, which means that from a sample of 46 flawed specimens at least 45 flaws must be detected to assure the 90 percent probability at a 95 percent confidence level. The higher the reliability requirements the larger the sample must be to demonstrate the required reliability. A large sampling is required to demonstrate high reliability; the smallest sample possible to demonstrate the 90/95 CL requirements of MIL A 83444 is 29 as noted above.

It is significant that small samples will not be sufficient to demonstrate a high degree of reliability. To use Packman's [76] numbers, suppose a lot of 10 flaw specimens are inspected and only 8 flaws are found. A rough estimate of detection probability is 80 percent, but because of the small sample size the true reliability will be lower and will depend upon the confidence level. For example, if a confidence level of 90 percent is needed then the resulting lower bound detection probability from Equation (16) is only 55 percent. So there is a 90 percent probability

that the true detection ability is greater than 55 percent. If more confidence is needed, the detection probability drops even lower. For example, if 99 percent confidence is needed then the resulting lower bound detection probability is only 38.8 percent. The best reliability that one can demonstrate with a small sample size is rather low. If the inspection had revealed all of the 10 flaws Equation (16) shows that there will be only a 65 percent confidence that the detection probability exceeds 90 percent. Even in an inspection experiment involving a sufficiently large sample the demonstrated probability of detection diminishes sharply if very many flaws are missed. *Table 7* taken from Yee [77] illustrates this for a lot size N of 30 and a confidence limit of 95 percent. The table shows that if 30 of the 30 flaws are detected the detection probability is 0.905 compared to a point estimate of 1.00. If however the number of flaw detections drops to 25 the probability of detection drops to 0.681 while the point estimate value is 0.833. Equation (16) for large N is cumbersome to use, and a number of approximations, including the chi-square distribution, have been used in place of it. Yee [77] includes some of these.

By conducting a statistically suitable inspection experiment for a given crack length, one can calculate the probability of crack detection for a given confidence level. This in theory can be done for a number of distinct crack lengths yielding a curve which gives the probability of crack detection as a function of crack length. An example of such a set of curves is shown in

TABLE 7. LOWER BOUND PROBABILITY OF DETECTION AS FUNCTION OF SUCCESSFUL INSPECTION DETECTIONS IN A LOT OF 30 WITH CONFIDENCE LIMIT OF 95 PERCENT [77]

Number of Successful Detections in 30 Trials (S)	Point Estimate of Probability of Detection (p)	Lower Bound Probability of Detection (pL)
10	0.333	0.193
15	0.500	0.339
20	0.667	0.501
25	0.833	0.681
29	0.967	0.851
30	1.000	0.905

Figure 65. As an example, *Figure 65* shows that the smallest crack which can be detected by ultrasonics with a 90/95 reliability is 0.09 inches. The flaw size for that case that would be used in the design then is 0.09 inch. In conducting an inspection experiment to find the flaw detection reliability as a function of crack length some practical difficulties occur. First, a significant number of specimens are required for each crack length, as already seen. The flaws are usually fabricated by making fatigue cracks, the lengths and exact shapes of which are difficult to replicate. Therefore, instead of finding the reliability for a given crack length, one normally groups the cracks into crack length intervals and determines the reliability for a given crack length interval. The inspection reliability would be determined for specimens where the crack lengths are grouped into equal intervals of say, 0.05-0.10 inch, 0.10-0.15 inch, 0.15-0.20 inch. The question which then arises is to which crack length within a given interval does the calculated reliability apply? Should the detection probability for the first interval be plotted for the smallest crack length, 0.05 inch, the mean 0.075 inch, or the longest, 0.10 inch? To what precise crack length in the interval do the results apply? Packman [76] and Yee [77] discuss a number of ways to handle this problem. The simplest procedure and the most conservative approach is to use the longest crack length in each interval. In other words, detection probability for a given interval should at the least apply to the longest crack per range. Therefore, in plotting detection probability versus crack length one uses as the crack length the upper limit of each interval. This method requires a large number of specimens. As already seen, to demonstrate a 90/95 CL reliability at least 29 specimens are required. Five equal intervals 5 X 29 or 145 specimens would be required. In addition, sharp dips can occur in the inspection reliability curve for this method. This method is straightforward and serves to illustrate the general procedure; the reader is referred to Packman [76] and Yee [77] for a discussion of other methods which yield better behaved curves (no sharp dips) with a smaller number of samples. As an example of the benefit of using either Packman's equal-sample-size, or optimized-probability method over the equal-flaw-size-interval method Packman's curves comparing the three are shown in *Figure 70*. The first method exhibits sharp dips much more prevalently than the other two.

C. The Human Factor in NDE

As seen in Section II, specific requirements for the training and certification of inspectors exist. Still the affect of human error on the reliability of NDI remains one of the strongest concerns in the NDE community. During discussions at the 1977 AGARD meeting [21], speakers continually voiced concern over inspector reliability. Two problems with inspector reliability are outstanding: performance is known to vary among inspectors and performance is diminished by boredom.

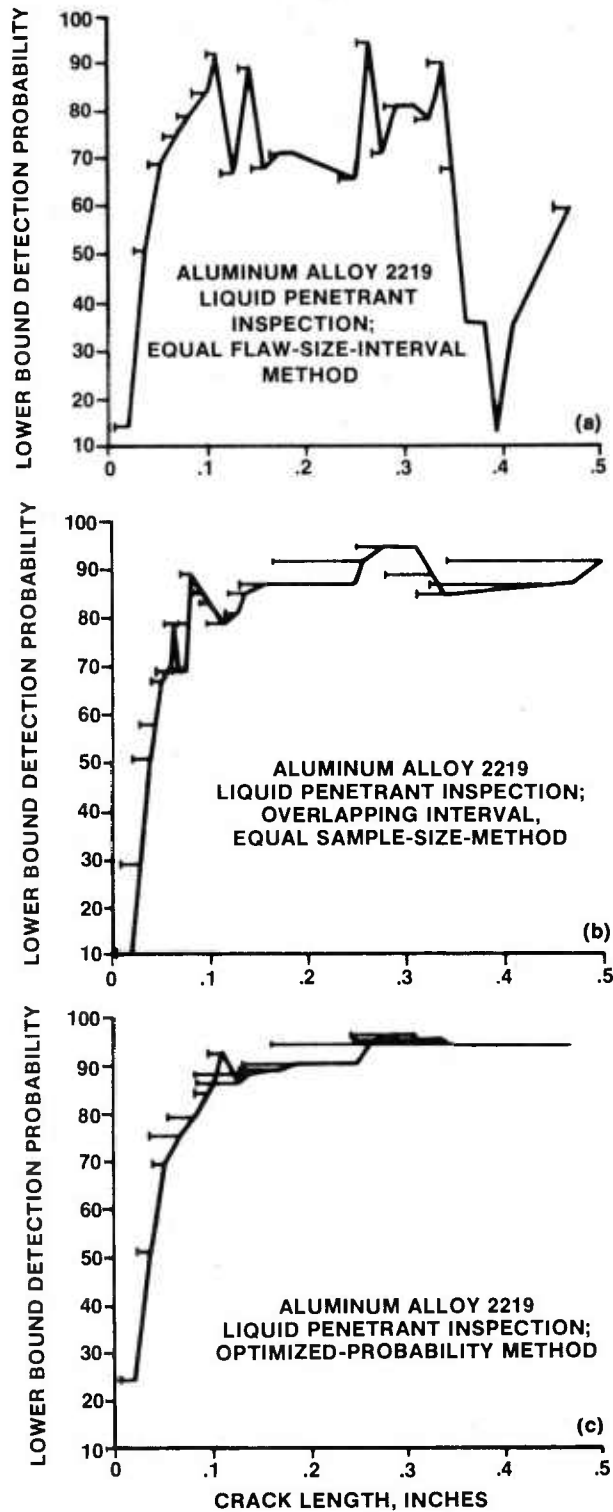


Figure 70. Comparison of lower-bound fatigue crack detection probability by three different plotting methods (95 percent confidence limits [76,77]).

The question of variability of inspector performance was examined recently by Jarfall and Magnusson [78]. Twelve bolted joint sheet specimens 2.5mm-thick, 2024-T3 aluminum were fabricated for use in an inspection program. Each specimen contained 14 bolt holes with bolts. Hence there were (14 X 12 =) 168 possible crack locations. These specimens were then inspected by inspectors from three aircraft operators. *Figure 71* shows the specimen. At the 168 locations a total of 56 fatigue cracks existed. The fatigue cracks were located at the faying surface as shown in the cross section view and were not visible from the outside. All inspectors chose ultrasonics as the most suitable inspection method. Inspectors 1 through 3 conducted the inspection from the countersink side while inspector number 4 inspected from the faying surface side. For comparison an x-ray examination was carried out although due to the presence of the bolthead the method was not sensitive. *Figure 72* shows the difference in the results of the four inspectors using ultrasonics in addition to the x-ray results. Excluding x-ray, of the 56 known cracks one inspector found 46, two inspectors found 47, and one found 55 cracks. The x-ray method was obviously inferior in this case. The performance of the four ultrasonic inspectors is illustrated in terms of crack area, *Figure 73*. It can be seen that two inspectors found cracks as small as 0.5mm^2 where, on the other hand, three inspectors missed a crack of 9mm^2 . In addition, an inspector with experience from the field of civil engineering only was given an opportunity to inspect the bolted joints. He selected the x-ray method and did not find a single crack. This study by Jarfall and Magnusson [78] indicates a considerable variability among inspectors, however it was not stated whether the inspectors were trained or certified under any certification standard such as SNT-TC-1A.

Two similar studies are discussed by Herr [73]— one with the magnetic particle method and one by the Delta Scan ultrasonic technique. The inspectors, representing industries from large manufacturers to small commercial testing labs, were all certified to the applicable specifications. The results from the magnetic particle method are shown in *Figure 74*, which gives the number of inspection trials and the number of misses for each flaw size. Misses for the 0.005 inch crack length are expected but one inspector missed a crack of 0.175 inch length. *Figure 75* shows the misses for a surface flaw inspected by the delta scan method. Again it can be seen that one inspector missed a crack greater than 0.225 inch long. The inspectors knew they were being tested so it is reasonable to assume that their results were better than would have been under production conditions.

Inspector performance reliability under production conditions over a sustained period has not been thoroughly examined. The problem of inspector boredom is of great concern. One has only to recall Kent's example (Section I) of the required inspection of 4000 fasteners in one airplane to appreciate the problem. According to Mar [79] one USAF base commander tried an ingenious but unsuccessful method to combat inspector boredom. These inspectors

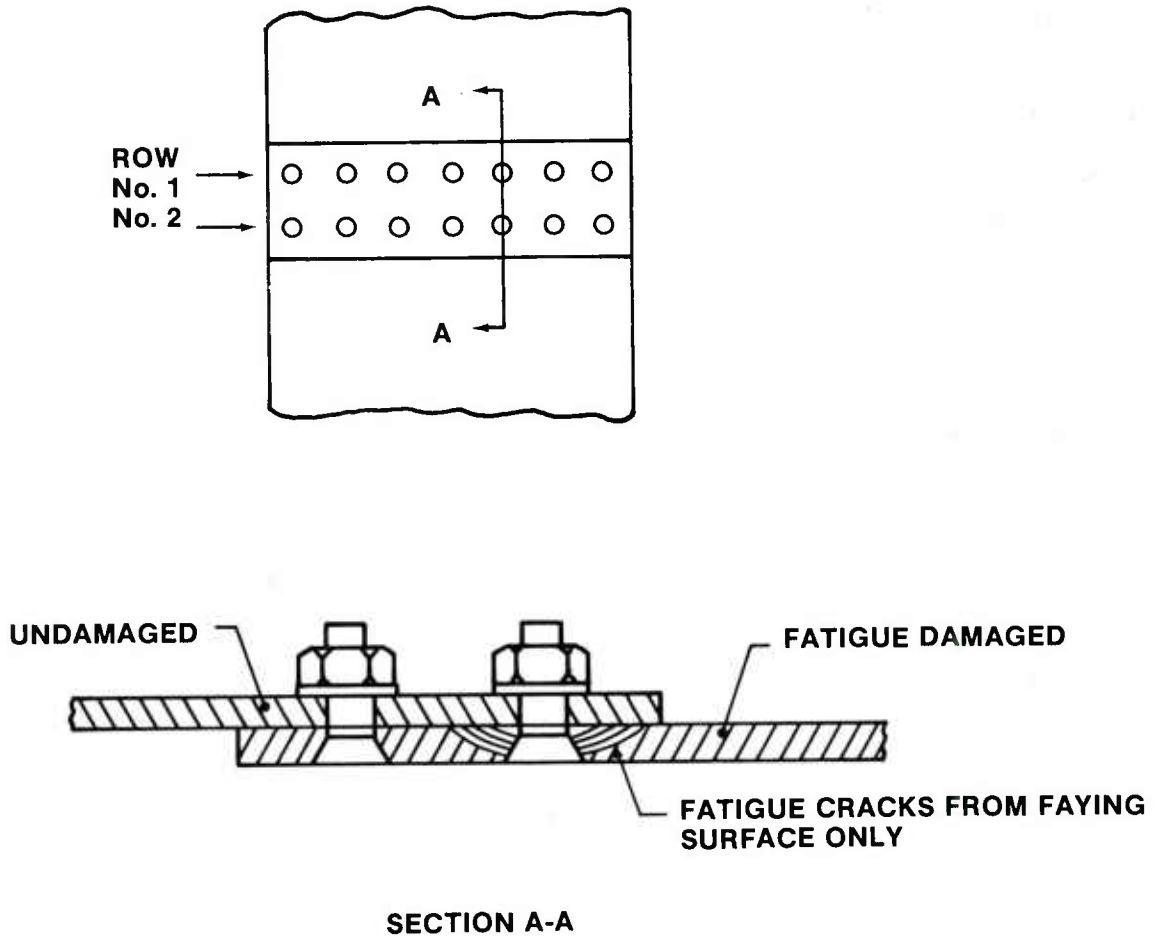


Figure 71. Bolted-joint fatigue-cracked specimen used in an inspection program [78].

	NUMBER OF MARKINGS			
	O	D	N	X
CORRECT DISTRIBUTION	112	56	0	0
INSPECTOR 1 ULTRA SONICS	74	46	10	38
INSPECTOR 2 ULTRA SONICS	112	47	9	0
INSPECTOR 3 ULTRA SONICS	104	55	1	8
INSPECTOR 4 ULTRA SONICS	111	47	9	1
INSPECTOR 5 X-RAY	107	13	43	5

12 SPECIMENS WITH 168 POSSIBLE CRACK LOCATIONS EXAMINED BY EACH INSPECTOR.

O = CORRECT DETERMINATION FOR LOCATION WITHOUT CRACK

D = CORRECT DETECTION OF CRACK

N = CRACK NOT DETECTED

X = CRACK BELIEVED TO EXIST AT LOCATION WITHOUT CRACK

Figure 72. Comparison of inspectors for finding cracks in bolted joints [78].

**NO. OF INSPECTORS
DETECTING THE CRACK**

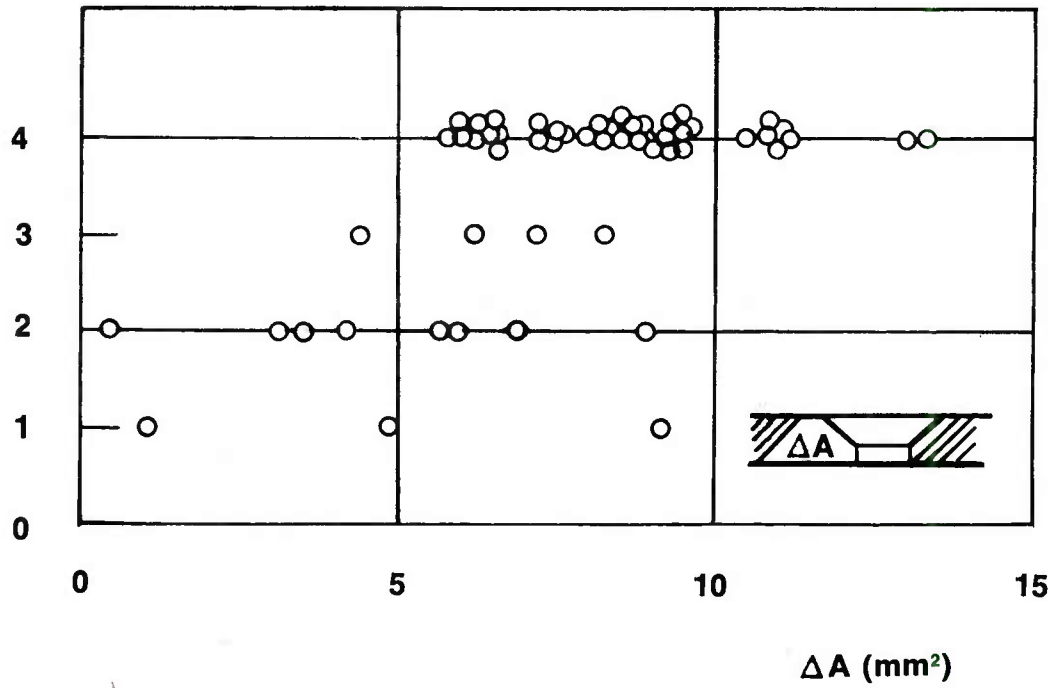


Figure 73. Number of inspectors detecting cracks of various sizes in a bolted joint [78].

<u>FLAW SIZE*</u>	<u>NUMBER OF TRIALS</u>	<u>NUMBER OF MISSES</u>
0.005	16	16
0.010	35	24
0.015	70	13
0.020	307	45
0.025	203	26
0.030	288	11
0.035	163	6
0.040	105	2
0.045	102	6
0.050	164	2
0.055	165	7
0.060	162	1
0.065	44	0
0.070	42	2
0.075	11	0
0.090	39	0
0.100	26	0
0.125	5	0
0.145	13	0
0.150	11	0
0.155	13	0
0.160	23	0
0.175	33	1
0.185	20	0
0.225	5	0
0.240	11	0
0.250	5	0
0.275	13	0
0.330	6	0
0.600	13	0
> 0.600	23	0
Totals	<hr/> 2136	<hr/> 162

*IMPLANTED SURFACE FLAW LENGTH (INCHES).

Figure 74. Crack detection ability of several inspectors using the magnetic particie method [73].

FLAW SURFACE LENGTH (INCHES)*	NUMBER OF TRIALS	NUMBER OF MISSES
LESS THAN 0.075	78	23
0.076 - 0.150	92	5
0.151 - 0.225	63	2
GREATER THAN 0.225	58	1
TOTALS	291	31

*Diameter of a semi-circular (half-penny) shaped flaw. Based upon simulated flaw estimated sub-surface response areas.

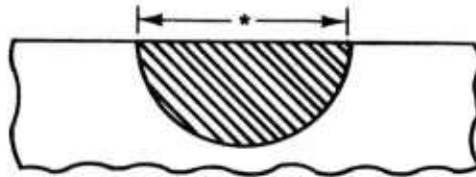


Figure 75. Crack detection ability of several inspectors using delta scan for semicircular surface flaws [73].

had the tedious job of looking for cracks in engine fan blades. The commander offered an all-expense-paid weekend at Las Vegas for anyone who found a crack. After a few days he gave up the idea because no inspectors found a crack. Even this incentive would not keep the inspectors interested in looking for cracks that occurred only once in every 10,000 blades. More automation, and improved equipment may solve some problems of human error associated with judgmental decisions but at the same time automation may contribute to boredom by making the inspector's duties more rote, more repetitive and less demanding of attention.

Aside from the necessary training and certification there is a difficulty in determining who should be an inspector and who should not — which personal qualities make a good inspector, which ones do not, and how one determines if a candidate has the requisite personal qualities. Forney [74] described a good inspector as a person who loves to fish and does not care if he catches anything or not — a person with that kind of patience and serenity. According to Galotto [80] psychologists should determine the qualities which make a good inspector and deal also with the problems of boredom arising from automation.

It is apparent that the overall reliability of NDI may be determined less by the accuracy of the various inspection methods than by a combination of other factors such as the field or production conditions under which the inspection is made and the reliability of the humans who carry out the inspections. It is probably less serious that a crack 0.10 inch long is missed because of test method sensitivity than that a 6 inch crack is missed because a bored or distracted inspector failed to look.

REFERENCES

1. Mullinix B.R. and Smith, D.G., *Fracture Mechanics Design Handbook*, US Army Missile Research and Development Command, Redstone Arsenal, Alabama, August 1977, Technical Report TL-77-8 (Previously Technical Report RL-77-5).
2. Smith, D.G. and Mullinix, B.R., *Fracture Mechanics Design Handbook for Composite Materials*, US Army Missile Research and Development Command, Redstone Arsenal, Alabama, September 1977, Technical Report T-78-6.
3. Berger, H., "Nondestructive Measurements: How Good Are They?," *Materials Evaluation*, Volume 34, Number 1, January 1976, pp. 18A-24A and 33A-34A.
4. *Economic and Management Aspects of Nondestructive Testing, Evaluation, and Inspection in Aerospace Manufacturing*, National Materials Advisory Board, 1977, NMAB-337, AD A049339.
5. Forney, D.M. Jr. and Cooper, T.D., "The Economic Implications of NDE: Opportunities and Payoff," AGARD Conference Proceedings, Number 234, September 1977.
6. Military Standard MIL-STD-1530 (USAF), "Aircraft Structural Integrity Program, Airplane Requirements," September 1972.
7. McMaster, R.C. "The Prevention of Technological Disasters," *Materials Evaluation*, Volume 27, Number 3, March 1969, pp. 17A-18A, 20A, and 22A.
8. North, D.M., "Crash to Boost FAA Scrutiny," *Aviation Week and Space Technology*, June 4, 1979, pp. 12-15.
9. North, D.M., "DC-10 Type Certificate Lifted," *Aviation Week and Space Technology*, June 11, 1979 pp. 47-50.

REFERENCES (Continued)

10. "How Safe?" *Newsweek*, June 11, 1979, p. 34.
11. Feazel, M., "DC-10s Return to Service as Carriers Assess Losses," *Aviation Week and Space Technology*, June 23, 1979, p. 26.
12. Hastings, C.H., "Military Standards for Nondestructive Tests," *Nondestructive Testing Standards—A Review*, ASTM STP 624, Harold Berger, Editor, American Society for Testing and Materials, 1977, pp. 30-37.
13. McMaster, R.C., Editor *Nondestructive Testing Handbook*, The Ronald Press Company, 1963.
14. McGonnagle, W.J., *Nondestructive Testing*, Gordon and Breach Science Publishers, Second Edition, 1966.
15. Schall, W.E. *Nondestructive Testing*, The Machinery Publishing Co. Ltd., 1968.
16. *Quality Assurance, Guidance to Nondestructive Testing Techniques*, Headquarters, US Army Materiel Command, April 1970, AMCP 702-10.
17. *Nondestructive Testing—A Survey*, National Aeronautics and Space Administration, 1973, NASA SP-5113.
18. Carpenter, J.L. and Stuhrke, W.F., *NDE—An Effective Approach to Improved Reliability and Safety—A Technology Survey*, Martin Marietta Corp., June 1976, NASA CR-134963.
19. *Nondestructive Evaluation*, National Materials Advisory Board, June 1969, NMAB-252, AD-692491.
20. Bolis, E. Editor, *Nondestructive Inspection Practices*, Advisory Group for Aerospace Research and Development, North Atlantic Treaty Organization, October 1975, AGARD-AG-201.

REFERENCES (Continued)

21. *Nondestructive Inspection Relationships to Aircraft Design and Materials*, Advisory Group for Aerospace Research and Development, North Atlantic Treaty Organization, September 1977, AGARD-CP-234, AD-A054 206.
22. Berger, H., *Nondestructive Testing Standards—A Review*, ASTM STP 624, American Society for Testing and Materials, 1977.
23. Cooper, T.D., Packman, P.F., and Yee, B.G.W., Editors, *Prevention of Structural Failure, The Role of Quantitative Nondestructive Evaluation*, American Society for Metals, 1975.
24. Military Specification MIL-A-83444 (USAF) "Airplane Damage Tolerance Requirements," July 1974.
25. Packman, P.F., "Fracture Toughness and NDT Requirements for Aircraft Design," *Nondestructive Testing*, Volume 6, Number 6, December 1973, pp. 314-324.
26. Forney, D.M. Jr., "NDI In The United States Air Force," *British Journal of NDT*, Volume 18, Number 3, May 1976, pp. 72-81.
27. Kent, H.M., "Unfulfilled Needs of Nondestructive Inspection of Military Aircraft," AGARD Conference Proceedings, Number 234, September 1977.
28. Packman, P.F., Pearson, H.S., Owens, J.S., and Young, G., "The Applicability of a Fracture Mechanics — Nondestructive Testing Design Criterion for Aerospace Structures," *Metals Engineering Quarterly*, Volume 9, Number 3, August 1969, pp. 52-62.
29. Hastings, C.H., "Nondestructive Tests as an Aid to Fracture Prevention Mechanics," *Journal of the Franklin Institute*, Volume 290, Number 6, December 1970, pp. 589-598.
30. Ehret, R.M., *Fracture Control Methods for Space Vehicles, Volume II Assessment of Fracture Mechanics Technology for Space Shuttle Applications*, National Aeronautics and Space Administration, August 1974, NASA CR-134597.

REFERENCES (Continued)

31. Kaplan, M.P. and Reiman, J.A. "Use of Fracture Mechanics in Estimating Structural Life and Inspection Intervals," *Journal of Aircraft*, Volume 13, Number 2, February 1976, pp. 99-103.
32. Davidson, J.R., "Rationale for Structural Inspections," in *Aircraft Safety and Operating Problems*, Conference held at Langley Research Center, Hampton, Virginia, October 18-20, 1976, NASA SP-416, pp. 355-368.
33. Military Specification MIL-I-6870C, "Inspection Program Requirements, Nondestructive Testing: For Aircraft and Missile Materials and Parts," March 1973.
34. Hagemaiier, D.J., McFaul, H.J. and Radtke, N.H. "Nondestructive Inspection on the DC-10," *Materials Evaluation*, Volume 27, November 1969, pp. 19A-20A and 25A-28A.
35. Hagemaiier, D.J. and McFaul, H.J., "Development of the DC-10 Nondestructive Testing Manual," *Materials Evaluation*, Volume 29, November 1971, pp. 249-255.
36. Hagemaiier, D., "State-of-the-Art Inspection of Aircraft Structures by Nondestructive Testing," Volume 33, September 1975, pp. 217-226 and 231.
37. Air Transport Association of America, Specification for Manufacturer's Technical Data, Nondestructive Inspection Manual, Para 2-9-0, 2-9-1, 2-9-2, May 1, 1967.
38. Recommended Practice for Nondestructive Testing Personnel Qualification and Certification, SNT-TC-1A, American Society for Nondestructive Testing.
39. Berry, F.C., "ASNT Recommended Practice for Nondestructive Testing Personnel Qualification and Certification (SNT-TC-1A) and Its Use," *Nondestructive Testing Standards—A Review*, Harold Berger, Editor, American Society for Testing and Materials, ASTM STP 624, 1977, pp. 53-62.
40. Hovland, H., "The Human Element in Nondestructive Testing," *Materials Evaluation*, Volume 27, Number 12, December 1969, pp. 13A-15A, 18A-19A.

REFERENCES (Continued)

41. Military Standard MIL-STD-410D, "Nondestructive Testing Personnel Qualification and Certification," July 1974.
42. Vary, A., Nondestructive Evaluation Technique Guide, National Aeronautics and Space Administration, 1973, NASA SP-3079.
43. *Nondestructive Testing Introduction RQA/MI and M3-5330.9*, George C. Marshall Space Flight Center, National Aeronautics and Space Administration, January 1967.
44. Flora, J.H., Gruber, H.T., Thomas, R.E. and Meister, R.P. *Multifrequency Eddy Current Inspection for Cracks Under Fasteners*, Air Force Materials Laboratory, December 1976, AFML-TR-76-209.
45. *Detection of Cracks Under Installed Fasteners*, Air Force Materials Laboratory, April 1974, AFML-TR-74-80.
46. Berger, H., Editor, *Practical Applications of Neutron Radiography and Gaging*, ASTM STP 586, American Society for Testing and Materials, 1975.
47. Barton, J.P., "Neutron Radiography — An Overview," *Practical Applications of Neutron Radiography and Gaging*, ASTM STP 586, Harold Berger, Editor, American Society for Testing and Materials, 1975, pp. 5-19.
48. Cutforth, D.C., "Neutron Sources for Radiography and Gaging," *Practical Applications of Neutron Radiography and Gaging*, ASTM STP 586, Harold Berger, Editor, American Society for Testing and Materials, 1975, pp. 20-34.
49. John, J., "Californium — Based Neutron Radiography for Corrosion Detection in Aircraft," *Practical Applications of Neutron Radiography and Gaging*, ASTM STP 586, Harold Berger, Editor, American Society for Testing and Materials, 1975, pp. 168-180.
50. Edenborough, N.B., "Neutron Radiography to Detect Residual Core in Investment Cast Turbine Airfoils," *Practical Applications of Neutron Radiography and Gaging*, ASTM STP 586, Harold Berger, Editor, American Society for Testing and Materials, 1975, pp. 152-157.

REFERENCES (Continued)

51. Dance, W.E., "Neutron Radiographic Nondestructive Evaluation of Aerospace Structures," *Practical Applications of Neutron Radiography and Gaging*, ASTM STP 586, Harold Berger, Editor, American Society for Testing and Materials, 1975, pp. 137-151.
52. Underhill, P.E., and Newacheck, R.L., "Miscellaneous Applications of Neutron Radiography," *Practical Applications of Neutron Radiography and Gaging*, ASTM STP 586, Harold Berger, Editor, American Society for Testing and Materials, 1975, pp. 252-267.
53. Hartbower, C.E., "Detection and Determination of Flaw Size by Acoustic Emission," *Nondestructive Inspection Practices*, AGARDograph Number 201, Bolis, E., Editor, 1975, pp. 387-448.
54. Dunegan, H.L., "Quantitative Capabilities of Acoustic Emission for Predicting Structural Failure," *Prevention of Structural Failure*, Cooper T.D., Packman, P.F., and Yee, B.G.W., Editors, American Society for Metals, 1975, pp. 86-113.
55. Forney, D.M., Jr. in Discussion Summary, Session I, AGARD Conference Proceedings, Number 234, September 1977.
56. van der Shee, E.J. and Bijlmer, P.F.A., "Critical Survey of Methods," *Nondestructive Inspection Practices*, AGARDograph Number 201, Bolis, E., Editor, 1975, pp. 91-128.
57. Green, A.T., Dunegan, H.L., Tetelman, A.S., "Nondestructive Inspection of Aircraft Structures and Materials Via Acoustic Emission," *International Advances in Non-destructive Testing*, 1977, Volume 5, pp. 275-289.
58. Brown, S.P., "Detection of Flaws in Metallic and Nonmetallic Composite Structures Using Liquid Crystal Technology," *Nondestructive Inspection Relationships to Aircraft Design and Materials*, AGARD Conference Proceedings, Number 234, AGARD-CP-234, 1977.
59. Brown, S.P., "Liquid Crystal and Neutron Radiography Methods," *Nondestructive Inspection Practices*, AGARDograph Number 201, E. Bolis, Editor, 1975, pp. 449-459.

REFERENCES (Continued)

60. Leith, E.N. and Uputnieks, J., "Wavefront Reconstruction with Continuous Tone Objects," *Journal of the Optical Society of America*, Volume 53, 1963, pp. 1377-1381.
61. Holloway, D.C., "Holography and Its Application to Photoelasticity," M.S. Thesis (TAM Report 329), Department of Theoretical and Applied Mechanics, University of Illinois, Urbana, Illinois, June 1969.
62. Irelan, V.G., Mullinix, B.R., Castle, J.G., "Real-Time Acoustical Holography," US Army Missile Command, Technical Report T-78-10, Redstone Arsenal, Alabama 35809, October 1977.
63. Archbold, E., Burch, J.M., Ennos, A.E., "Recording of In-Plane Surface Displacement by Double Exposure Speckle Photography," *Optica Acta*, Volume 17, Number 12, 1970, pp. 883-898.
64. Schaeffel, J.A., "Acoustical Speckle Interferometry," US Army Missile R&D Command, Technical Report T-79-39, Redstone Arsenal, Alabama 35809, 22 March 1979.
65. Southworth, H.L., Steele, N.W., and Torelli, P.P., "Practical Sensitivity Limits of Production Nondestructive Testing Methods in Aluminum and Steel," Air Force Materials Laboratory, AFML-TR-74-241, March 1975.
66. Anderson, R.T., Delacy, T.J., and Stewart, R.C., "Detection of Fatigue Cracks by Non-destructive Testing Methods," Convair Aerospace Division of General Dynamics, Report Number GDCA-DBG 73-002, March 1973.
67. Fredrick, S.F., "Service Life of Reusable Structures Based on NDT," McDonnell Douglas Astronautics Co., Report MDC G2668, December 1971.
68. Rummel, W.D., Todd, P.H., Jr., Frecska, S.A., Rathke, R.A., "The Detection of Fatigue Cracks by Nondestructive Testing Methods" (Martin Marietta Aerospace) NASA CR-2369, February 1974.

REFERENCES (Continued)

69. Rummel, W.D., Todd, P.H., Rathke, R.A., and Castner, W.L., "The Detection of Fatigue Cracks by Nondestructive Test Methods," *Materials Evaluation*, Volume 32, October 1974.
70. Lord, R.J., Evaluation of the Reliability and Sensitivity of NDT Methods for Titanium Alloys," (McDonnell Aircraft Company) Air Force Materials Laboratory, AFML-TR-703-107, Volume II, June 1974.
71. Neuschaefer, R.W., and Beal, J.B. "Assessment of and Standardization for Quantitative Nondestructive Testing," George C. Marshall Space Flight Center, NASA TM X-64706, September 1972.
72. Pettit, D.E., and Hoepfner, D.W. "Fatigue Flaw Growth and NDI Evaluation for Preventing Through Cracks in Spacecraft Tankage Structures," Lockheed — California Company, report of research performed under NASA Contract NAS9-11722, September, 1972.
73. Herr, J.C., "Human Factors in NDE" *Prevention of Structural Failure*, Cooper T.D., Packman, P.F., Yee, B.G.W., Editors, American Society for Metals, 1975, pp. 226-241.
74. Forney, D.M., Jr., in Discussion Summary, Session III, AGARD Conference Proceedings, Number 234, September, 1977.
75. Gulley, L.R., Jr., "NDE Horror Stories," Proceedings of the Interdisciplinary Workshop for Quantitative Flaw Definition, Science Center, Rockwell International, Thousand Oaks, California, June 17-20, 1974, Air Force Materials Laboratory Report AFML-TR-74-238, pp. 5-67.
76. Packman, P.F., et. al., "Reliability of Flaw Detection by Nondestructive Inspection," *Metals Handbook*, ASM, 8th Edition, Volume II, 1976, pp. 414-424.
77. Yee, B.G.W., Chang, F.H., Couchman, J.C., Lemon, G.H., and Packman, P.F., "Assessment of NDE Reliability Data" (General Dynamics and Vanderbilt University) National Aeronautics and Space Administration, NASA CR-134991, October 1976.

REFERENCES (Concluded)

78. Jarfall, L., and Magnusson A., "Crack Detection in Bolted Joints," *Nondestructive Inspection Relationships to Aircraft Design and Materials*, AGARD Conference Proceedings, Number 234, AGARD-CP-234, 1977.
79. Mar, J. in Discussion Summary, Session III, AGARD Conference Proceedings, Number 234, September, 1977.
80. Galotto, C.P., in Preface, AGARD Conference Proceedings, Number 234, September, 1977.

APPENDIX A

The following pages, which appeared in AGARDograph No. 201, give two examples of an airplane's NDT manual, referred to in the US Air Force as the airplane's "dash 36." Two distinct types of airplanes are represented; this appendix is for a fighter whereas Appendix B is for a large transport. The manual excerpts are included here to illustrate the high degree to which the airplane's inspection is planned and to illustrate the degree to which the instructions to the inspector are detailed and specified.

T.O. 1F-104A-36S-4

OPERATIONAL SUPPLEMENT**TECHNICAL MANUAL****NONDESTRUCTIVE INSPECTION PROCEDURES**

USAF SERIES

**F-104A, B, C, D
F, RF AND TF-104G (MAP)**

AIRCRAFT

THIS PUBLICATION SUPPLEMENTS T.O. 1F-104A-36 DATED 17 APRIL 1970. Reference to this supplement will be made on the title page of the basic manual by personnel responsible for maintaining the publication in current status.

COMMANDERS ARE RESPONSIBLE FOR BRINGING THIS SUPPLEMENT TO THE ATTENTION OF ALL AFFECTED AF PERSONNEL.

PUBLISHED UNDER AUTHORITY OF THE SECRETARY OF THE AIR FORCE

10 JANUARY 1973

1. PURPOSE.

To add new procedures for inspection of the vertical stabilizer front and rear beam mounting pads.

2. INSTRUCTIONS.

a. In Section III, page 3-35, new paragraphs 3-105 through 3-110 are added as follows:

3-105. F-104 NDI PROCEDURE - Vertical Stabilizer Lower Beams.

3-106. General. Both the forward and rear beams of the vertical stabilizer are susceptible to stress corrosion cracking in the lower beam section, commonly referred to as the mounting pad section. See figure I (Sheet I of 6). This inspection procedure outlines ultrasonic and eddy current techniques to detect cracks without removal of the stabilizer from the aircraft, and without paint removal which is required when using the present T.O. 1F-104A-36 procedures.

3-107. Description of Defects. Refer to figure I (Sheet 2 of 6).

1. Cracks initiating from or extending into the four attaching fastener holes - Inspect using the eddy current bolt hole probe technique.

1

T.O. 1F-104A-36S-4

2. Cracks initiating from or extending into the four counterbore areas of the fastener holes – Inspect using the eddy current pencil probe technique.

3. Cracks extending in the forward-aft direction between the four fastener holes and large cracks extending from steps 1 and 2 – Inspect using the ultrasonic technique.

3-108. Equipment/Materials Required.

1. Ultrasonic Requirements.

- a. Detector-ultrasonic flaw, FSN 6635-018-5829.
- b. Transducer-Type SFZ, 10 MHz, Part No. 57A2279, Automation Industries, Inc., or equivalent. FSN 6635-945-1220.
- c. Calibration Block – 1-inch block of aluminum, see View A, figure 1 (Sheet 3 of 6) or aluminum shear wave test block. FSN 6635-018-5832.
- d. Couplant-Light Grease.

2. Eddy Current Requirements.

- a. Detector, ED-520 Magnaflux Corp or equivalent. FSN 6635-167-9826.
- b. Probe – Bolt hole expandable 1/2 – 11/16-inch. FSN 6635-018-5839, or equivalent.
- c. Probe – Pencil. FSN 6635-409-8845, or equivalent.
- d. Calibration Blocks – See Views A and B, figure 1 (Sheet 3 of 6).

3-109. Inspection Procedures: The order of inspection operation is recommended as follows:

1. Ultrasonic Inspection Procedure.

NOTE

Ultrasonic inspect both front and rear beams for large defects. No fastener removal is required except to confirm "suspect" crack indications.

- a. Remove fillets to expose lower portions of both front and rear stabilizer beams.
- b. Clean and remove rough or loose paint of areas coming in contact with the ultrasonic transducer. Area identified by "U" on figure 1 (Sheet 1 of 6).
- c. Ultrasonic instrument calibration – Position the 10 MHz longitudinal wave transducer on the calibration block directing the sound beam through the one inch thickness. See View A, figure 1 (Sheet 3 of 6). Adjust the sweep length and sensitivity controls to display 10 back reflections on the cathode ray tube (CRT). See View A, figure 1 (Sheet 4 of 6).

d. Adjust the marker controls or use a grease pencil to show 6 inches of material thickness.

e. Apply couplant to the transducer face and place it on the area to be inspected. See View B, figure 1 (Sheet 4 of 6). Adjust the sensitivity control to obtain a 2 inch high signal at the 6.5 inch material thickness marker. This signal will be obtained by moving the transducer slightly until a maximum reflection is received from one of the two fastener holes on the opposite side of the mounting pad. See View B, figure 1 (Sheet 4 of 6), beam No. 1.

f. Scan all inspection areas as indicated on both right and left sides of the mounting pads. Note figure 1 (Sheet 5 of 6), which shows the areas to be scanned. Inspection results will be analyzed as follows:

- (1) Defect signals less than 2 inches in amplitude should be disregarded unless there is a complete loss of back reflection from the opposite side of the mounting pad.
- (2) Disregard defect signals outside the 6 inch marker position on the CRT.
- (3) Disregard signals from the small diameter holes located on the aft edge of the rear beam mounting pad flange. These signals will appear at the 3 inch marker position. Note small diameter holes in View B, figure 1 (Sheet 4 of 6).

CAUTION

Scanning outside of indicated inspection areas will produce false indications. Also, occasional signals may result from fillet areas of base that may appear to be defects. Evaluate these carefully. Note fillet position in View B, figure 1 (Sheet 4 of 6).

(4) Confirm all defect indications by visual (10x), eddy current, or penetrant methods. Stabilizer may have to be removed if defect indications do not come to any exposed surfaces.

2. Eddy Current Inspections – If no defects have been confirmed as a result of the ultrasonic inspection, continue to inspect using eddy current techniques.

NOTE

Remove one attach fastener at a time and inspect for cracks using both the eddy current pencil and bolt hole probes. Confirm cracks by visual or penetrant inspections.

a. Calibrate the pencil probe according to the instructions contained in T.O. 33B2-9-1 using the flat eddy current test block shown in View B, figure 1 (Sheet 3 of 6). This block is an accessory of the ED-520 eddy current tester. Obtain at least a 50 microampere deflection from the 0.020-inch deep slot in the test block. Record equipment settings for ease in resetting equipment when pencil probe and bolt hole probe are used alternately for each hole and counterbore inspection.

b. Calibrate the 9/16-inch diameter bolt hole probe (used for front beam holes) according to instructions contained in T.O. 33B2-9-1 using the test block shown in View A, figure 1 (Sheet 3 of 6). An alternate and easier technique is to insert the probe in the 5/8-inch diameter test hole and press the tip of the probe away from the hole wall and note deflection of needle. Adjust lift-off control until there is no needle deflection when the tip of the probe is moved away from the hole wall. During this operation the needle is brought on scale with the balance control. Adjust sensitivity controls (both function control and screwdriver adjustment) until at least a 50 microampere deflection is obtained from the slot in the hole. Again, record equipment settings for ease in resetting between alternate inspections with the pencil probe.

The 5/8 and 11/16-inch diameter holes in the test block are used if probes other than the 9/16-inch diameter probe is used for the rear beam inspections. Record equipment settings if more than one eddy current bolt hole probe is used.

c. Remove one of the four fasteners from the front beam mounting pad and clean all foreign material from the hole and counterbore. Do not remove paint.

d. Using the pencil probe, scan the fillet radius and all surface areas inside the counterbore. Scan all accessible radii and internal surfaces on exposed areas of the mounting pads. (See View A, figure 1 (Sheet 6 of 6).)

CAUTION

Scanning near sharp outside radii or steel such as fasteners will produce edge effect, resulting in sharp downscale deflections resembling defect indications.

e. Remove pencil probe and replace with 9/16-inch diameter bolt hole probe. Position controls to previously recorded positions. Check operation using test standard hole.

f. Adjust the collar on the probe to inspect for defects at the edge of the hole at the counterbore. Rotate in a 360° circle and note any sharp downscale deflections. (See View B, figure 1 (Sheet 6 of 6).)

g. Continue to inspect the entire length of the fastener hole in 0.100-inch increments.

h. Confirm indications detected using eddy current inspections by visual (10x) or penetrant inspections.

i. Reinstall the fastener after proper corrosion protection and remove second fastener. Inspect with bolt hole probe and pencil probe (counterbore area) after proper cleaning.

j. Complete inspection of front beam inspection by removing and inspecting one fastener at a time.

k. Repeat inspection of rear beam holes, counterbores, and adjacent areas similar to the front beam inspection.

l. Record and report all cracks for proper disposition.

b. Figure 1 (Sheets 1 through 6) of this supplement is figure 3-19 (Sheets 1 through 6) of the basic manual.

T.O. 1F-104A-36S-4

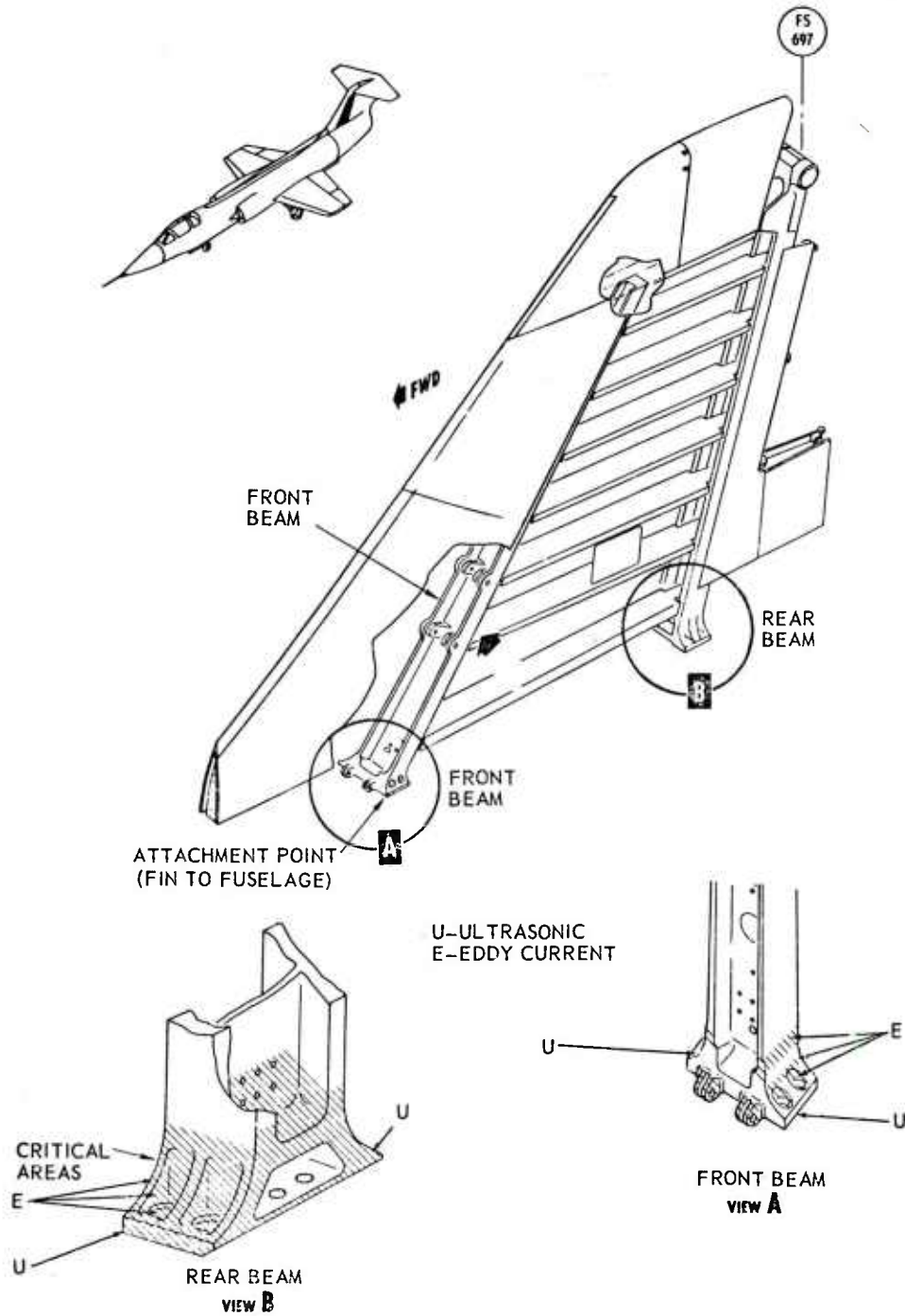


Figure 1. Forward and Rear Beams (Sheet 1 of 6)

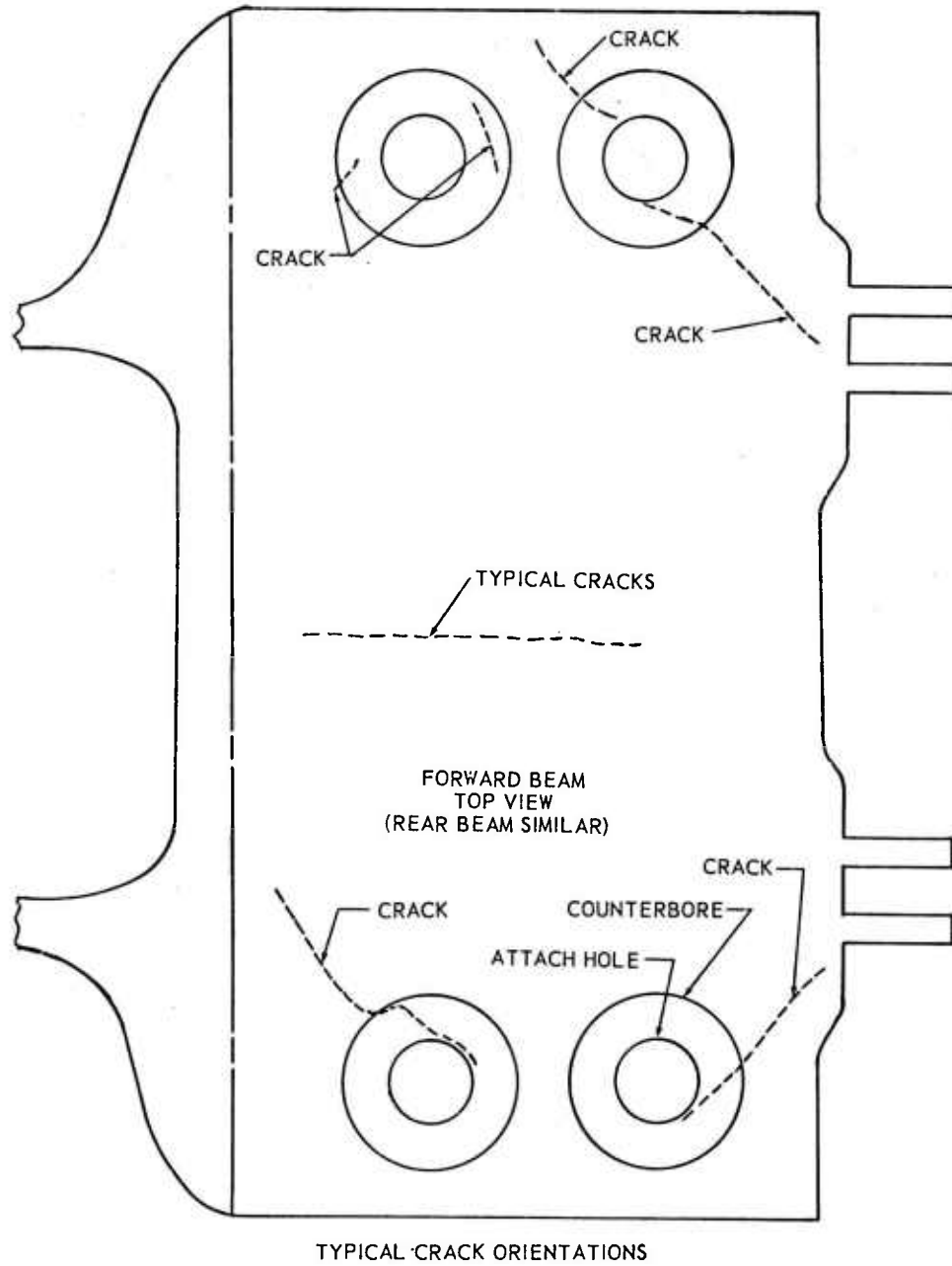
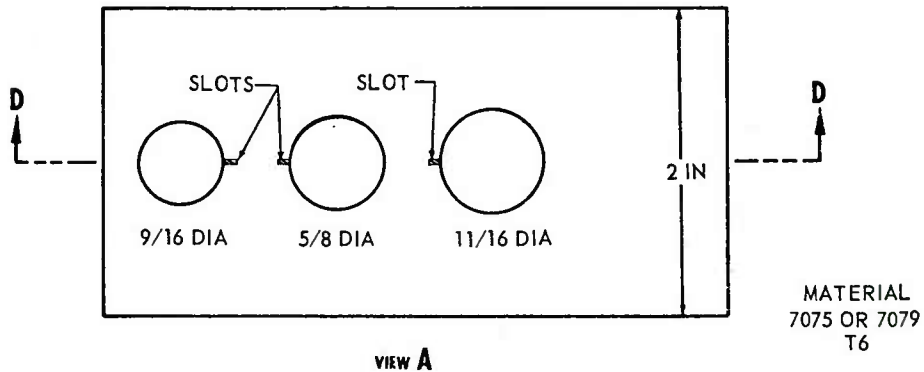


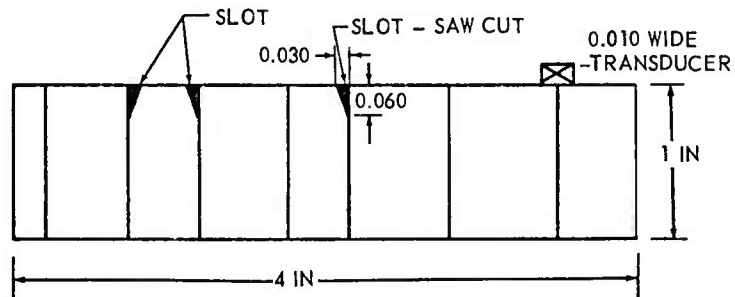
Figure 1. Forward and Rear Beams (Sheet 2 of 6)

T.O. 1F-104A-365-4

STANDARD ULTRASONIC & EDDY CURRENT BOLT HOLE

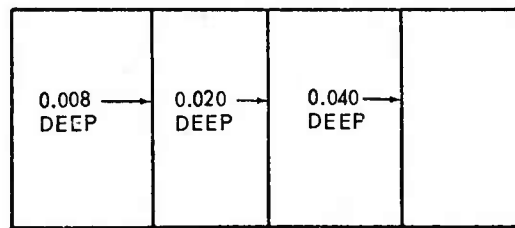


VIEW A



SECTION D-D

TEST BLOCK-EDDY CURRENT PENCIL

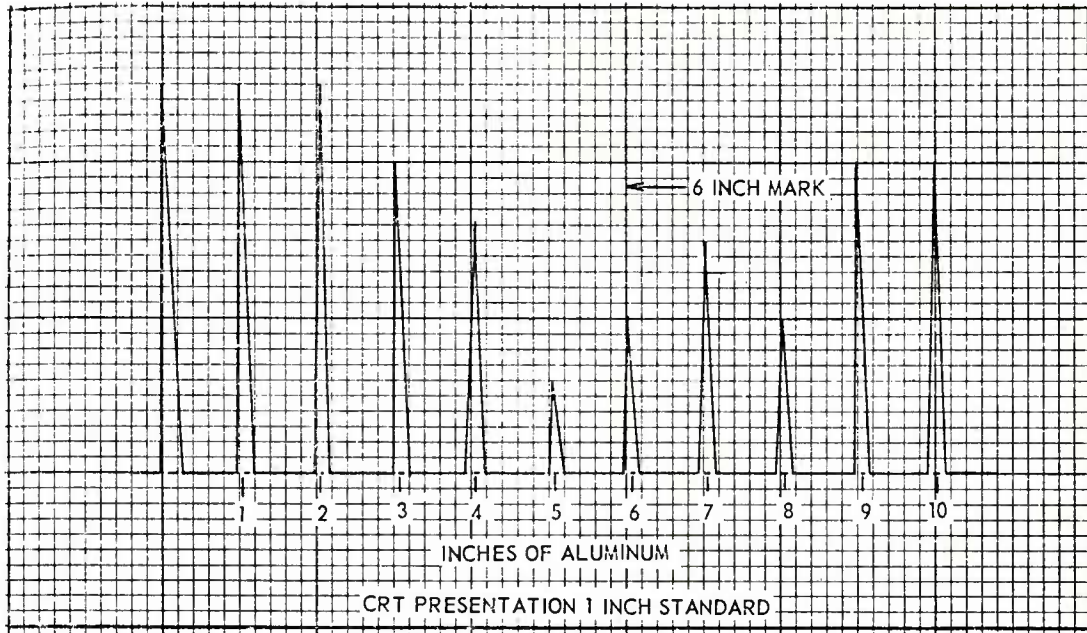


VIEW B

BLOCK FURNISHED
WITH ED-520
3-1/8 X 1-3/8 X 5/16
SLOT WIDTH 0.006

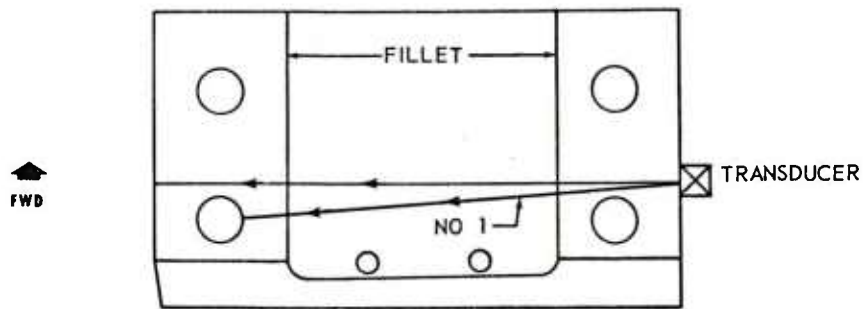
Figure 1. Forward and Rear Beams (Sheet 3 of 6)

T.O. 1F-104A-36S-4



VIEW A

ULTRASONIC CALIBRATION



VIEW B

REAR BEAM (FORWARD BEAM SIMILAR)
LOOKING AT BOTTOM

Figure 1. Forward and Rear Beams (Sheet 4 of 6)

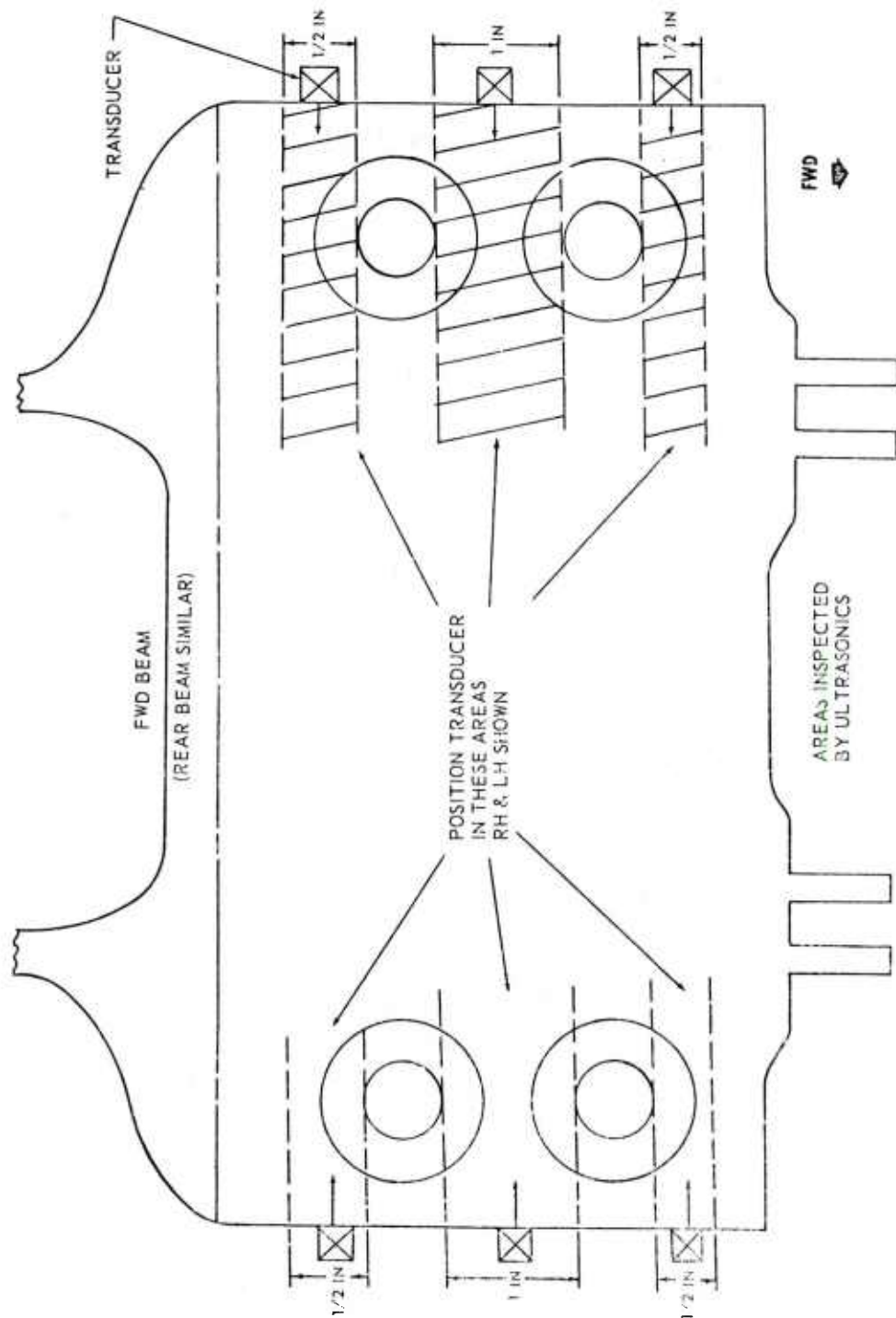
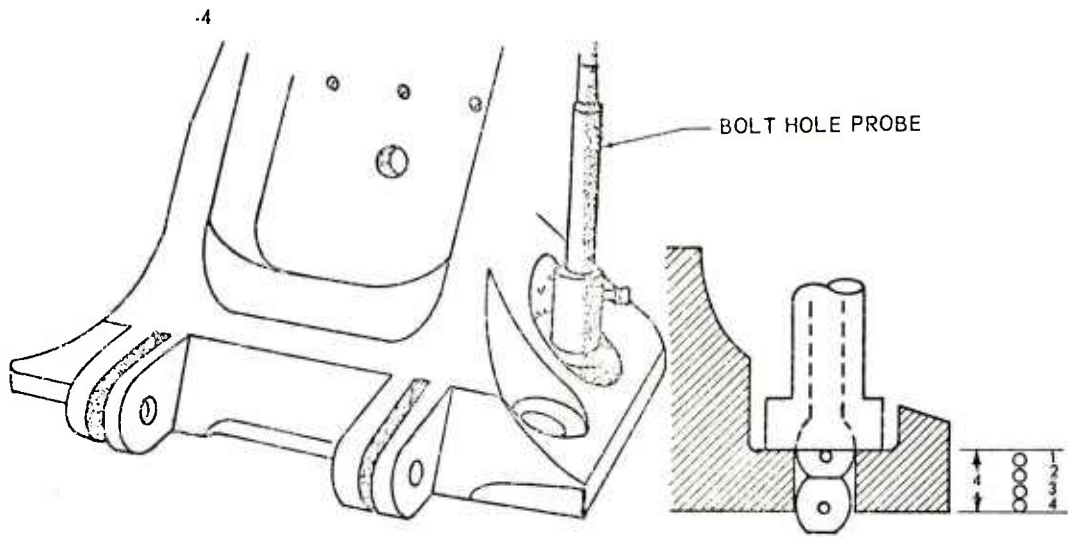
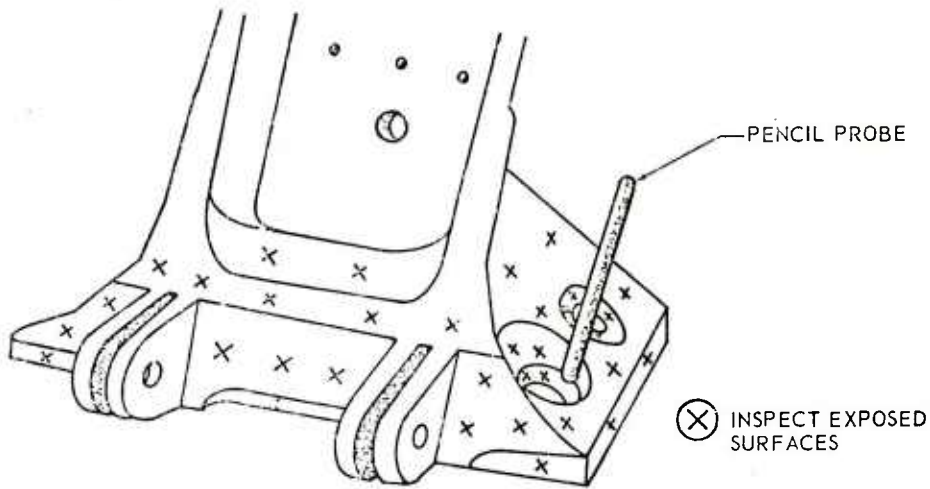


Figure 1. Forward and Rear Beams (Sheet 5 of 6)



VIEW B

ATTACH HOLE INSPECTION - FWD BEAM
(REAR BEAM SIMILAR)



VIEW A

PENCIL PROBE INSPECTION - FWD BEAM
(REAR BEAM SIMILAR)

Figure 1. Forward and Rear Beams (Sheet 6 of 6)

THE END

T.O. 1F-104A-36S-5

OPERATIONAL SUPPLEMENT

TECHNICAL MANUAL

NONDESTRUCTIVE INSPECTION PROCEDURES

USAF SERIES

F-104A, B, C, D
F, RF, AND TF-104G (MAP)

AIRCRAFT

THIS PUBLICATION SUPPLEMENTS T.O. 1F-104A-36. Reference to this supplement will be made on the title page of the basic manual by personnel responsible for maintaining the publication in current status.

COMMANDERS ARE RESPONSIBLE FOR BRINGING THIS SUPPLEMENT TO THE ATTENTION OF ALL AFFECTED AF PERSONNEL.

PUBLISHED UNDER AUTHORITY OF THE SECRETARY OF THE AIR FORCE

8 MARCH 1973

1. PURPOSE.

To add a new eddy current procedure for the knob installed on the tip tank and to improve the existing magnetic particle inspection procedure.

2. INSTRUCTIONS.

a. The existing TIPTANK LATCH KNOB procedure, paragraphs 2-122 through 2-128 are replaced as follows:

- 2-122. TIPTANK LATCH KNOB, Part No. 764825, Models F-104A, B, C, D and Part No. 776640-1, Models F/RF/TF-104G.
- 2-123. DESCRIPTION. (See figure 2-26) The tiptank latch knob is attached to the tip tank as indicated in the figure. The latch knob is made from 4340 steel. Two inspection procedures are provided - - An eddy current procedure for the installed knob, and a magnetic particle inspection for the knob removed from the tip tank.

F.O. 1F-13A-365-5

- 2-124. DEFECTS. In-service cracks have been developing at the 6 and 12 o'clock positions of the knob. Complete failure of the knob at the intersection of the 0.500-inch diameter shank and the knob has occurred on a number of occasions.
- 2-125. PRIMARY NDI PROCEDURE FOR KNOB INSTALLED IN TIPTANK - EDDY CURRENT.
1. NDI equipment.
 - a. Crack detector, Magnaflux ED-520, or equivalent, Stock No. 6635-167-9826.
 - b. Probe, specially designed Magnaflux probe, Part No. 209199. Magnaflux Corp., 7300 W. Lawrence Ave., Chicago, Illinois 60656. Note design of probe in figure 2-26.
 - c. Test standard, tiptank knob with circumferential slot as shown in figure 2-26.
 2. Preparation of airplane. Remove tiptank in accordance with applicable technical procedures.
 3. Preparation of part. Clean tip of knob as necessary to permit good contact between part and probe.
 4. Instrument calibration.
 - a. Connect probe to ED-520 and check battery condition.
 - b. Slide probe onto tip of test standard. Orient coil in probe away from the slotted portion of the standard.
 - c. Rotate function switch to "LO" position. Starting at the zero position of the "LIFT-OFF/FREQ" control rotate dial until the needle changes direction, e.g., changes from up-scale direction to downscale. During this operation the needle is kept on scale by using the "BALANCE" control.
 - d. To correct for lift-off (minimum movement of needle due to coil-test piece distance variations) wiggle the probe slightly while adjusting the "LIFT-OFF/FREQ" control. Lift-off correction is extremely important and must be done very carefully.
 - e. Rotate probe slowly around the tip of the knob and note the deflection from the test standard slot. Adjust the "SENSITIVITY INC" control for a maximum of $50 \pm$ scale units. (Refer to figure 2-26.)
 5. Inspection. (Inspect with knob in vertical position, see figure 2-26.)
 - a. Slide probe onto knob taking care to seat it properly.
 - b. Wiggle probe to minimize lift-off. This operation is required for each knob inspected because of physical differences between knobs.
 - c. Slowly rotate probe 360° and note deflections. Small needle movements of 20 or 30 units may occur throughout the rotation due to surface variations on the knob or probe wobble. Upscale deflections in excess of 50 units shall be interpreted as "suspected" crack indications. Crack indications will appear at the 6 or 12 o'clock knob positions.
 - d. To confirm defect indications remove tip tank knob in accordance with technical manuals and inspect by magnetic particle inspection method. See below.

2-126. PRIMARY PROCEDURE FOR TIP TANK LATCH KNOB REMOVED FROM TIP TANK AND CONFIRMATION OF EDDY CURRENT INDICATIONS.

1. NDI equipment.
 - a. Magnetic inspection unit, portable hand probe DA 200, Stock No. 6635-022-0372, or equivalent.
 - b. Magnetic particle solution, fluorescent, Stock No. 6850-841-1347, or equivalent.
 - c. Light unit, test, portable (black light), Stock No. 6635-611-5617, or equivalent.
 - d. Indicator, field, magnetic variation, 0-6 Oersted range, Stock No. 6635-391-0058, or equivalent.
 - e. (Alternate magnetic inspection unit). Stationary type MB-3, Stock No. 6635-055-6596, or equivalent.
2. Preparation of airplane. Remove tip tank from aircraft and remove knob in accordance with technical manuals.
3. Preparation of part. Remove any paint, corrosion, grease, or dry film lubricant from the entire tip tank latch knob.
4. Inspection procedure.
 - a. Portable hand probe.
 - (1) Position Pulse/AC switch to AC.
 - (2) Position sensitivity control to maximum sensitivity.
 - (3) Place tip tank latch knob between probe legs as indicated by figure 2-26.
 - (4) Press test switch and spray magnetic particle solution on part. Keep test switch pressed for at least 5 seconds after application of solution.
 - (5) In a darkened area using the black light, inspect in the critical areas for cracks. Service cracks have occurred at either the 6 or 12 o'clock positions at the intersection of the 0.500-inch diameter shank and the knob. Also, inspect for deep or sharp grooves in this area. Cracks or grooves are not acceptable in the knob area.
 - (6) Evaluate defect indications by examining the part with optical devices. Mark and report indicated defects.
 - (7) Demagnetize the part after inspection.
 - b. Stationary or portable magnetic particle systems, 7500-10,000 ampere turn capability.
 - (1) Position the knob in the magnetizing coil as noted in figure 2-26.
 - (2) Apply current for one second while spraying the part with magnetic particle solution.
 - (3) Observe for defect indications and evaluate suspect indications similar to that described for the portable hand probe technique.

T.O. 1F-104A-36S-5

2-127. SYSTEMS SECURING. Clean areas inspected, restore finishes, recoat the knob with dry film lubricant per MIL-L-46010, Stock No. 9150-142-9309, and reinstall, in accordance with applicable technical orders.

b. Figure 1 of this supplement is figure 2-26 of the basic manual.

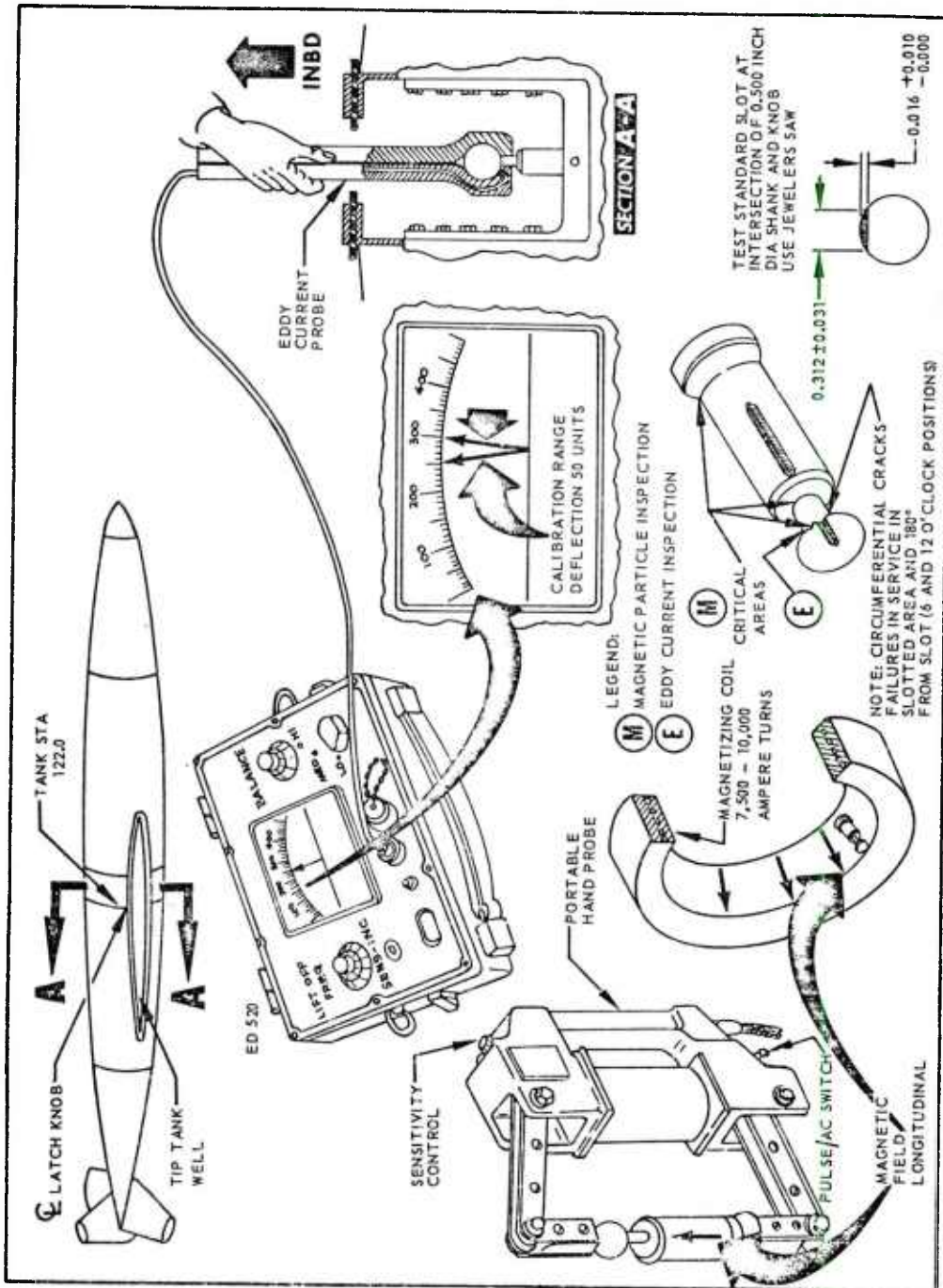


Figure 1. Tiptank Latch Knob.

THE END

5/(6 blank)

APPENDIX B

NON-DESTRUCTIVE TEST MANUAL

**Inspection Procedures for Boeing Jet Transports
Boeing Document D6-7170**

The following pages are reproduced directly
from the relevant test manuals.

EFFECTIVITY
MODEL: ALL 707 AND 720
SERVICE BULLETIN
REFERENCE: 2330

BOEING Commercial Jet
NONDESTRUCTIVE TEST MANUAL

PART 4 - ULTRASONIC

HORIZONTAL STABILIZER

1. Purpose

- A. Service experience shows that cracks can occur in top and bottom lugs of horizontal stabilizer spar terminal fittings, P/N 65-3409-5 or -6. The cracks originate at the bolthole and propagate along the flash line. This longitudinal wave technique is recommended for detecting these cracks.

NOTE: Cracks cannot be distinguished from inclusions with this procedure.

2. Equipment

- A. Any ultrasonic equipment which satisfies the requirements of recommended procedure may be used.
- (1) Transducers
 - (a) 5-mc/s, 1/4-inch diameter crystal, mounted in 3/8-inch diameter case
 - (2) Crack comparison standard, fabricated as shown in detail I
 - (3) Transducer positioning fixtures, fabricated as shown in details II and III
 - (4) Couplant. Light oil or grease is satisfactory

3. Preparation for Inspection

- A. Clean surface of terminal fitting thoroughly to ensure good contact between transducer positioner and fitting.
- B. If painted surface is rough, smooth lightly with abrasive cloth.
- C. Coat inspection area with couplant.

Horizontal Stabilizer Outboard Front Spar Terminal Fitting
Figure 1 (Sheet 1)

Jan 15/72
+

Part 4
55-10-07
Page 1

BOEING Commercial Jet
NONDESTRUCTIVE TEST MANUAL

4. Instrument Calibration

A. Calibration for Inspecting Inboard Side of Bolt Hole

- (1) Place transducer in positioning fixture. Place fixture on comparison standard so as to direct sound beam into artificial crack area. (See detail IV.)
- (2) Move fixture forward and aft to obtain a maximum signal response from crack.
- (3) Identify position of maximum response on oscilloscope. Hold transducer in this position.
- (4) Adjust sensitivity of instrument until vertical response indication on oscilloscope is approximately 70 percent of saturation.
- (5) Note position of transducer on standard at which maximum response is obtained.

B. Calibration for Inspecting Outboard Side of Bolt Hole

- (1) After inspecting inboard side of bolt hole, calibrate instrument for inspecting outboard side using same procedure used for calibrating inboard side.

5. Inspection Procedure

A. Inspection of Inboard Side of Bolt Hole

- (1) Place transducer in positioning fixture. Place positioning fixture on lug so as to direct sound beam toward inspection area. (See detail IV.)
- (2) Scan area by moving fixture in a forward and aft pattern to a distance of approximately 1/2-inch on each side of maximum scan position established in calibration procedure.
- (3) If a crack indication is detected, a response will appear on the oscilloscope similar to the response received from the simulated crack in the comparison standard. Lateral movement of crack response occurs as transducer is moved back and forth on the lug.
- (4) Compare indications with those of standard for determination of cracks. Any indication up to or greater than that obtained from standard is positive indication of crack.

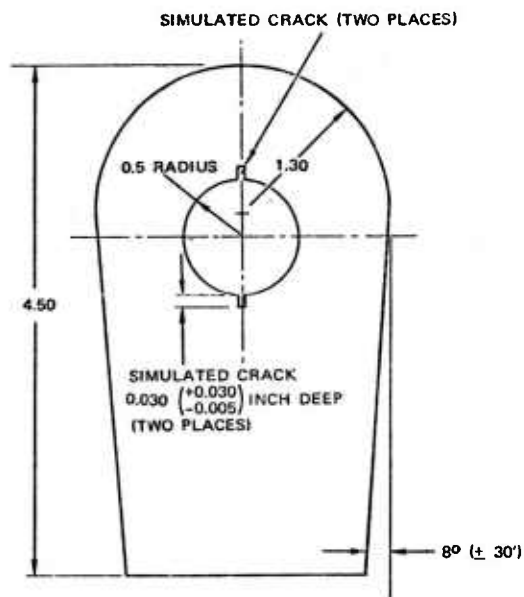
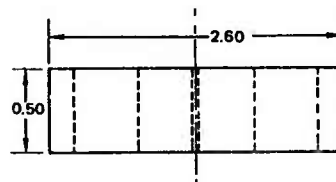
Horizontal Stabilizer Outboard Front Spar Terminal Fitting
Figure 1 (Sheet 2)

BOEING *Commercial Jet*
NONDESTRUCTIVE TEST MANUAL

- (5) Verify crack indications by removing pin, cleaning area, and checking by visula or other means.

B. Inspection of Outboard Side of Bolt Hole

- (1) After calibrating instrument, repeat procedure on outboard side of bolt hole.



- NOTE: 1. ALL DIMENSIONS
IN INCHES
 2. FABRICATE FROM
ALUMINUM
 3. TOLERANCE ± 0.030
ON ALL DIMENSIONS
EXCEPT AS NOTED

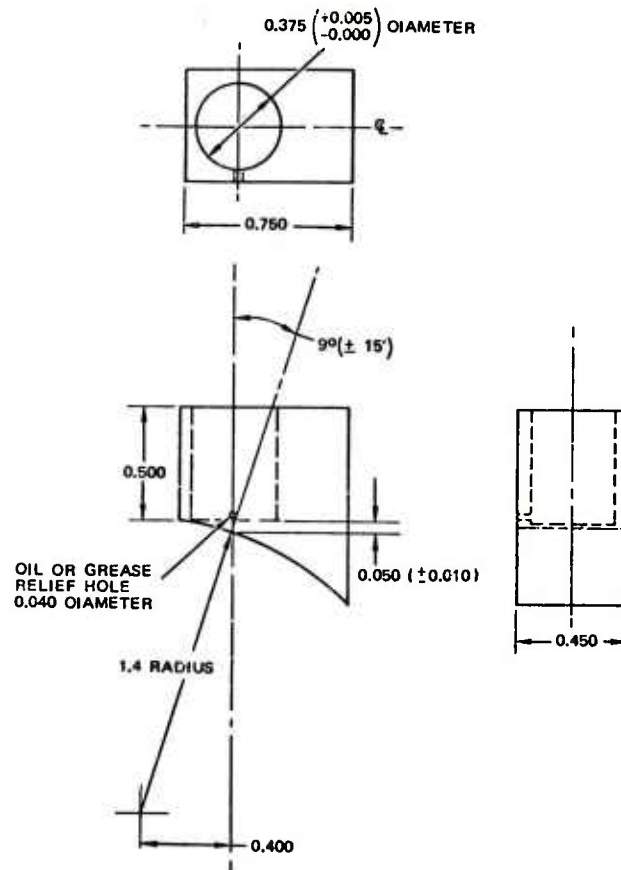
COMPARISON STANDARD
DETAIL 1

Horizontal Stabilizer Outboard Front Spar Terminal Fitting
Figure 1 (Sheet 3)

Jan 15/72
+

Part 4
55-10-07
Page 3

BOEING *Commercial Jet*
 NONDESTRUCTIVE TEST MANUAL



- NOTE: 1. MAKE FROM LUCITE
 2. ALL DIMENSIONS
 IN INCHES
 3. ± 0.030 TOLERANCE
 ON ALL DIMENSIONS
 EXCEPT AS NOTED

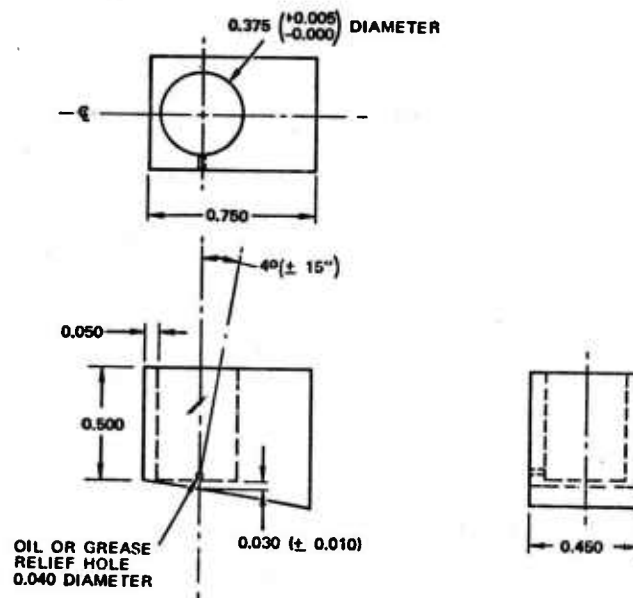
TRANSDUCER POSITIONING FIXTURE
 DETAIL II

Horizontal Stabilizer Outboard Front Spar Terminal Fitting
 Figure 1 (Sheet 4)

Part 4
 55-10-07
 Page 4

Jan 15/72

BOEING *Commercial Jet*
NONDESTRUCTIVE TEST MANUAL



TRANSDUCER POSITIONING FIXTURE

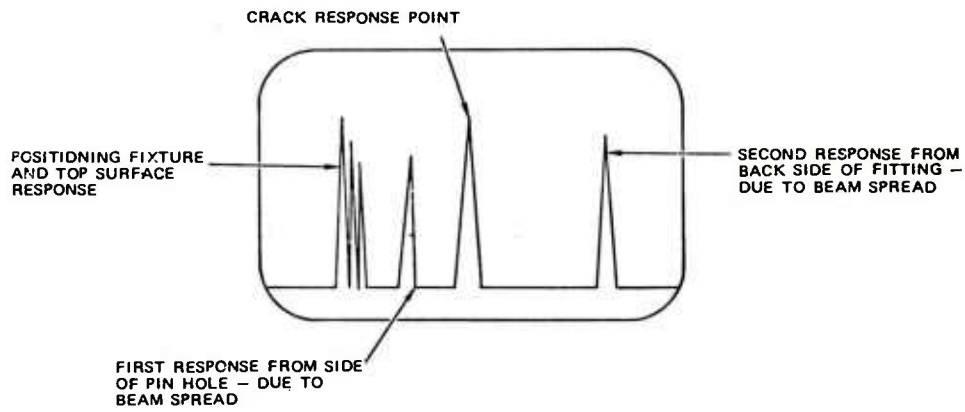
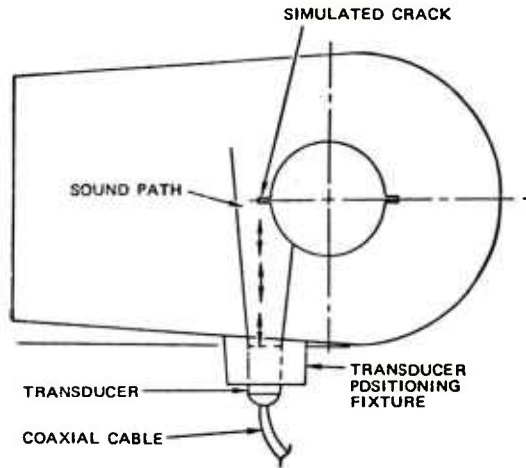
DETAIL III

Horizontal Stabilizer Outboard Front Spar Terminal Fitting
 Figure 1 (Sheet 5)

Jan 15/72

Part 4
 55-10-07
 Page 5

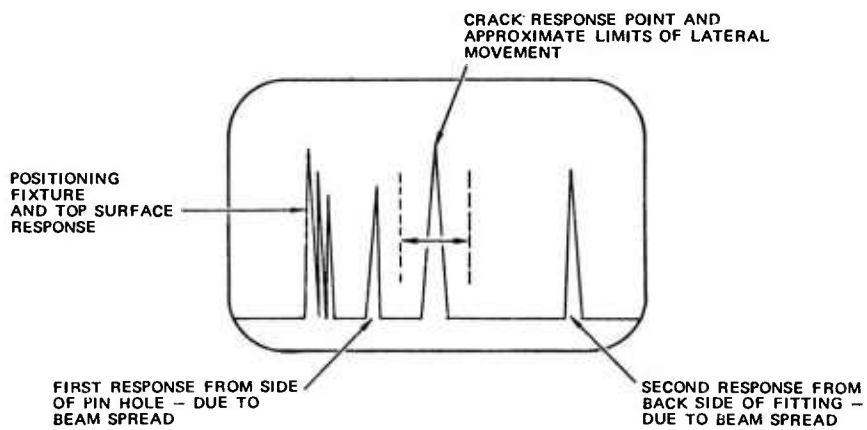
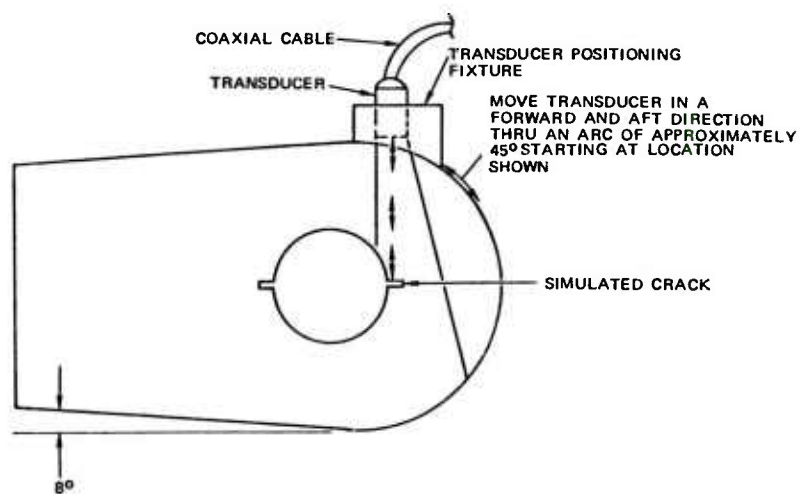
BOEING *Commercial Jet*
NONDESTRUCTIVE TEST MANUAL



**CALIBRATION OF EQUIPMENT
 DETAIL IV**

Horizontal Stabilizer Outboard Front Spar Terminal Fitting
 Figure 1 (Sheet 6)

BOEING *Commercial Jet*
NONDESTRUCTIVE TEST MANUAL



**CALIBRATION OF EQUIPMENT
 DETAIL IV (CONTINUED)**

Horizontal Stabilizer Outboard Front Spar Terminal Fitting
 Figure 1 (Sheet 7)

Jan 15/72

Part 4
 55-10-07
 Page 7

EFFECTIVITY
MODEL: ALL

BOEING Commercial Jet
NONDESTRUCTIVE TEST MANUAL

PART 6 - EDDY CURRENT

STRUCTURES - GENERAL

1. General

- A. The technique for inspecting fastener holes in aluminum parts was developed from data derived with Boeing-built probes and equipment specified in following procedure.

2. Equipment

- A. Instrument Set - Any eddy-current unit designed for crack detection which is comparable to those listed below.

- (1) Magnaflux, Magnatest ED-500, ED-510, ED-520
- (2) Uresco FC-2001
- (3) Foerster, Defectometer 2.154

- B. Probes - Probes used in this procedure should have the following characteristics:

- (1) Diameter should be adjustable to obtain a snug fit in the hole.
- (2) Probe should be adjustable to permit depth penetration into hole to be adjusted.
- (3) Movement of the coil area perpendicular to the axis of the hole from its set depth must be minimal in order to reduce edge effect interference. Axial probe movement should not produce edge effect interference greater than 20 percent of the meter response from the calibrating crack in the test block.
- (4) Probe should not give interfering responses from normal handling pressures or manipulation, or from normal operating pressure variations on the sensing coil.

<u>Hole Diameter</u>	<u>Probe Diameter</u>
3/16	0.1875 inch
1/4	0.2500 inch
5/16	0.3125 inch
3/8	0.3750 inch
7/16	0.4375 inch
1/2	0.5000 inch

Fastener Holes in Aluminum Parts
Figure 1 (Sheet 1)

Jan 15/73

Part 6
51-00-00
Page 1

TR-- RL-80-C


NONDESTRUCTIVE TEST MANUAL

- C. Test Blocks - Test blocks with suitable natural cracks or artificial notches to simulate cracks in each of the hole sizes being tested. A Standard test block should meet the following requirements:
- (1) Block should be of aluminum alloy similar to the material being tested. Aluminum having conductivity within 5 percent of that of the part being tested is satisfactory.
 - (2) Block should contain a suitable range of hole diameters to permit calibration of instrument for diameter of each hole to be tested.
 - (3) The crack or notch in the block must give an eddy-current instrument calibration comparable to that obtained from the recommended Boeing test block. Recommended test blocks with applicable diameters are as follows:

<u>Hole Diameter</u>	<u>Probe Diameter</u>
3/16	0.1875 inch
1/4	0.2500 inch
5/16	0.3125 inch
3/8	0.3750 inch
7/16	0.4375 inch
1/2	0.5000 inch

NOTE: See detail I for details of calibration test blocks.

3. Preparation for Inspection

- A. Clean loose dirt and paint from inside and around fastener hole.
- B. Remove buildup of paint, sealant, etc., from around outside of hole where probe will bear.

NOTE: If surface of hole is extremely rough, a 1/64-inch cleanup ream may be necessary.

4. Instrument Calibration

- A. Attach appropriate probe to instrument.
- B. Turn instrument on and allow to warm up per manufacturer's instructions.
- C. Select appropriate test block and place probe in hole. Probe should fit snugly but not so tight as to cause excessive wear of probe. Expand loose probe to obtain snug fit.

Fastener Holes in Aluminum Parts
Figure 1 (Sheet 2)


NONDESTRUCTIVE TEST MANUAL

- D. Adjust instrument for lift-off.
- (1) Place sensitive (coil) part of probe on a flat surface of material to be inspected. Because of edge effect interference, place coil at least 1/4 inch away from edge of part.
 - (2) Manipulate probe to obtain maximum eddy-current effect.
 - (3) Place a single sheet of ordinary writing paper (approximate thickness 0.003 inch) between probe and material.
 - (4) Remove paper and note direction and amount of deflection of needle.
 - (5) Adjust lift-off control to obtain minimum needle movement when shim is removed. When no needle movement is noted, instrument and probe have been calibrated.
- E. Insert probe in hole in test block, and adjust depth in hole to obtain maximum needle deflection on meter from edge crack (center of coil approximately 0.025 inch deep for 0.030-inch edge crack).
- F. Adjust sensitivity to obtain a minimum of 10% full scale meter deflection from standard crack. Instrument is now calibrated for detection of edge cracks in hole to be inspected.
- G. Insert probe in test block, and adjust depth in hole to obtain maximum needle deflection from crack located between ends of hole in test block. Tighten setscrew on collar of probe.
- H. Repeat step F. Instrument is now calibrated for detection of cracks between ends of hole.

5. Test Procedure

- A. Adjust collar on probe to set depth of penetration into hole at 0.025 inch from top end of hole.
- B. Tighten collar on probe and insert probe into hole. Adjust balance control to bring needle approximately to midscale.
- C. Slowly scan entire circumference of hole. Note position of any needle deflection of 10% of full scale or greater, giving a positive crack response.

NOTE: A positive crack response is characterized by rapid deflection of the meter needle over a short scan distance. Deflection occurs as the coil moves over the crack. This movement is equivalent to an arc of approximately 40 degrees in a 1/4-inch fastener hole, and 20 degrees in a 1/2-inch hole.

Fastener Holes in Aluminum Parts
Figure 1 (Sheet 3)

Jan 15/73

Part 6
51-00-00
Page 3

**NONDESTRUCTIVE TEST MANUAL**

- D. Note locations of any questionable indications, i.e., crack-like indications causing needle deflection of less than 10% of full scale, or indications not conforming to a positive crack indication. Perform a 1/64-inch cleanup ream and repeat test, paying particular attention to areas where indication was noted. Note location and response of all positive crack indications.
- E. Repeat steps B through D at incremental depths of 0.050 inch and 0.025 inch from bottom end of hole. Calibrate instrument as directed in calibration procedure for each step.
- F. When hole is reamed to clean up or remove cracks, perform eddy-current test after each increase in hole diameter.
- G. Recheck calibration of instrument with test block periodically to ensure proper sensitivity of instrument.
- H. Repeat procedure for each hole in area to be inspected.

Fastener Holes in Aluminum Parts
Figure 1 (Sheet 4)

Part 6
51-00-00
Page 4

Jan 15/73


NONDESTRUCTIVE TEST MANUAL

EFFECTIVITY
MODEL: ALL

PART 6 - EDDY CURRENT

STRUCTURES - GENERAL

1. General

- A. The technique for inspecting bolt holes in steel parts was developed from data derived by experiment with Boeing-built probes and equipment specified in following procedure.

2. Equipment

- A. Instrument Set - Magnaflux ED-500 or ED-510
 B. Hole Probes - Probes to suit diameter of holes

<u>Hole Diameter</u>	<u>Probe Diameter</u>
3/16 inch	0.1875 inch
1/4 inch	0.2500 inch
5/16 inch	0.3125 inch
3/8 inch	0.3750 inch
7/16 inch	0.4375 inch
1/2 inch	0.5000 inch

- C. Test Blocks - Use test block to establish sensitivity of system for each size hole. Fabricate blocks of low carbon steel (4130, 4140, or 4340) to dimensions shown in detail I.

3. Preparation for Inspection

- A. Clean loose dirt and paint from inside and around fastener hole.
 B. Remove buildup of paint, sealant, etc., from around fastener hole where probe will bear.

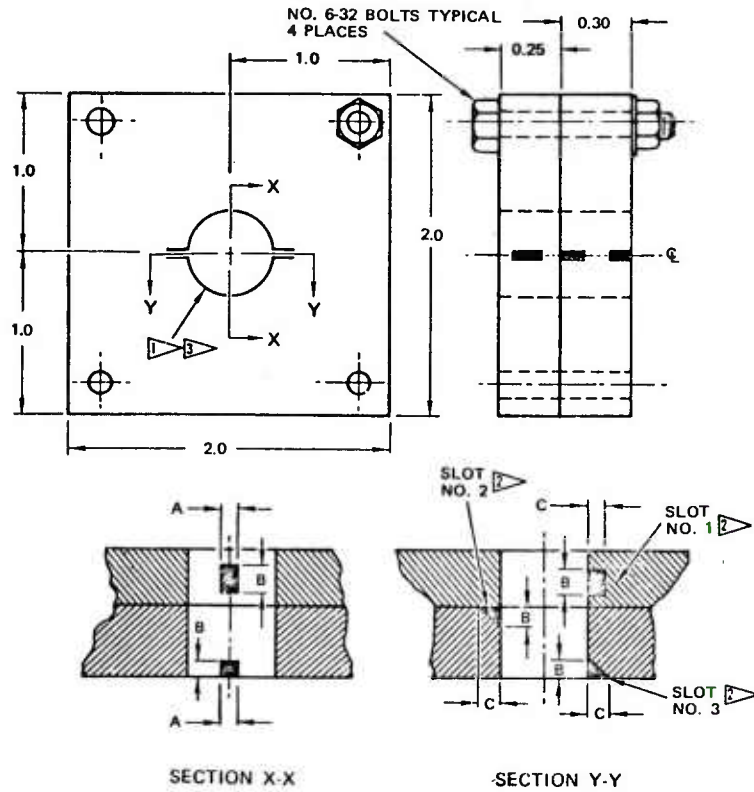
NOTE: If surface of hole is extremely rough, a 1/64-inch cleanup ream may be necessary.

4. Instrument Calibration

- A. Turn instrument on and allow to warm up 15 minutes.
 B. Connect Boeing probe to instrument.

Fastener Holes in Steel Parts
 Figure 2 (Sheet 1)

BOEING Commercial Jet
NONDESTRUCTIVE TEST MANUAL



- NOTES:
- TOLERANCE ON ALL DIMENSIONS ± 0.050 INCH EXCEPT AS NOTED
 - ALL DIMENSIONS IN INCHES
 - 1 FINISH REAM HOLE AND DO NOT DEBURR
 - 2 ELECTRIC DISCHARGE MACHINE PER GIVEN DIMENSIONS
 - 3 HOLE DIAMETER (6 STANDARD)
0.1875 0.2500 0.3125
0.3750 0.4375 0.5000
TOLERANCE $+0.005$ ON ALL HOLES
 -0.000

SLOT NUMBER	A	B	C
	WIDTH	LENGTH	DEPTH
1	0.005	0.060	0.030
2	0.005	0.030	0.030
3	0.005	0.030	0.030
TOLERANCE	$+0.000$ -0.001	± 0.001	± 0.001

CALIBRATION TEST BLOCK DATA
DETAIL I

Fastener Holes in Aluminum Parts
Figure 1 (Sheet 5)

Jan 15/73

Part 6
51-00-00
Page 5

BOEING
Commercial Jet
NONDESTRUCTIVE TEST MANUAL

C. Adjust instrument controls.

- (1) Set frequency selector at (9).
- (2) Adjust liftoff control to about midrange.
- (3) Adjust sensitivity to maximum.
- (4) Adjust instrument for liftoff.
 - (a) Place sensitive (coil) part of probe on a flat surface of material to be inspected. Because of edge effect interference, place coil at least 1/4 inch away from edge of part.
 - (b) Manipulate probe to obtain maximum eddy-current effect.
 - (c) Place a single sheet of ordinary writing paper (approximate thickness 0.003 inch) between probe and material.
 - (d) Remove paper and note direction and amount of deflection of needle.
 - (e) Adjust liftoff control to obtain minimum needle movement when shim is removed. When no needle movement is noted, instrument and probe have been calibrated.

D. Place probe in proper hole in test block.

NOTE: Probe should fit snugly in hole of test block as well as in holes of part to be tested. A folded paper shim may be inserted into slot of the probe to expand probe and make a snug fit.

E. Adjust penetration depth of probe so that center of coil crosses middle of notch in test block. Tighten setscrew on collar of probe.

F. Bring needle to center of scale by means of balance control.

G. Rotate probe slowly in test hole. Note meter deflection as probe crosses notch. Deflection should be 150 microamperes (MA) or greater, reduce sensitivity to obtain approximately a 150-MA deflection from the center-scale position. Instrument and probe are now calibrated for inspection.

NOTE: Unsatisfactory steel, fastener hole probes - Occasionally, a probe may be selected which is extremely sensitive to the notch in the test block. This probe may cause a deflection of 400 MA or more. Minimum instrument sensitivity adjustment may not reduce this deflection to the specified 150 MA. This probe must be discarded; it is too sensitive to be used for inspection of steel holes.

Fastener Holes in Steel Parts
Figure 2 (Sheet 2)

Jan 15/73

Part 6
51-00-00
Page 7

BOEING ~~Commercial Jet~~
NONDESTRUCTIVE TEST MANUAL

5. Test Procedure

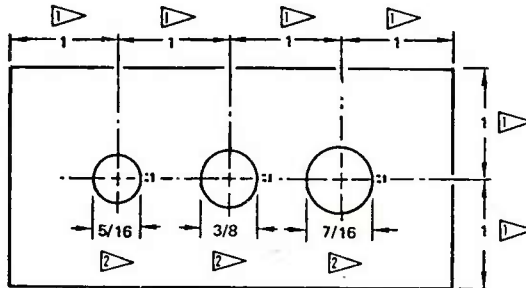
- A. Adjust collar on probe to set depth of penetration of probe into hole at 0.050 inch. Slowly scan the complete circumference of the hole first at a depth of 0.050 inch from top of hole; then readjust collar and scan at incremental depths of 0.050 inch, measured along axis of hole, and 0.050 inch from bottom of hole.
- B. Note position of each indication giving positive response of approximately 150 MA deflection or greater.

NOTE: A positive response is characterized by the rapid deflection (up-scale) of the meter needle over a short scan distance. The deflection occurs as the probe coil travels over the crack, a distance of approximately 0.1 inch. In fastener hole inspection, this movement is equivalent to an arc of approximately 40 degrees for a 1/4-inch fastener hole and 20 degrees for a 1/2-inch fastener hole.

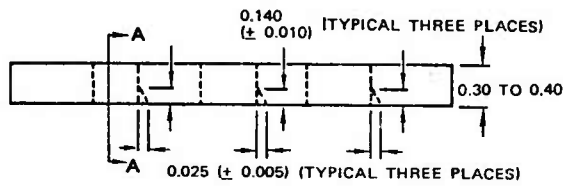
- C. Note location of questionable indications, i.e., less than 100 MA, or indications not conforming exactly to a positive crack indication. Perform a cleanup ream of hole and repeat eddy current test, paying particular attention to area where crack indication was noted. Perform a cleanup ream of hole if an irregular response is obtained which interferes with a proper eddy current hole inspection. Note location and response of all positive eddy current indications.
- D. After reaming hole to remove crack, perform eddy current check after each increase in hole diameter.
- E. Recheck test block periodically to assure proper instrument sensitivity.
- F. Repeat procedure for each hole in inspection area.

Fastener Holes in Steel Parts
Figure 2 (Sheet 3)

Jan 15/73

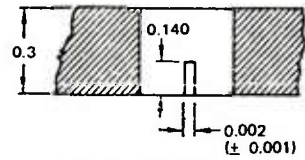


PLAN VIEW



-  TOLERANCE ON ALL DIMENSIONS ± 0.050
-  REAM HOLES FOR SMOOTH FINISH

NOTE: ALL DIMENSIONS IN INCHES



SECTION A-A
(TYPICAL)

CALIBRATION TEST BLOCK DATA

DETAIL I

Fastener Holes in Steel Parts
Figure 2 (Sheet 4)

Jan 15/73

Part 6
51-00-00
Page 9

EFFECTIVITY
MODEL: ALL

PART 6 - EDDY CURRENT

STRUCTURES - GENERAL

1. General

- A. When aluminum alloys are subjected to high temperatures, hardness of the metal decreases and conductivity values increase. The extent of damage to a structural area can be determined accurately by using an eddy current instrument to measure conductivity of the material.
- B. Aluminum structure can withstand moderate heat (up to 500°F) for short periods of time without significant loss of strength. Structure that exhibits an increase of conductivity without discoloration of the green or yellow primer (excluding surface smut) may be considered as meeting the design minimum properties providing the conductivity does not exceed the following limits. Values are for bare material. Clad material will have higher readings dependent upon thickness of the surface coating.

Alloy and Condition	%IACS (International Annealed Copper Standard)
2024-T3, T4	33.5%
7079-T6, T611	34.0%
7075-T6	35.0%
7075-T73	42.5%
7178-T6	34.0%
2014-T6	40.0%

NOTE: The above limits are applicable only to structure that does not exhibit primer discoloration.

- C. Structure exhibiting primer discoloration must be considered as having been exposed to temperatures in excess of 500°F. Conductivity readings are not recommended for predicting strength in this region. Any conductivity change above or below the nominal undamaged reading is considered suspect.

2. Equipment

- A. Instrument - Magnatest ED-500, FM-100, or FM-120, or equivalent. The FM-120 is portable; therefore, it is most practical for use on aircraft structures because of accessibility problems.
- B. Probe - Flat, surface type

Investigation of Fire Damage on Aircraft Structure
Figure 3 (Sheet 1)


NONDESTRUCTIVE TEST MANUAL

3. Preparation for Testing

- A. Thoroughly clean area to be inspected to ensure good contact between probe and surface.

4. Instrument Calibration

- A. Attach probe to instrument.
- B. Turn instrument on and allow to warm up according to manufacturer's instructions.
- C. Adjust instrument for lift-off according to manufacturer's instructions.

5. Inspection Procedure

- A. If area to be inspected is large, a grid system may be used to ensure complete coverage of the area. It is suggested that the area be laid out in a manner which will allow rechecking of test results.
- B. Identify material to be tested. Refer to the appropriate Structural Repair Manual.
- C. Make test readings on unaffected material to obtain comparative data.

NOTE: If different types of material are used in inspection area, make sample readings from each type. Take sample readings on unaffected portion of structure periodically during test to ensure proper calibration of the instrument.

- D. Having established the normal readings to be expected from the unaffected structure, make inspection readings from the suspected area, starting on what appears to be satisfactory material, and working toward the center of the suspected area. Any rapid change in readings from those obtained on the unaffected material is reason to believe that the material under probe has been affected by heat.

NOTE: It is possible for the meter needle to deflect rapidly to either side of the scale when damaged material is encountered. This deflection is caused by a rapid change in the material conductivity.

- E. By working the probe back and forth over the area, it is normally possible to determine a definite demarcation line between affected and unaffected material. This should be drawn on the airframe and rechecked in order to verify that all of the affected material has been detected.

Investigation of Fire Damage on Aircraft Structure
Figure 3 (Sheet 2)

Jan 15/73

Part 6
51-00-00
Page 11

6. Conversion Factors

A. To convert N% IACS to conductivity units in meters/ohm-mm squared, perform the following operation:

(1) $N \times 0.58 = \text{Conductivity unit in meters/ohm-mm squared}$

(a) Example: Given 31% IACS

$$N = 31$$
$$31 \times 0.58 = 17.98 \text{ meters/ohm-mm squared}$$

B. To convert conductivity units in meters/ohm-mm squared to % IACS, perform the following operation:

(1) $\frac{\text{meters/ohm-mm squared}}{0.58} = \% \text{ IACS}$

(a) Example: Given 17.98 meters/ohm-mm squared

$$\frac{17.98}{0.58} = 31\% \text{ IACS}$$

C. To convert N% IACS to resistivity units in micro ohm-cm, perform the following operation:

(1) $\frac{1}{N} \times 172.41 = \text{Resistivity units in micro ohm-cm}$

(a) Example: Given 100% IACS

$$N = 100$$
$$\frac{1}{100} \times 172.41 = 1.7241 \text{ micro ohm-cm}$$

D. To convert resistivity units in micro ohm-cm to % IACS, perform the following operation:

(1) $\frac{172.41}{\text{micro ohm-cm}} = \% \text{ IACS}$

(a) Example: Given 1.7241 micro ohm-cm

$$\frac{172.41}{1.7241} = 100\% \text{ IACS}$$

Investigation of Fire Damage on Aircraft Structure
Figure 3 (Sheet 3)

DISTRIBUTION

	No. of Copies
Defense Metals Information Center Battelle Memorial Institute 505 King Avenue Columbus, Ohio 43201	1
Defense Technical Information Center Cameron Station Alexandria, Virginia 22314	12
Commander US Army Foreign Science and Technology Center ATTN: DRXST-SD3 220 Seventh Street, NE Charlottesville, Virginia 22901	1
Office of Chief of Research and Development Department of the Army ATTN: DARD-ARS-P Washington, DC 20301	1
Commander US Army Electronics Command ATTN: DRSEL-PA-P -CT-DT -PP, Mr. Sulkolove Fort Monmouth, New Jersey 07703	1 1 1
Commander US Army Natick Laboratories Kansas Street ATTN: STSNLT-EQR Natick, Massachusetts 01760	1
Commander US Army Mobility Equipment Research and Development Center Fort Belvoir, Virginia 22060	1

DISTRIBUTION (Continued)

	No. of Copies
Commander ATTN: STEAP-MT Aberdeen Proving Ground, Maryland 21005	1
Chief Bureau of Naval Weapons Department of the Navy Washington, DC 20390	1
Chief Bureau of Ships Department of the Navy Washington, DC 20315	1
Naval Research Laboratory ATTN: Dr. M. M. Krafft Code 8430 Washington, DC 20375	1
Commander Wright Air Development Division ATTN: ASRC Wright-Patterson AFB, Ohio 45433	1
Director Air Force Materiel Laboratory ATTN: AFML-DO-Library Wright-Patterson AFB, Ohio 45433	1
Director, Army Materials and Mechanics Research Center ATTN: DRXMR-PL -MT, Mr. Farrow Watertown, Massachusetts 02172	1 1
Commander White Sands Missile Range ATTN: STEWS-AD-L White Sands Missile Range, New Mexico 88002	1

DISTRIBUTION (Continued)

	No. of Copies
Jet Propulsion Laboratory California Institute of Technology ATTN: Library/Acquisitions 111-113 4800 Oak Grove Drive Pasadena, California 91103	1
Sandia Laboratories ATTN: Library P.O. Box 969 Livermore, California 94550	1
Commander US Army Air Defense School ATTN: ATSA-CD-MM Fort Bliss, Texas 79916	1
Technical Library Naval Ordnance Station Indian Head, Maryland 20640	1
Commander US Army Material Development and Readiness Command ATTN: DRCMT Washington, DC 20315	1
Headquarters SAC/NRI (Stinfo Library) Offutt Air Force Base, Nebraska 68113	1
Commander Rock Island Arsenal ATTN: SARRI-RLPL-Technical Library Rock Island, Illinois 61201	1
Commander (Code 233) Naval Weapons Center ATTN: Library Division China Lake, California 93555	1
Department of the Army US Army Research Office ATTN: Information Processing Office P.O. Box 12211 Research Triangle Park, North Carolina 27709	1

DISTRIBUTION (Continued)

	No. of Copies
ADTC (DLDSL) Eglin Air Force Base, Florida 32542	1
University of California Los Alamos Scientific Laboratory ATTN: Reports Library P.O. Box 1663 Los Alamos, New Mexico 87545	1
Commander US Army Materiel Development and Readiness Command ATTN: DRCRD DRCDL 5001 Eisenhower Avenue Alexandria, Virginia 22333	1 1
Director Defense Advanced Research Projects Agency 1400 Wilson Boulevard Arlington, Virginia 22209	1
Commander US Army Research Office ATTN: DRXRO-PH, Dr. R. Lontz P.O. Box 12211 Research Triangle Park, North Carolina 27709	2
US Army Research and Standardization Group (Europe) ATTN: DRXSN-E-RX, Dr. Alfred K. Nedoluha Box 65 FPO New York 09510	2
Headquarters Department of the Army Office of the DCS for Research Development and Acquisition Room 3A474, The Pentagon ATTN: DAMA-ARZ Washington, DC 20310	2
US Army Materiel Systems Analysis Activity ATTN: DRXSY-MP Aberdeen Proving Ground, MD 21005	1

DISTRIBUTION (Concluded)

	No. of Copies
IIT Research Institute ATTN: GACIAC 10 West 35th Street Chicago, Illinois 60616	1
DRSMI-LP, Mr. Voigt	1
DRSMI-R, Dr. Kobler	1
-RL, Mr. Comus	1
-RLA, Mr. Pettey	1
Dr. Mullinix	1
Mr. Schaeffel	50
-EO	2
-ED	2
-ES	1
-EM	1
-EP	1
-EE	1
-ET	3
-RT	1
-RR, Dr. Hartman	1
-RPR	3
-RPT (Record Set)	1
(Reference Set)	1